POLITECNICO DI TORINO

Master Degree in Biomedical Engineering

Master Thesis

The effect of retinal inhibitory interneurons on ganglion cell spiking during saccade-like stimulation: model and experiments

---

ETH *zürich*

IOB

Supervisor
Prof. Valentina AGOSTINI

External supervisors
Prof. Andreas HIERLEMANN
Prof. Felix FRANKE
PhD(c) Annalisa BUCCI

Candidate
Filippo GALLUZZI
257727

Academic Year 2020-2021

"Io, Francesco Guccini, eterno studente
Perchè la materia di studio sarebbe infinita
E soprattutto perchè so di non sapere niente . . ."

Francesco Guccini

Abstract

Your eyes are probably performing saccades scrolling on the screen, or on the page you printed out to read the abstract of this thesis. Yet you do not have the perception that they are moving, you do not realise what happens during these movements, your perception is remaining stable, you have perfect control of your visual scene.

This experienced stability is partially accompanied by an impairment of the visual system's sensitivity proximal to saccades, a phenomenon known as saccadic suppression. This phenomenon already starts in the retina and it is supported by three mechanisms.
Two of them are probably mediated by lateral networks of retinal inhibitory interneurons. More precisely by wide field amacrine cells and horizontal cells networks. However, the underlying physiological aspects remain unclear.

Here, to develop intuitions on the role of these networks in retinal saccadic suppression, we present a phenomenological model which describes their function. We designed, in MATLAB, the architecture and functionality of the lateral networks of interneurons based on their actual physiological and functional properties. We validated our model with previously reported data and new data collected through the introduction of a novel experimental protocol.

We demonstrated the capability of the model to capture the functionality of the wide field amacrine cells network in retinal saccadic suppression. Furthermore, we found that the crucial feature of such a network in mediating suppression is the interaction timescale.
We observed, both in model predictions and experiments, that the horizontal cells network might play a role in retinal saccadic suppression. However we found that its influence in modulating RGCs activity varies among cell types.

Acknowledgements

Contents

List of Figures

List of Tables

List of Abbreviations

AAV	Adeno-Associated Virus
AC	Amacrine Cell
BC	Bipolar Cell
CC	Center Compartment
CCS	Central Component (of) Suppression
CNS	Central Nervous system
cGMP	cyclic Guanosine-MonoPhosphate
CSS	Circular Saccade Suppression protocol
DA model	Dynamical Adaptation model
ESS	Extraretinal Saccadic Suppression
GCL	Ganglion Cells Layer
FR	Firing Rate
GCS	Global Component (of) Suppression
GDP	Guanosine-DiPhosphate
GTP	Guanosine-TriPhosphate
HC	Horizontal Cell
INL	Inner Nuclear Layer
IPL	Inner Plexiform Layer
IRP	Inner Retina Pathway
MC	Michelson Contrast
MI	Modulation Index
NAC	Narrow-field Amacrine Cell
nRGC	new model transient ON-RGC type
ONL	Outer Nuclear Layer
OPL	Outer Plexiform Layer
PrC	Peripheral Compartment
PR	PhotoReceptor
PSAM	Pharmacologically Selective Actuator Molecule
PSEM	Pharmacologically Selective Effector Molecule
RF	Receptive Field
RGC	Retinal Ganglion Cell
RPE	Retinal Pigment Epithelium
RSS	Retinal Saccadic Suppression
SC	Surround Compartment
SCS	Surround Component (of) Suppression
WAC	Wide-field Amacrine Cell

List of Symbols

$I(t)$	ligth intensity temporal evolution	$photons * s / \mu m^2$
$I_Y(t)$	fast component of ligth intensity temporal evolution	$photons * s / \mu m^2$
$I_Z(t)$	slow component of ligth intensity temporal evolution	$photons * s / \mu m^2$
τ_y, τ_z	time constants of light transmission to photoreceptors	ms
γ	weigth of the fast component of light intensity	
$c(t)$	cone temporal evolution	mV
τ_c	time constant of phototransduction	ms
α_c	gain of phototransduction	$\mu m^2 / (photons * s) / mV$
β_c	gain adaptation of phototransduction	$\mu m^2 / (photons * s)$
$h(t)$	horizontal cell temporal evolution	mV
$\tau(ch)$	time constant of cones-horizontal cells transmission	ms
α_{ch}	gain of cones-horizontal cells transmission	
β_{ch}	gain adaptation of cones-horizontal cells transmission	
α_{hc}	gain of horizontal cells inhibition feedback onto cones	
$IRP(t)$	inner retina pathway temporal evolution	mV
μ, σ	period and std of the fast $IRP(t)$	ms
τ_1	time constant of the intermediate $IRP(t)$	ms
τ_2	time constant of the slow $IRP(t)$	ms
$I_g(t)$	combination of $IRPs(t)$	mV
α_g	weigth of derivative part of I_g	
$RGC_g(t)$	model retinal ganglion cell types	$spikes/s$
τ_{hc1}, τ_{hc2}	time constants of the horizontal cells inhibition feedback	ms
α_{hh}	gain of horizontal cells mutual connection in *spatial model*	
$\overline{C_C}(t), \overline{H_C}(t)$	center cone and horizontal cell temporal evolutions in *asymmetric model*	mV
$\overline{C_S}(t), \overline{H_S}(t)$	surround cone and horizontal cell temporal evolutions in *asymmetric model*	mV
$\alpha_{hh,cs}$	gain of horizontal cells mutual connection in the center-surround direction	
$\alpha_{hh,sc}$	gain of horizontal cells mutual connection in the surround-center direction	
$fb_{C1}(t), fb_{C2}(t)$	center inhibition feedback blocks temporal evolution	mV
$fb_{S1}(t), fb_{S2}(t)$	surround inhibition feedback blocks temporal evolution	mV
τ	time constant of the new introduced $IRP(t)$	ms
Δt_{flash}	time of flash from saccade onset	ms
SS	Suppression strength	$\%$

To my family…

Chapter 1

Introduction

1.1 Motivation

The retina is the most direct window to the outside world. Thanks to it we perceive everything that is around us. All its complexity is packed into 200 μm of tissue where a dense and layered network of neurons is specialized in detecting and processing all the information present in the visual scene.

Despite decades of research on the retina, all its components and its functionality, much is still unclear about its underlying mechanisms. The partial completeness of the information we have about the retina is what drives basic research, towards total comprehension.

Among the countless tasks that the retina performs, it is also responsible for providing us with a part of the visual stability we benefit from every day. In fact, we perceive the world as continuous and coherent, even though the visual flow is anything but continuous. Eye movements, such as saccades, are among the most common sources of discontinuity within the visual flow. Although we are all aware that our eyes move continuously, we continue to perceive the world around us as stable. For what reason?

Disruptions in continuity due to saccades are minimized by a reduction in the visual system's sensitivity. The visual system, indeed, has found a way to discard all the incoming redundant information within the time of the saccade - a phenomenon known as saccadic suppression.

A novel study by Idrees et al. (2020a) reports that saccadic suppression starts at the retinal level and then protracts to the CNS level. Moreover, such retinal saccadic suppression is the result of three different components (i.e., central,surround and global components of suppression), which originate in distinct locations of the retinal ganglion cells' receptive field. Thus, the retina, among its innumerable tasks, also participates in saccadic suppression, with three different components of suppression (Idrees et al., 2020b).

But what are the mechanisms underlying retinal saccadic suppression? Hypotheses have emerged regarding the origin of the three components of suppression but they are accompanied by uncertainty. In order to interpret the already obtained results on retinal saccadic suppression, we built a model. Such a model describes the possible mechanisms underlying retinal saccadic suppression in order to develop intuition or even make predictions.

1.2 Our and my contributions

We present a model whose purpose is to describe retinal saccadic suppression and to explore the origins of its three components of suppression. Based on assumptions and real data, we built a model that can simulate the functioning of the three different components of suppression separately. We compared its output with experimental data and demonstrate its qualitative consistency with them.

I personally took care of the construction of the phenomenological model (*asymmetric model*)

starting from an extension (*spatial model* by Felix Franke, F.F. and Annalisa Bucci, A.B. (Bucci et al., 2019)) of an already published model (*temporal model* by F.F. (Drinnenberg et al., 2018)). In addition, I carried out the tests run on the model and its validation through comparison with previous experimental data (Idrees et al., 2020b) and new experimental data collected by us.

I participated in the experiments, within the limits of what the regulations imposed (e.g., I did not personally conduct the sacrifice of animals), in equal measure with A.B. We collected the cellular responses thanks to the spike sorting algorithm developed by F.F and Roland Diggelmann (Diggelmann et al., 2018). Always in collaboration with A.B. we conducted a preliminary analysis of cellular responses to a novel experimental protocol (theoretically designed by A.B., F.F. and me and then coded by A.B.). I personally handled the final analysis, adding statistics also, in order to compare experimental data's and model's results.

I also collaborated in minor part on the immunohistochemistry protocols and tissue imaging (A.B.).

1.2.1   Assumptions

- The central component of suppression acts from the very center of the receptive field. Its origins lie in nonlinear signal processing of pathways within the retina.

- The global component of suppression acts from the periphery of the receptive field. Perhaps its origins are founded on one of the two lateral networks of inhibitory interneurons of the retina: the wide field amacrine cells network. Wide field amacrine cells mediate signals within one of the innermost retinal layers connecting distant regions of the same retina.

- The surround component of suppression acts from the immediate surround of the receptive field. Our hypothesis is that its source has to be found in the other lateral network of inhibitory interneurons of the retina: the horizontal cells network. Horizontal cells connect neighboring regions of the retina by mediating signals in one of the outer retinal layers.

1.2.2   A phenomenological model that accounts for retinal saccadic suppression functioning

Both lateral networks of interneurons connect different regions of the receptive field of a retinal ganglion cell. The model therefore simulates, through a multicompartmental structure, different areas of the receptive field itself.

- The central component of suppression's operation is modelled by a cascade of filtering blocks with threshold nonlinearities (Idrees et al., 2020b).

- The functioning of the global component of suppression is modelled through the introduction of a filtering block aimed at reproducing wide field amacrine cells. This block interconnects different modeled areas of the receptive field in a deep level of the retina.

- The working principle of the surround component of suppression is modelled through the introduction of interconnection terms aimed at reproducing the network of horizontal cells. Such interconnective terms are embedded in the modeling of one of the outermost layers of the retina.

1.2.3 Experimental validation of the model

- For the central and global components of suppression, we used data reported by Idrees et al. (2020b) and verify that the model can simulate the functionality of the global and the central components of suppression in retinal saccadic suppression. What emerged is that "timing is king" in suppression, and wide-field amacrine cells network's action is strictly related to it.

- For the surround component of suppression, we ran experiments on mice and explore the possibility of the engagement of the horizontal cells network in retinal saccadic suppression. We chemogenetically perturbed horizontal cells to highlight their possible role as suppressors. We then compared our real results with predictions given by the model, and we found commonalities. Horizontal cells network might have a role in retinal saccadic suppression: the question we need to ask is, which one?

1.3 Outline

The rest of this thesis is organized as follows. The first two chapters are introductory, they are aimed at presenting the principles underlying this thesis: the functioning of the retina and the saccadic suppression. The methods for the creation of the model are then outlined through the presentation of what has already been presented by others and what we have included anew. Results and discussion are presented in the final part of the thesis.

In particular, in Chapter 2, we provide a general outlook of the retina, the main cell types that populate it and their functional role. In addition, we analyze more in detail the center-surround architecture of retinal ganglion cells' receptive field. In Chapter 3 we provide details regarding retinal and extraretinal saccadic suppression. We also report the main results obtained and the hypotheses (i.e., the basis of the model) regarding the different spatial origin of retinal saccadic suppression (Idrees et al., 2020b).

In Chapter 4, we introduce the importance and utility of models in interpreting real data. We also give the example of a phenomenological model of the retina asking whether it can be used in modelling retinal saccadic suppression. In Chapter 5 we describe our new model, which is inspired by the one described in Chapter 4. We illustrate how both the horizontal and wide field amacrine cells networks have been built and on which theoretical basis.

In Chapter 6 we present the results we obtained regarding modelling the functionality of retinal saccadic suppression. Predictions regarding the global component of suppression are compared with real data reported by Idrees et al. (2020b). With respect to the surround component of suppression, we illustrate the results we obtained experimentally and compare them with the predictions provided by the model. Finally, in Chapter 7 we discuss the limitations of the model and future direction of research.

Chapter 2

The retina: the brain's window on the world

The retina is a layered, $\simeq 200$ μm thick, light-sensitive neural network lining the back of the eye. In the human eye, the pupil (i.e., variable diaphragm), the crystalline lens and the cornea (i.e., refractive apparatus) work as optical processors and provide the retina with a focused image (Fig. 2.1, left). The retina transforms the incoming light into a neural message suitable for transmission to the brain.
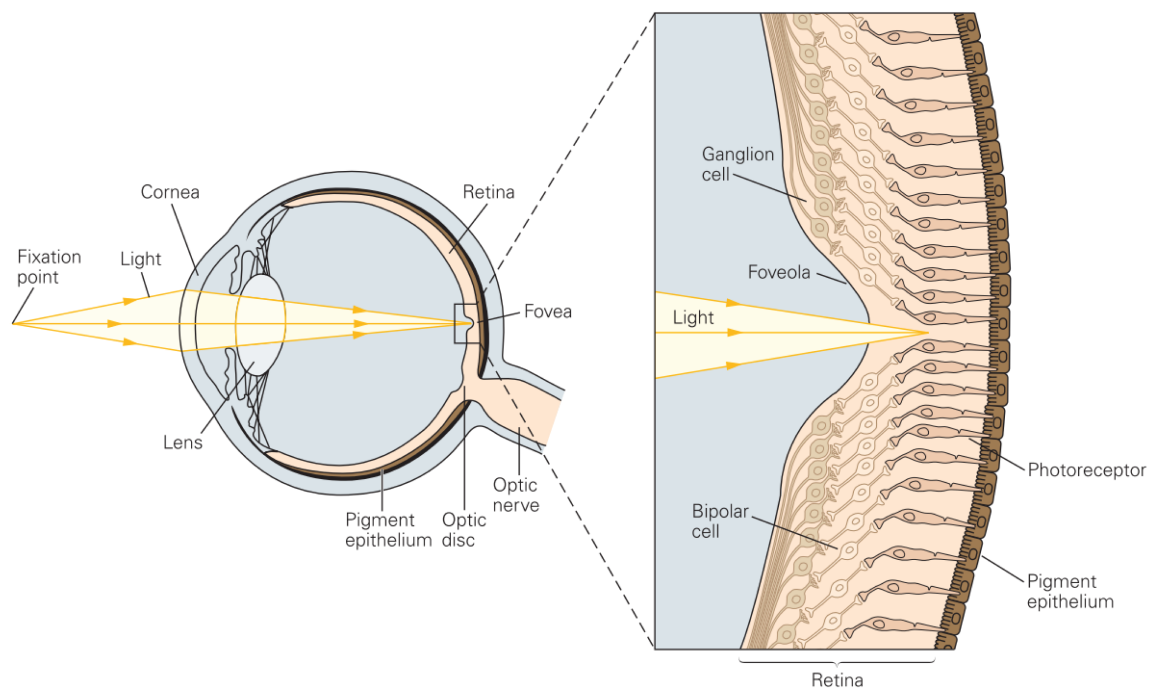
FIGURE 2.1: **The eye project the visual scene onto the retina's photoreceptors.** **Left**| Light from the visual field is refracted by the cornea and crystalline lens and focalised on the retina. **Right**| Stratified organisation of the retina. The light's processing starts with photoreceptors, the signal is passed firstly to bipolar cells and then to ganglion cells. In the very center of gaze, the foveola, light has direct access to the photoreceptors. The direct access is guaranteed by the shifted aside proximal neurons, this accounts for higher resolution in the foveola. (Adapted from Kandel, E. R, Schwartz, J.H, & Jessel (2013))

2.1 The layered neural structure of the retina

The retina is the neural entry of the visual system. Its cells are organized in a layered architecture (Fig. 2.2), from light receptors that acquire the incoming light, to ganglion cells that send the visual information to the brain in the form of spike trains.

Visual processing starts with phototransduction (i.e., transduction of light into a nervous signal). This process begins in the photoreceptors (**PRs**) layer (the "outer nuclear layer", **ONL**), which synapses onto bipolar cells (**BCs**) in the "outer plexiform layer" (**OPL**). BCs synapse, in turn, onto the ganglion cells (**RGCs**) processes (in the "inner plexiform layer", **IPL**) (Fig. 2.1, right). The axons of RGCs converge at the level of the optic disk to form the optic nerve, where the first spikes are generated to carry the signal to the rest of the central nervous system (**CNS**).

There are two other types of neurons in the retina, horizontal (**HCs**) and amacrine cells (**ACs**). They are placed in the "inner nuclear layer" (**INL**) and are primarily responsible for lateral interactions within the retina. HCs synapse both PRs and BCs in the OPL, ACs bind BCs and RGCs in the "inner plexiform layer" (**IPL**).
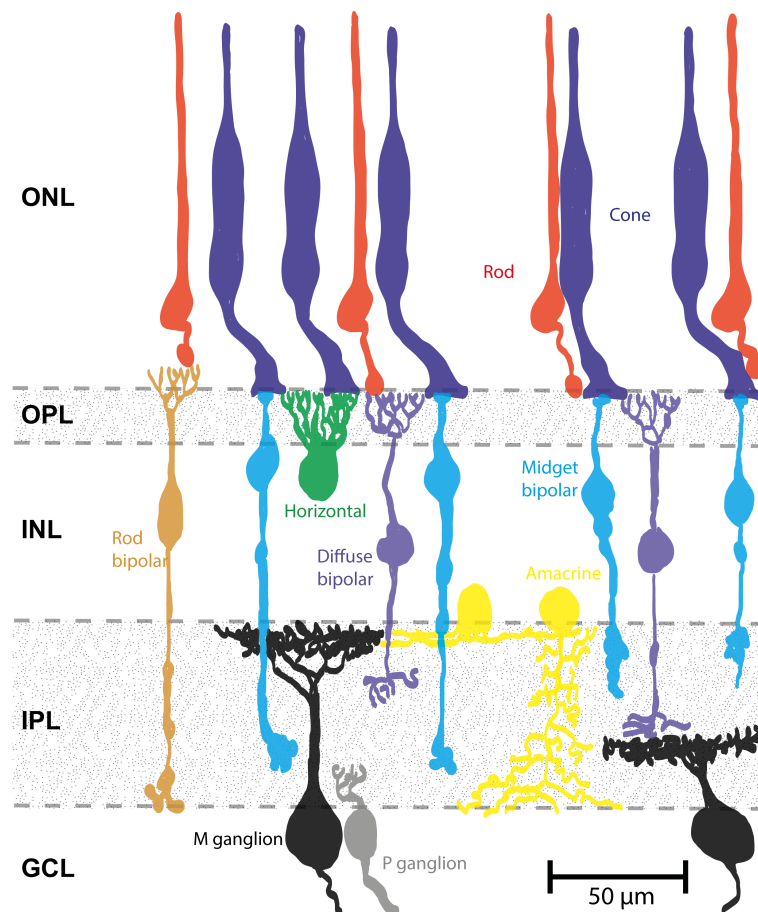
FIGURE 2.2: **The layered structure of neurons in the macaque monkey's retina**. Synaptic layers are shown patterned, cellular layers are shown unpatterned. (M ganglion, magnocellular ganglion cell; P ganglion, parvocellular ganglion cell). (Adapted from Polyak (1942)).

2.1.1 The photoreceptors layer: cones and rods

The ONL of the mammalian retina hosts two main types of PRs: rods and cones (100 and 6 millions, respectively, in the human retina). Both neurons share the same 4-regions structure:

1. the outer segment, attached to pigment epithelium (**RPE**, Fig. 2.1, right), where the light sensitive molecules are found (i.e., pigment, chromophore, opsin).

2. the inner segment.

3. the cell body.

4. the synaptic terminal in the OPL. It is different from cones (cone pedicle) and rods (rod spherule) (Fig. 2.5).

While rods are specialized for scotopic (i.e., dim light or night) vision, cones are specialized for photopic (i.e., daylight or bright light) vision. In the human fovea, the high-resolution part of the retina, cones display the highest density and no rods are found.

The phototransduction mechanism

Phototransduction is the conversion from an input light, consisting of photons, into an electrical current.
In both cones and rods, the transduction channels between the outer and the inner segment are **cGMP** (cyclic guanosine-monophosphate)-gated non-selective cation channels, open in darkness. The Na^+ and Ca^{2+} free flow makes the cell polarized at *-40 mV* in its rest condition. This causes a steady release of glutamate from the synaptic terminal (aka *dark current*).
When a PR's outer segment is hit by a photon, the photon triggers the hydrolysis of cGMP. A cascade of events yields a decrease in glutamate release from the synaptic terminal.
Specifically: the visual pigment of photoreceptors consists of an opsin protein, covalently bound to a chromophore, usually the *11-cis* retinal, aldehyde of vitamin *A1* (i.e., retinol). When a photon hits the outer segment of the photoreceptor the covalent bond between opsin and chromophore breaks, and it activates the pigment (i.e., all-trans-retinal). This is the only light-dependent event of the process. The chromophore's concentration in cones and rods is similar ($\simeq 3.5mM$) so that a photon has the same $\simeq 40\%$ probability to activate a pigment molecule in both the two types of PRs.
Once activated, the pigment attaches to a protein G, called transducin that, in its inactivated nature, binds to GDP (Guanosine diphosphate). The link between the activated pigment and the transducin makes the exchange of GDP for GTP (Guanosine triphosphate) possible. One single activated pigment could cause the reactions of multiple transducins that will bring to multiple exchanges of GDP for GTP. This mechanism makes the amplification of the signal possible.
GTP then binds to cGMP-PDE (phosphodiesterase) that hydrolyses the cGMP present in the outer segment, leading to the decrease in glutamate release. A single molecule of cGMP-PDE could hydrolyse more than 1000 molecules of cGMP. Hence the amplification is maintained.
 Once the PR produces a light response it must decay again to its steady state, in order to be ready for another light stimulus. In cones, such reset takes minutes, while in rods it takes hours, and it consists of four main steps, which yield the pigment in its activable form (i.e., *11-cis* retinal):

- The visual pigment is partially quenched when it is phosphorylated by a G-protein receptor kinase (GRK). This mechanism is $\simeq 50$ times faster in cones than in rods.

- The phosphorylate visual pigment is then fully inactivated due to the binding with a protein called arrestin. The amount of arrestin is $\simeq 7$ times larger in cones than in rods.

- GTP is hydrolyzed into GDP again. This mechanism is mediated by a regulator of G-protein signalling (RGS9) whose concentration is $\simeq$ 10 times higher in cones as compared to rods.

- Guanylyl cyclase (GC) restores the concentration of free cGMP in the outer segment of the photoreceptor.
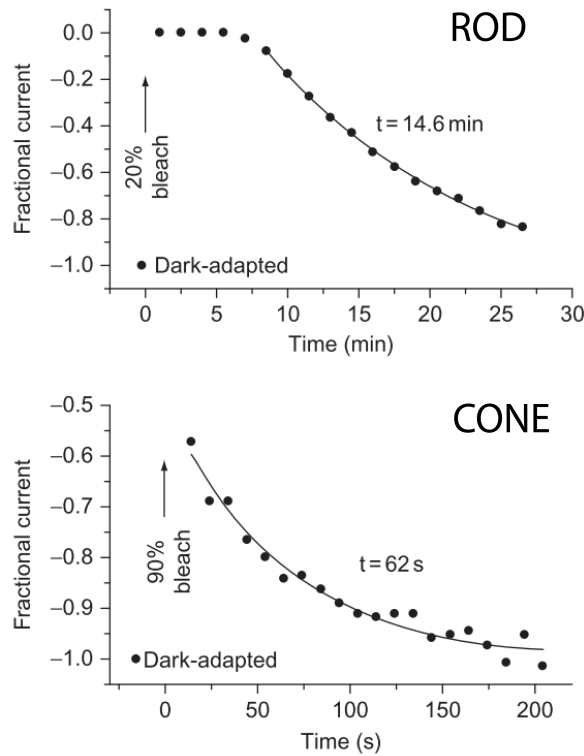
FIGURE 2.3: **Comparison of rod and cone dark adaptation**. Darkness recovery trends of the current in salamander rod (**top**) and red cone (**bottom**). Cells were previously subjected to bright light that activated 20 % and 90 % of the rod pigment and the cone pigment respectively. The fit (*solid line*) is done by a single exponential decay function. Cone's recovery current shows to be faster than rod's one. (Adapted from Kefalov (2010))

The two types of PRs show different adaptation dynamics in response to light. While rods saturate fastly in presence of bright light (Fig. 2.3, top), cones can adapt their range of responses in function of the ambient light (Fig. 2.3, bottom). This mechanism, also known as "gain adaptation", is not clearly understood but it is thought to be related to Ca^{2+} exchange in the outer segment.

In sum, a light stimulus provokes a cascade of events that finally yields a change in the glutamate release at the level of the synaptic terminal of the photoreceptor. Such change in the release of glutamate leads to hyperpolarization, in bright light, or depolarization, in darkness.

2.1.2 Horizontal cells as first functional processors of the visual scene

Horizontal cells are interneurons that populate the INL. Their axons spread widely in the OPL and connect each other through electrical synapses (i.e., gap junctions) to form the HCs network. Each HC receives synaptic inputs from either cones or rods and feeds them back with a neurotransmitter release altering signal. HCs are a small portion of the whole INL, occupying only 5% of the whole cell population. In most mammals, there are two different types of HCs (Szikra et al., 2014), with and without axon. Mice and rats, differently, are

provided with only the axon-bearing type of horizontal cells (L Peichl, Gonzälez-soriano, 1994).

Horizontal cells functional roles

Traditionally cones' HCs have two main functions in processing the visual signal:

1. They enhance contrast at stimulus edges (i.e., the interface between bright and dark regions) by providing cones with inhibition feedback (*local signal processing*). The inhibition feedback allows the cone response to have a sharper evolution. This change in the cone's evolution is captured by the inner retina processing paths and finally driven to RGCs. This mechanism increases the temporal resolution of the visual function.

2. Since their processes widely spread in the OPL, via their gap-junctions connections (Janssen-Bienhold et al., 2001), it is believed they record the overall level of illumination, subtracting it from the signal coming from phototransduction (*global signal processing*). This function would allow to fully exploit the dynamic range of photoreceptors. Thus, HCs might also have a role in PRs' gain adaptation.
   Their mutual coupling makes their receptive field (**RF**) much larger than the dendritic field; in addition, the fact that this coupling is mediated by gap junctions makes the signal transmission nearly instantaneous. (i.e $\simeq$ ms-dozens of ms).

Recent evidence shows implication of HCs in colour discrimination (Yoshimatsu et al., 2019). It is suggested they influence the absorption spectra of photoreceptors. Furthermore, a possible role of HCs has been proposed in the center-surround antagonism and surround activation in BCs. This might be due not only to the negative feedback to cones, but also to a direct influence of HCs onto BCs. This mechanism will be discussed later in this chapter (2.2). Recent evidence hints at the presence, besides the negative feedback from HCs to cones, of positive feedback that could link HCs and cones (Jackman et al., 2011). The mechanism under this effect remains unclear. Likely, it involves the activation of AMPA receptors in HCs and the subsequent increase of postsynaptic Ca^{2+} release.

Horizontal cells inhibition feedback onto cones terminal: a controversial mechanism

The mechanism by which HCs provide cones with negative feedback is unclear. However, different agents have been proposed to be responsible (Kramer and Davenport, 2015): *(1)* a conventional neurotransmitter, GABA, *(2)* protons, unconventional neurotransmitter and *(3)*, ephaptic signalling that does not involve any kind of neurotransmitter.

1. GABA is the main inhibitory neurotransmitter in the brain. In non-mammalian retinas, HCs have been found to embed biosynthetic enzymes for GABA. It seems that HCs are depolarized by glutamate release at the level of the cone terminal, this would drive a GABA release back onto the cone terminal (Fig. 2.4, left). The activation of $GABA_A$ receptors in the cone terminal would hyperpolarize them reducing the glutamate release.

2. Ca^{2+} channels in cone terminals proved to be sensitive to extracellular pH, it was then suggested that HCs could regulate the synaptic cleft *pH*. For this hypothesis, HCs depolarization could lead to a proton efflux toward the HCs dendritic tips. This efflux would then modulate the permeability of Ca^{2+} channels on the cone's side with a time constant of approximately $\simeq$ 200 ms (Fig. 2.4, right).
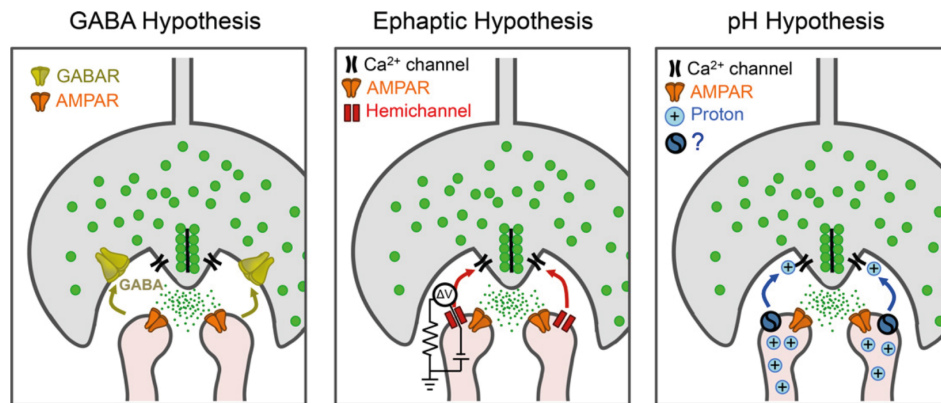
FIGURE 2.4: **The three possible mechanisms that could mediate negative feedback from horizontal cells to cones**. Glutamate (*green*) is released by cones and activates receptors (AMPAR) on HCs. HCs give inhibitory feedback onto cones' terminal via γ-Aminobutyric acid receptors (GABAR, *left*), an ephaptic mechanism (*centre*), or synaptic pH changes (*right*). (Reproduced from Kramer and Davenport (2015)).

3. For the ephaptic theory, HCs are believed to be passed by ion current and to have high extracellular resistance. These two things together would produce an extracellular voltage change that could be felt by voltage-gated Ca^{2+} channels in the cone terminal. Thus, an outward current from HCs would cause an extracellular depolarization. Such depolarization would reflect in an intracellular hyperpolarization at cone terminal level, causing almost instantaneous inhibition feedback ($\simeq 35$ ms) (Fig. 2.4, centre).

HCs mediated lateral inhibition could be a mixture of all these three mechanisms as well as only one. Someone believes that GABA acts only indirectly within the PR's synapse (Chapot, Euler, and Schubert, 2017). Ephaptic transmission might contribute as a fast component, while protons mediate a slower component (Vroman et al., 2014). Alternatively, ephaptic and proton feedback might contribute differently depending on light stimulation conditions (Kemmler et al., 2014).

2.1.3 Bipolar Cells as first differentiators of retinal output

Bipolar Cells (BCs) are placed in the INL, they synapse with the PRs' terminals in the OPL, process and pass the signal in the IPL to RGCs.
BCs are divided into cone-bipolar cells and rod-bipolar cells, according to which kind of PR's terminal they bind (Fig. 2.5). They exist in ON and OFF versions, their RF has a center-surround architecture (see 2.2.1), and they exist in transient and sustained types. In addition, BCs exist in several subtypes, which mark the beginning of differentiation of retinal output into several parallel pathways.

Cones bipolar cells

Cone-bipolar cells could be divided into two major subgroups: ON-BCs and OFF-BCs.
The OFF-BCs channels express AMPA and kainate type receptor, cation channels opened by glutamate. It means that in presence of a bright stimulus OFF-BCs hyperpolarize just as the PRs; these channels are called "sign conserving". The ON-BCs, vice versa, depolarize in presence of a bright stimulus because they express the metabotropic receptor mGluR6 that, if bound with glutamate, causes the closing of the cation channel TRPM1. The ON pathway
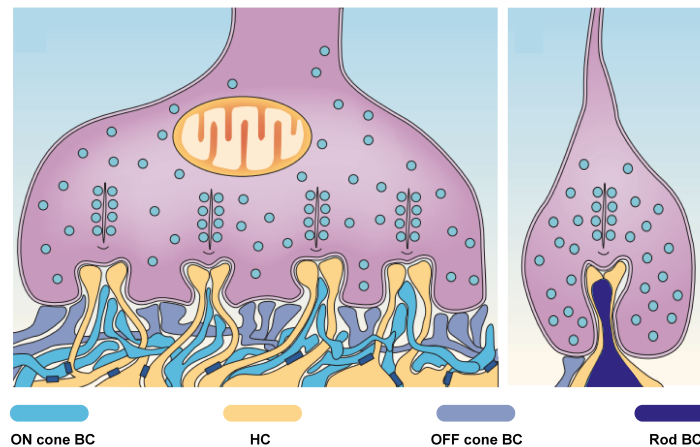
FIGURE 2.5: **Schematic of cone and rod terminals in the mammalian retina**. **Left**| Cone pedicle, the synaptic terminal of cones. Four presynaptic ribbons host HCs and ON cone bipolar cells dendrites. OFF cone bipolar cells' dendrites connect at the base of the cone pedicle. **Right**| Rod spherule, the synaptic terminal of rods. The only one presynaptic ribbon hosts HCs and rod bipolar cells dendrites. OFF cone bipolar cells' dendrites form contacts at the base. (Adapted from Wässle (2004))

channels are so-called "sign inverting".

BCs, depending on the temporal evolution of their response, can be divided into transient BCs (i.e., expressing rapid inactivating glutamate receptors) or sustained BCs (i.e., expressing slow inactivating glutamate receptors).

Cone-BCs synapse RGCs in the IPL through a really complex synaptic terminal. This synaptic terminal not only involves the cone-BCs but also ACs which, in turn, synapse to BCs and RGCs (Fig. 2.6, left). This makes the BC as much an integrating system that links even different parts of the outer and the inner retina.

Rods bipolar cells

Rods-bipolar cells are depolarized by bright stimuli, as such they are ON-BCs. Although they all terminate deeper in the IPL, near to the RGCs layer, they are not directly engaged in a synaptic connection with RGCs. They fit into cones' processing pathway via a particular interneuron (i.e., AII amacrine cells) to indirectly influence RGCs (Fig. 2.6, right). AII ACs form excitatory synapses with rods-BCs, thus they are depolarized by light. They form excitatory gap junctions with ON cone-BCs and inhibitory chemical synapses onto OFF cone-BCs terminal.

2.1.4 Amacrine cells: the most diverse and least known, but essential, cells of the retina

Amacrine cells (ACs) are the most diverse class in the retina: over 60 types of ACs have been found in mice so far (Yan et al., 2020). ACs are also the less well-understood retina's cells, although they are assigned many of the tasks related to signal shaping in the IPL. ACs play almost the same interstitial role as HCs in the OPL but carried out in the IPL.

Amacrine cells classification and functional roles

The major distinction in ACs' population wants them to be divided into narrow field ACs (**NACs**) and wide field ACs (**WACs**).

NACs (usually glycinergic) are involved in local calculations and work as shapers of BC and RGC signals. WACs (GABA-ergic), by opposition, transmit remote inhibition to RGCs. 16
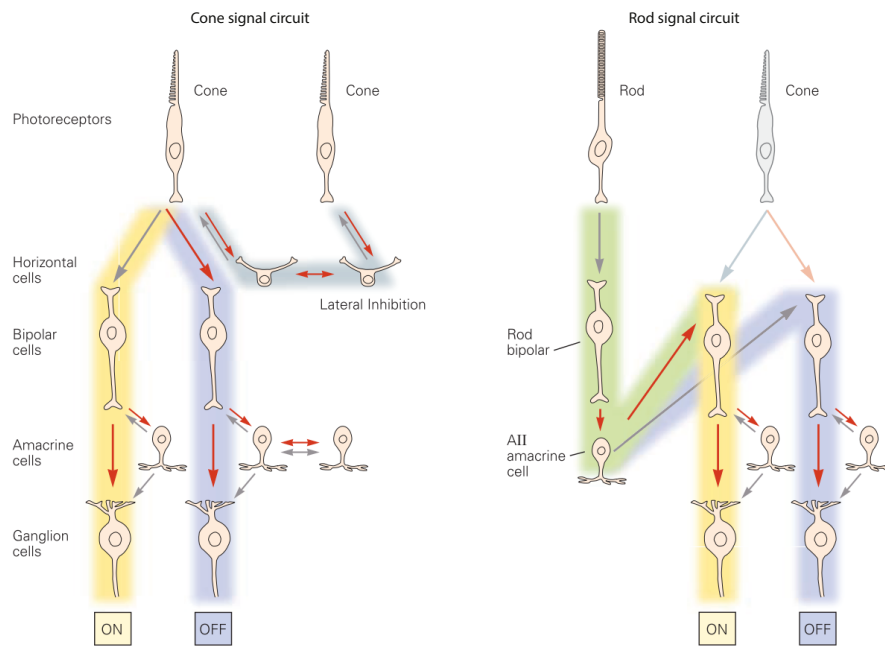
FIGURE 2.6: **Differences in cones' and rods' downstream circuitry**. **Left**| The cone signal circuit embeds both the split into ON and OFF pathways and the pathway for lateral inhibition in the outer layer. *Red arrows* stand for sign-conserving connections, *grey arrows* stand for sign inverting ones. **Right**| The rod signal circuit has neither the split nor the lateral inhibition pathway. The only rod-bipolar cell responds to bright contrast changes, thus it is an ON bipolar cell. Rods' signals reverse into cones' circuits via AII amacrine cells. (Reproduced from Kandel, E. R, Schwartz, J.H, & Jessel (2013)).

types of WACs have been documented so far (Bin Lin and Richard H. Masland, Lin, and Masland, 2008), their subclassification is hard since they spread very sparsely in the whole retina ($\simeq 10 - 20 cells/mm^2$).

The presumed roles of ACs are various, among the most important ones: *(i)* temporal shaping of RGC responses usually carried out by NACs; *(ii)* Inhibition related to global movements of the background, carried out by WACs.

The actions of different types of ACs, together with the differentiation of pathways introduced by BCs, make the further network of RGC (in the INL) so diversified in responses.

2.1.5   Retinal Ganglion Cells: the retinal output

Retinal ganglion cells (RGCs) receive signals from BCs and ACs. They represent the retinal output and they send a frequency modulated spike train (i.e., firing rate, **FR**) to the brain. RGCs are the only cells with a well-defined axon, all the RGCs' axons form the optic nerve, the gateway to the CNS.

The total number of RGCs covers only 1% of the cells in the ONL. The RGCs, however, need to take in all the information from the upstream layer, which requires a great deal of processing within the retina. It is as if the inner layers of the retina are working as feature extractors in order to bring an optimized version of what has been detected upstream, to the brain.

Retinal ganglion cells classification

More than 30 types of RGCs have been reported in mice (Baden et al., 2016) and they spread throughout the whole retina: each point of the retina is covered by the receptive field of at least one RGC.

The very first functional classification of RGCs is between ON and OFF RGCs. This splitting

comes from the previous BCs division: ON cone-BCs, and ON rod-BCs contact, directly and indirectly respectively, ON-RGCs with excitatory synapses. OFF cone-BCs and ON rod-BCs (inverted in sign via AII ACs) contact OFF-RGCs.

In presence of bright stimuli, ON-RGCs increase their FR and OFF-RGCs decrease it, vice-versa in presence of a dark stimulus OFF-RGCs increase their FR while ON-RGCs lower it. This splitting mechanism alone is a time optimization method: what if only one of these two types of retinal ganglion cells existed?

Imagine that ON-RGCs fire at 10 $spikes/s$ in their steady-state and in presence of a bright stimulus they increase the FR by a factor of 10. If a bright step is provided upstream they would fire at 100 $spikes/s$ and the CNS would be able to detect this change in 10ms. If, instead of a bright step, a dark step is provided, the decrease of the FR could be detected by the CNS much slower.

The ON-OFF splitting at both the BCs' level and RGCs' one is, therefore, necessary to rapidly detect changes in the visual scene.

Among the RGCs types that are differentiated by their response to bright or dark stimuli, there are also the ON-OFF RGCs that respond indifferently to both positive and negative contrast changes.

RGCs are also classified according to the temporal evolution of their response. As transient and sustained BCs exist, both ON and OFF-RGCs are also divided into these two classes. In addition, RGCs are subject to temporal shaping by ACs which, directly or indirectly (i.e., via BCs), influence the time course of the RGCs responses.

Transient RGCs can rapidly communicate changes in the visual scene to the CNS. Their response is typically fast, and they resting firing rate is quickly restored after the detection of stimulus changes. Conversely, sustained RGCs have a less sharp temporal evolution that better follows stimulus timing.

The temporal sharpening of the RGCs responses bypasses one of the possible time resolution problems of PRs. In fact, PRs are quite slow in responding to the stimulus (e.g., it takes 40ms for cones to reach the peak of the response), too slow to guarantee a proper visual readout. The given increase of the temporal sharpness of the response allows RGCs to accurately detect signal changes in the whole visual scene.

Other RGCs types   Other different functional classifications have been proposed to cluster RGCs types. One of them has been found in brisk transient RGCs (ON and OFF polarities). These are known as the cells with the shortest latency, the largest cell body, and the fastest axons among all RGCs. It has been proposed that their fast transmission might serve the purpose of "switch" for visual attention (Wässle, 2004). Sluggish RGCs, in contrast, display a more delayed response to stimuli.

Evidence of colour-coding RGCs have been found as well. The clearest example is given by the blue-ON pathway that exclusively connects blue-cone, blue ON cone-BCs and finally blue ON-RGCs (Chang, Breuninger, and Euler, 2013).

Interestingly, a subtype of RGCs deals with the very complex task of motion extrapolation. *Texture motion* RGCs (Fig. 2.7, top) respond to moving textures regardless of the direction of the spatial pattern (Turner, Schwartz, and Rieke, 2018). They can detect fine grating shifts shown in the receptive field even if the average light level remains constant, this is achieved by the fact that RGCs only accept BCs' depolarizations instead of both depolarizations and hyperpolarizations.

Object-motion-sensitive RGCs (OMS) (Fig. 2.7, centre), differently from texture motion RGCs, specifically detect the differential motion in a visual scene (Chen, Liu, and Tian, 2014). These cells only fire when a local patch that falls onto the receptive field moves differently as compared to the background. They remain silent if the patch moves together with the background. It has been found that this particular detection is due to the presence of polyaxonal
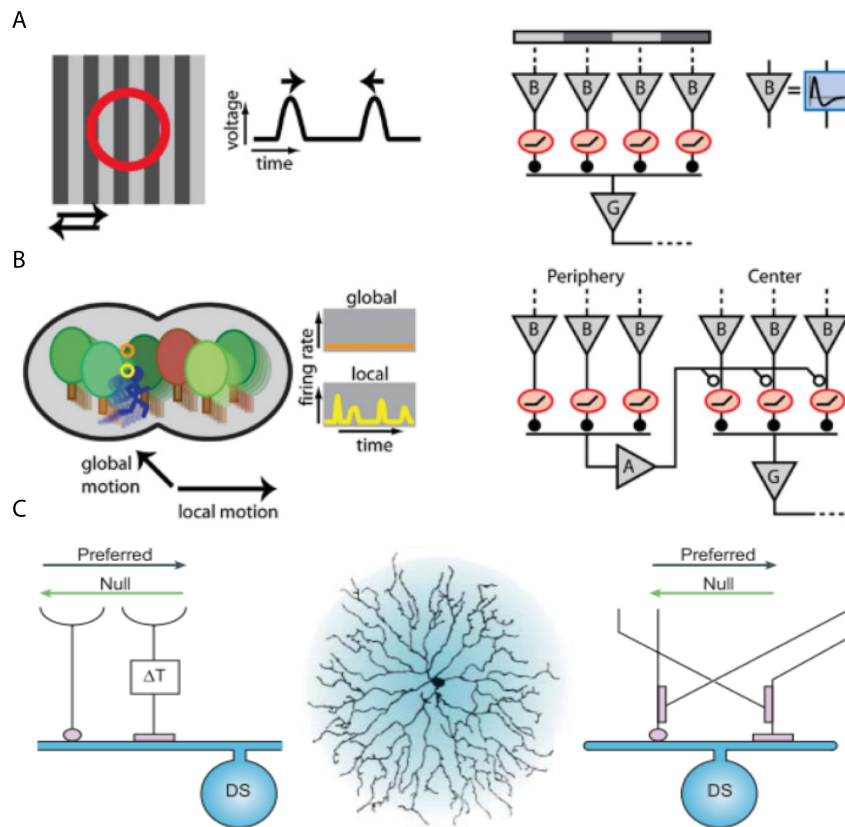
FIGURE 2.7: **Functional types of RGCs**. **a**| Modelling of RGCs sensitive to texture motion (Hochstein and Shapley, 1976). *Left:* RGC shows activation when a fine grating shifts in either direction over the receptive field. *Right:* the presented grating excites some bipolar cells and inhibits the others. Only the depolarized BCs communicate to the ganglion cell downstream which fires transiently on every shift. (Reproduced from Gollisch and Meister (2010)). **b**| Modelling of RGCs sensitive to differential motion (Ölveczky, Baccus, and Meister, 2003). *Left:* Object-motion-selective RGCs remain silent under global motion, they fire if a patch of the image moves differently from the background. *Right:* receptive field periphery and receptive field center communicate via inhibition from amacrine cells . If the motion in the periphery and in the center is synchronous the firing is suppressed. If the motion is not synchronous then RGCs in the receptive field center fire. (Reproduced from Gollisch and Meister (2010)). **c**| Direction selective RGC modelling (Barlow and Levick, 1965). *Left:* The DS cell receives an excitatory input and a delayed inhibitory input from two neighbouring image locations. The cell responds to movement of a stimulus only in the preferred direction and not in the null direction. *Right:* more recent model of DS RGC (S.I. Fried; T.A. Muench; F.S. Werblin, 2004). The cell receives excitatory input from the preferred side and inhibitory input from the null side. The excitatory input from the preferred side also receive presynaptic inhibition from the null side.The null side, vice-versa, receives presynaptic excitation from the preferred side. (Reproduced from Wässle (2004)).

ACs in the near surround of the RF (Baccus et al., 2008): if both in this zone and in the RF the same motion falls, then the interneurons (i.e., ACs) inhibit the center making it silent. If vice-versa only a patch in the RF moves on a static background, the near surround will not be able to detect any kind of motion so that the interneurons will not be able to drive any inhibitory signal to the central RF, letting it fire.

Direction-selective ON-RGCs (Fig. 2.7, bottom) and direction-selective ON-OFF RGCs (oDS-GCs, ooDSGCs) report movement in their preferred direction dependently (oDSGCs) or independentely (ooDSGCs) of the sign of contrast of the patch object with respect to the background (Sun et al., 2006; Weng, Sun, and He, 2005).

2.2 Receptive field center-surround architecture

The receptive field (RF) of a cell is the area in the visual space which more likely influences the neuron's firing rate.

The RFs of most RGCs exhibit a characteristic center-surround architecture, such property was found for the first time in mammalian retinas in the 50's (Kuffler, 1953).

If a small spot, brighter or darker than the ambient illumination, is shown to the RF of a RGC it causes different reactions depending on the precise location of the spot (Fig. 2.8). If the spot is of the same polarity of the RGC it might:

- increase RGC's FR if located in the very center of the RF.

- inhibits RGC's FR if located at the surround of the RF (i.e., surround antagonism).

By opposition, if the spot is of the opposite polarity of the RGC it might:

- inhibits RGC's FR if located in the very center of the RF.

- increase RGC's FR if located at the surround of the RF (i.e., surround activation).

The most important functional consequence of the RF center-surround architecture is the capability of RGCs to detect strong spatial contrast, such as object edges.

2.2.1 The origins of the center-surround mechanisms

BCs already have their RFs organized in a center-surround manner (Dacey et al., 2000) and as such, they are subject to both center-surround antagonism and surround-activation.

The biological origin of the whole center-surround mechanism has not yet been fully understood. Certainly, part of its source resides in the OPL and it is mediated by HCs. However, another part of the origin of the center-surround mechanism may reside in deeper layers, where lateral networks of interneurons have considerable extent (i.e., ACs).

The center-surround mechanism's origins in the OPL are attributed to synaptic opposition between PRs and HCs at the level of the synaptic connection with BCs (i.e., at the cone pedicle). HCs and their network play a fundamental role in the center-surround mechanism due to both inhibitory feedback onto cone terminals and feedforward transmission to BCs. In feedforward transmission to BCs, HCs would release GABA to BCs terminals (expressing $GABA_A$ receptors) causing inhibition for OFF-BCs and excitation for ON-BCs (Thoreson and Mangel, 2012). ON and OFF $GABA_A$ receptors' activation depends on the chloride potential in the synaptic cleft, such receptors use different chloride transporters though. Thus, the chloride efflux leads to opposite BCs reactions (ON-BCs depolarize, OFF-BCs hyperpolarize).

The hypothesised origins of the center-surround's mechanism in the IPL are attributed to the shaping effects of ACs on BCs and RGs. Several ACs give rise to a network in the IPL that covers a remarkable area. The presence of a spatial network of ACs could naturally provide BCs with an extended surround, expanding the origins of center-surround mechanisms to also the IPL.
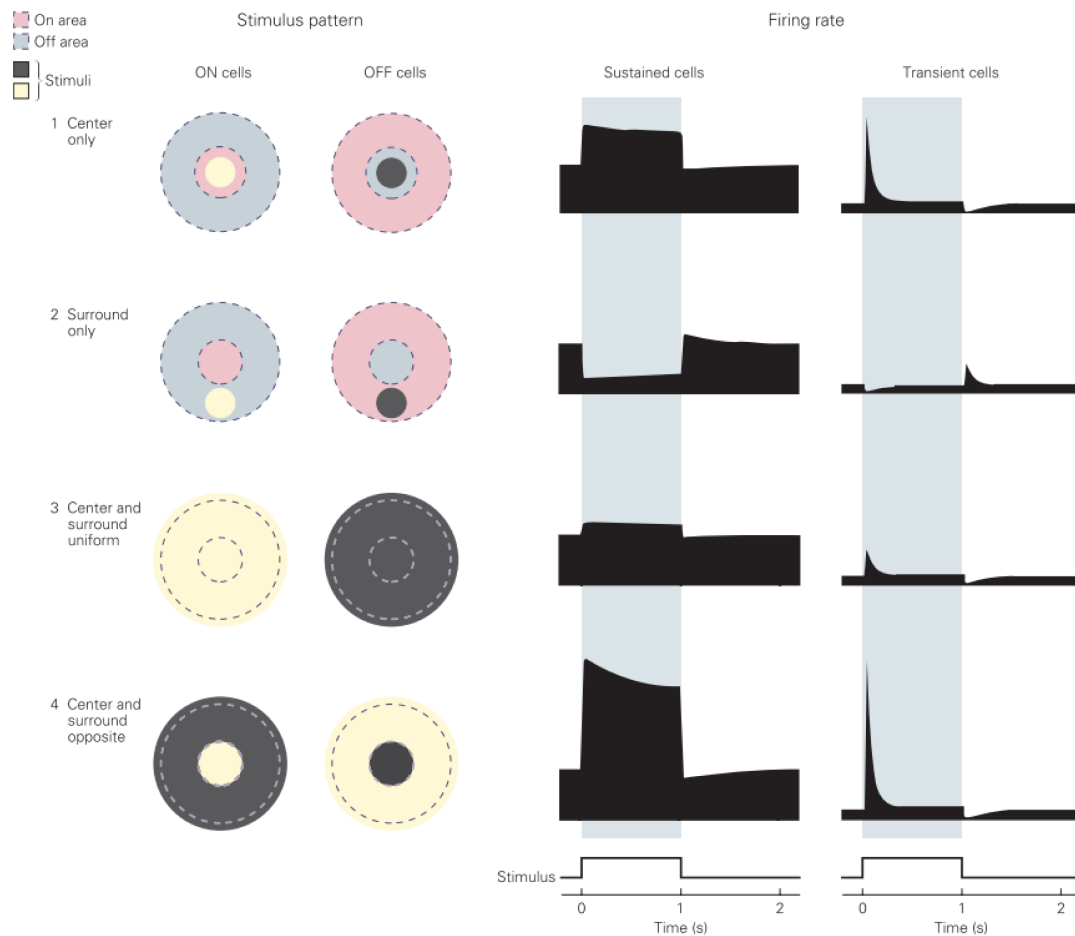
FIGURE 2.8: **RGCs center-surround antagonism**. The stimulus changes from a uniform gray field to the pattern of bright (*yellow*) and dark (*black*) regions indicated on the *left*. The dashed internal circle indicates the RF center while the dashed external one the RF surround. **1-2**| If the same stimulus that excites the RF center is applied to the RF surround, the firing is suppressed. **3**| Full field stimulation elicits a response like that of **1**, but much smaller in amplitude. **4**| Stimulation of the RF center combined with the opposite stimulus' polarity in the RF surround produces the strongest response. (Reproduced from Kandel, E. R, Schwartz, J.H, & Jessel (2013)).

Chapter 3

Saccadic suppression: a tool for visual stability

As was previously mentioned in Chapter 2 (2.1.1), PRs' signal evolution, and especially all the signals downstream, do not stay active for all the stimulation time. Cones and rods restore their steady-state voltage if the stimulation lasts too long and is constant. It means that if we fixate a particular image in front of us it will disappear as soon as the PRs reset their steady-state value. We know from experience that this vanishing does not happen, the visual perception of all our surroundings appears continuous and coherent. Therefore, how can we refresh PRs' attention and ensure proper visual function?

3.1   Saccadic movements

Every second or every half a second our eyes, even if we try to maintain the gaze fixed, produce movements that divert the gaze from the fixed object, these movements are called saccades. Saccades thus allow the visual system to restore the visual function avoiding the PRs to reset their steady state. This mechanism avoids the fixed image on the gaze to suddenly disappear.

The presence of saccadic eye movements is now well established: the gaze is diverted for a certain period ($\simeq 40ms$) to be then focused again on the previous object in the visual scene or a new one to which we want to focus attention.

Saccadic eye movements are not the only type of eye movements. In the literature proofs of other movements could be found. The others are called *drifts*, and, unlike saccadic movements, they are slower and happen between saccades or at any time when other eye movements are not happening. Even if they have been long considered random movements, recently, evidence has been found about their possible functions (Malevich, Buonocore, and Hafed, 2020).

Although in humans the image on the fovea shifts with each saccade, we perceive a stable visual world. We do not even notice the sudden visual scene change, neither a supposed blurred image in between the two fixations. Where does all the information detected in this period end? Is it even detected? These questions have interested many scientists[1].

3.2   Saccadic suppression

Brief peri-saccadic stimuli's perception has proved to be reduced in a multitude of studies[2]. It is well established that saccadic eye movements produce a temporal window of suppression in visual sensitivity[3], what is controversial is how they can bring to such an effect and

---

[1]Thiele et al., 2002; Wurtz, Joiner, and Berman, 2011.

[2]Ross, Burr, and Morrone, 1996; Burr, Morrone, and Ross, 1994.

[3]Bremmer et al., 2009; Idrees et al., 2020b; Idrees et al., 2020a; Binda and Morrone, 2018.

by whom this effect is led.

This suppression mechanism is known as *saccadic suppression* and it depends on the presented stimulus. There is evidence that, if high-frequency gratings are used as stimuli, less saccadic induced suppression would arise. On the contrary, with low-frequency gratings, stimuli's detection after saccades onset is more impaired (Wurtz, 2008).

3.2.1   The controversial origins of saccadic suppression

Although saccadic eye movements are well described as perceptual phenomena, what has still to be discovered is their real underlying mechanism. There are two main currents of thoughts regarding the origin of saccadic movements and the related onset of saccadic suppression. A first hypothesis wants extraretinal mechanisms as the basis of saccadic suppression (i.e., extraretinal saccadic suppression, **ESS**). A second hypothesis considers the possibility that saccadic suppression originates at the retinal level modulating RGCs' activity (i.e., retinal saccadic suppression, **RSS**).

Retinal mechanisms of suppression do not deny the existence of extraretinal mechanisms too in saccadic suppression (Wurtz, 2008) . It is likely that the visual-only function has a role in visual stability. Retinal mechanisms of suppression could help, or even only ease, the downstream processing done at the extraretinal level.

Extraretinal saccadic suppression

For the "extraretinal hypothesis", the CNS is responsible for saccadic suppression. Three main extraretinal mechanisms could explain visual stability together with saccadic suppression:

1. *Corollary discharge* | The perceptual suppression, could result from intrinsic knowledge of planned eye movements. This mechanism, known as corollary discharge, could be mediated by signals that come from (pre-)motor areas (Wurtz, 2008). Corollary discharge, also known as efference copy, is intended as a copy of the signal that the system sends to the parietal cortex to make it aware of the forthcoming saccade.

2. *Visual masking* | For the visual masking hypothesis, the produced image between the two fixation times has to be seen as a blurred image, in contrast with the sharpened images of both the fixations (Binda and Morrone, 2018). The blurred, low-contrast image produced in between is then masked by the high-contrast ones before and after the saccade. This hypothesis is supported by evidence about the potential detection of blurred images between the two fixations (Wurtz, 2008).

3. *Proprioception* | Proprioceptors feedback onto CNS (Wurtz, 2008) . However, it is unlikely that proprioceptors signals sent by the eye muscles suppress vision as properly as corollary discharge for example. This is due to timing issues: saccadic suppression arises even before the real onset of the saccade; proprioceptors have the machinery to act 100 or more milliseconds after the onset of the saccade.

ESS: how to deal with it experimentally   Extraretinal saccadic suppression (ESS) is usually studied via psychophysical experiments (Binda and Morrone, 2018).

A saccadic movement is induced in the subject. The presented image suddenly changes in a specific location recalling the subject attention, for example. A probe flash (i.e., light spot) is then presented to the subject after the onset of the induced saccade in another specific location of the screen.

Varying the relative timing between saccade and flash onsets the subject is more or less

capable to rightly localize the flash on the screen. For farther times of flash from saccade onset, subjects are more capable to correctly pinpoint the flash, while for shorter times of flash from saccade onset they can't fairly locate it. From now on we will refer as the time of flash from saccade onset as a variable, named Δt_{flash}.
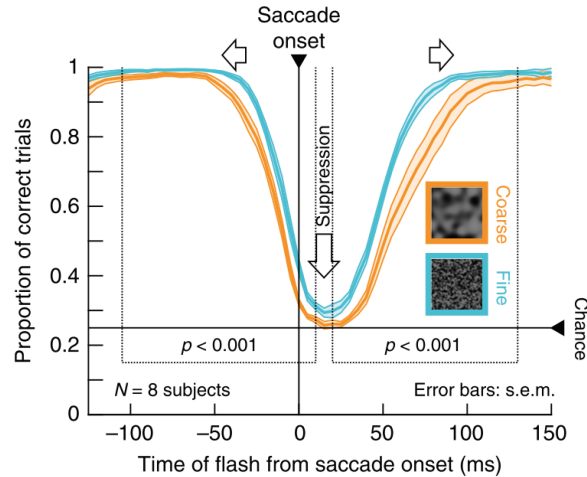
FIGURE 3.1: **Extraretinal saccadic suppression depends on the content shown**. Summary of psychophysical experiments to evaluate the timing and power of saccadic suppression. *X-axes*: time of the presented spot from the onset of the induced saccade. *Y-axes*: percentage of correct trials in rightly identifying the position of the spot after the saccade. Saccades were induced using both background coarse textures and fine textures. Perceptual saccadic suppression started earlier and lasted longer with presented coarse background textures. (Reproduced from Idrees et al. (2020a))

Flash detection capacity also depends, as previously mentioned, on the content of the image presented to the subjects. Idrees et al. (2020a) proved it showing the subjects two different types of textures as background of the "inducing-saccades" stimuli. The first background shown was a fine texture, whose blobs' dimensions were comparable with BCs receptive field's size, while the second was a coarse texture, whose blobs' dimensions were analogous to RGCs RF's size.
In the absence of induced saccades, probe flashes were rightly detected both with the fine and coarse texture background. Nevertheless, if the saccade was induced, saccadic suppression came into play and detection's impairing was different from coarse to fine texture backgrounds.
Coarse texture in the background produced larger suppression peaks and longer periods of suppression if compared to responses using fine textures as background (Fig. 3.1).

Retinal saccadic suppression

For the "retinal hypothesis" (i.e., retinal saccadic suppression, RSS) perceptual saccadic suppression could be the result of the visual consequences of retinal image shifts (García-Pérez and Peli, 2011, Castet et al., 2001). In this hypothesis, all the saccadic suppression, or only a part of it, relies on visual-only mechanisms.

Retinal saccadic suppression: evidence of existence   Idrees et al. (2020a) used the same paradigm described above to verify that perceptual saccadic suppression originates in the retina. They used both mouse and pig isolated retinas and designed the same fine and coarse textures with blobs dimensions analogous to BCs and RGCs RFs size of both the species.
Since the retina pieces were fixed and could not make real saccades, they had to externally induce an effect similar to a saccade. This was done introducing *saccade-like* stimuli. The saccade was externally induced presenting a moving texture to the fixed tissue (Fig. 3.2, a),

a probe flash was then shown at different time delays from the texture displacement. Using the same paradigm, they then changed the protocol replacing texture displacements with texture jumps (Fig. 3.2, b) or even structure free luminance steps (Fig. 3.2, c).
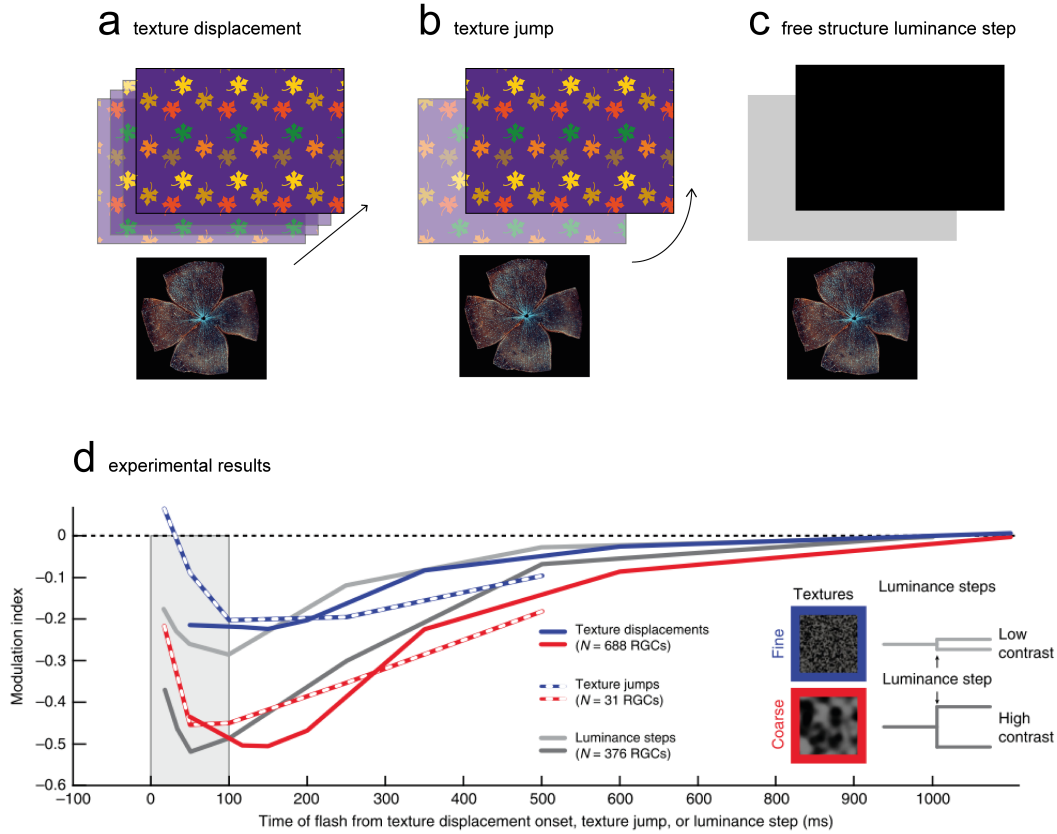
FIGURE 3.2: **Different approaches to externally induce saccadic movements' like effects**. In fixed retinas, saccadic movements' effects have to be externally driven. They could be recreated presenting saccade-like stimuli: a texture that shifts(**a**) or jumps(**b**) from one position to another, for example. Alternatively, the same effects could be recreated presenting to the tissue simple changes in contrast(**c**). **d**| Proofs that the three approaches lead to similar effects in the suppression's profiles. Coarse texture displacements, coarse texture jumps and high-contrast luminance steps lead to similar effects, as well as fine texture displacements, fine texture jumps and low-contrast luminance steps. (Adapted from Idrees et al. (2020a))

RGCs responses were then measured using multi-electrode array (MEA) and the amount of suppression at different times of flash from saccade onset was calculated via the introduction of a suppression index: the modulation index (**MI**, see B.4 for more details) (Fig. 3.2, d). The only change in background luminance (i.e., structure free luminance steps' protocol) has the same suppression effect of texture displacements in RGCs responses. Specifically, high contrast steps reflect coarse texture displacements while low contrast steps reflect fine texture ones. It is as if larger coarse texture blobs result in high contrast changes in individual receptive fields. Smaller fine texture blobs result in some sort of luminance averaging within the same RF, yielding small changes in contrast.

To prove that RGCs responses suppression did not depend on the saturation induced by simulated saccades themselves, they looked at cells that did not respond to simulated saccades at all. Their flash induced responses were still suppressed.

Different stimulus interactions were studied, such as the presentation of the flash before the simulated saccade instead of after it. The response to the saccade-like stimulus was subjected to suppression induced by the presence of a flash before. This reveals that more stimulus-stimulus interaction could lead to RSS.

Retinal saccadic suppression originates in different areas of the receptive field It is now clear that at least a part of perceptual saccadic suppression is carried out by the retina, what remains unclear is what mechanisms give birth to retinal saccadic suppression (RSS).

Idrees et al. (2020b) went deeper into the analysis of the underlying mechanism that could cause RSS. They managed to highlight how RSS acts differently on ON-RGCs and OFF-RGCs. In addition, using different protocols and pharmacology, they distinguished different spatial origins of RSS. They found three different components of retinal saccadic suppression:

1. The global component of suppression (**GCS**): it acts from the periphery of the RF center of the RGC.

2. The central local component of suppression (**CCS**): it acts from the very center of the RF of the RGC.

3. The Surround local component of suppression (**SCS**): it acts from the near surround of the RF of the RGC.

The global component of suppression To investigate if some mechanisms involved in saccadic suppression originate in the periphery of the receptive field, Idrees et al. (2020b) designed a protocol that would allow observing the suppression of RGC responses under the influence of only the global component of suppression.

A constant grey mask ($[1000x1000]$ μm) was overlapped to the usual texture displacement's stimulus. Texture displacements (i.e., saccades) were shown only beyond the borders of the mask, while probe flashes were presented in the whole area. The MI profiles of RGCs in the "flash-only" regions were considered to investigate the influence of the peripheral regions in which the saccade was shown.

They found asymmetries between suppression of ON and OFF RGCs responses. OFF-RGCs seem not to be affected by the "peripheral-only" saccade. Conversely, "peripheral-only" MI profiles of ON-RGCs change (i.e., change in timing and strength of suppression) if compared to the full-field saccade stimulus (Fig. 3.3, b), as such ON-RGCs are targeted by the GCS. The GCS has a specific action timing ($\Delta t_{flash} \simeq 100 - 400ms$), it recovers earlier than the combination of all the components together (i.e., full field condition).

Who is responsible for the global component of suppression and acts from the periphery of the RF? It is most likely that wide field amacrine cells give origin to this effect: treating ex vivo retinas with *SR-95531*, a GABA$_A$ receptor antagonist, the MI profile flattens at zero (Fig. 3.3, b *top*). WACs earned the role of global suppressors in retinal saccadic suppression. Nonetheless, using almost the same pharmacology (*SR-95531* and *Picrotoxin* $100\mu m$, two GABA$_A$ receptors antagonists) but presenting to the cells both the saccade and the flash, the strength of suppression does not change much (3.3, c). The GCS has thus a low influence on the whole amount of suppression.

Central and Surround components of suppression. To explore the possibility that a portion of retinal saccadic suppression originated in either the RF center (CCS) or RF surround (SCS) Idrees et al. (2020b) designed a new stimulation protocol.

The new stimulation protocol was aimed at detaching the CCS and the SCS: a grid was used. Each square of the grid could receive as stimulus either the saccade or the flash and, in between each square, 100 μm gaps with mean overall luminance were presented (Fig. 3.4, a). Once again, the RGCs activity from the "flash-only" region was studied.
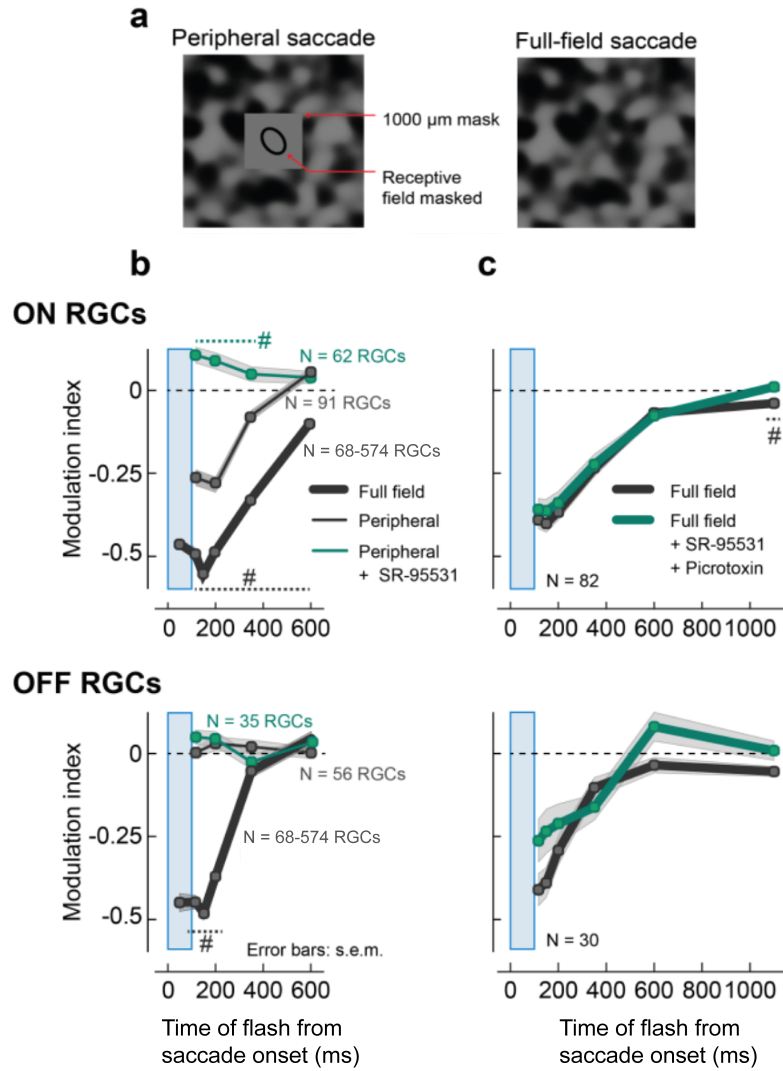
FIGURE 3.3: **The global component of suppression.** **a** | Visual stimulation paradigm used to probe the global component of suppression. Saccade-like stimuli were presented either full field (*right*) or only in the periphery (*left*) of the RGCs' RF using a 1000x1000 μm^2 grey mask. Probe flashes were presented in both the two regions. **b** | MI's populations (*mean* $\pm$ *s.e.m*) of ON-RGCs (*top*) and OFF-RGCs (*bottom*) for full field and peripheral only saccades. Responses to peripheral only saccades were studied also adding pharmacology (GABA$_A$ receptor blocker - 5μm SR95531). The *blue window* indicates the timing of the saccade. Probe flashes were presented at 50 and 150 (only for full-field saccade), 117, 200, 350, 600 and 2100 ms after the saccade onset. The coarse background texture had 300μm spatial scale. **c** | MI's populations (*mean* $\pm$ *s.e.m*) of ON-RGCs (*top*) and OFF-RGCs (*bottom*) for full field saccades. Pharmacological agents (5μm SR95531 + 100μm Picrotoxin) were added for the test condition. The *blue window* indicates the timing of the saccade. Probe flashes were presented at 117 ms, 150, 200, 350, 600, 1100 697 and 2100ms (baseline) after saccade onset. The coarse background texture had 150μm spatial scale. (Reproduced from Idrees et al. (2020b))

The lack of suppression in OFF-RGCs in the "surround-only" saccade case confirms what mentioned in the section above: they are affected by only very local mechanisms of suppression (i.e., central component of suppression) (Fig. 3.4, c).

The MI profile of ON-RGCs changes for earlier Δt_{flash} ($\simeq 100 - 150ms$), if the presented saccade was either full field or surround-only (Fig. 3.4, b). In the surround-only saccade case the MI profile shows persistent suppression for later Δt_{flash}.

One could think that the missing suppression (in the surround-only saccade case) for earlier Δt_{flash} was due to the lack of the GCS. But most likely WACs do not cause the later suppression since the GCS is supposed to recover faster ($\simeq 400ms$ after the onset of the saccade) than what is shown in Fig. 3.4, b.

Thus, the decreased suppression for earlier Δt_{flash} does not have its origin in the GCS. There
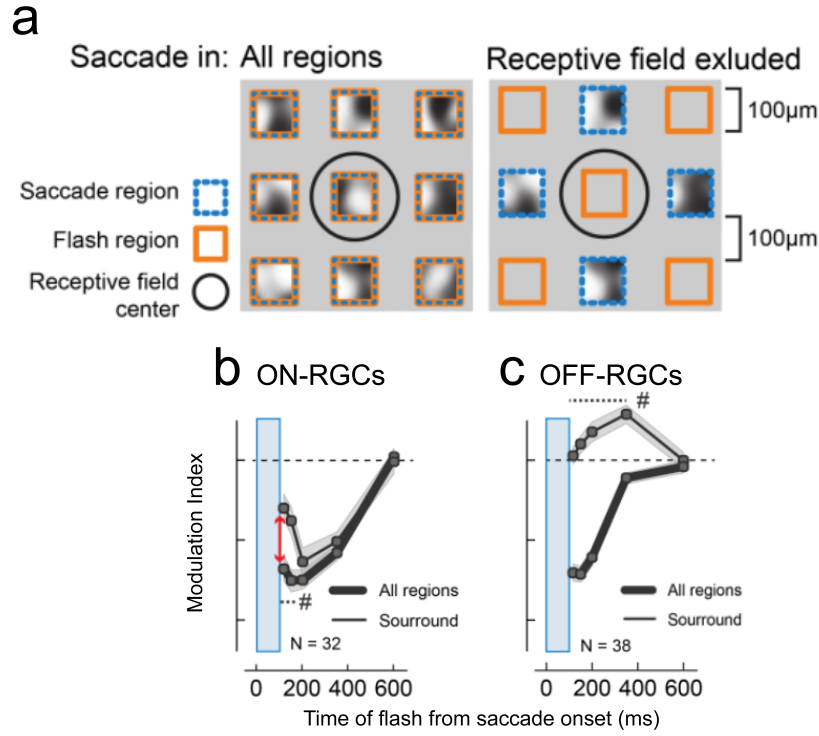
FIGURE 3.4: **Central and surround components of suppression**. **a** | Visual stimulation paradigm used to probe the central and surround components of suppression. Saccades and flashes were presented in $100x100\ \mu m^2$ square regions, separated by $100\mu m$ gaps with mean overall luminance. *Left*: Saccades and flashes in all regions. *Right*: Saccades and flashes presented in alternate regions. **b** | MI populations (*mean $\pm$ s.e.m*) of ON-RGCs for all regions saccades and flashes and saccades excluded from RGC RF center. The *blue window* indicates the timing of the saccade. *Red arrow* indicates a significant loss in suppression for early flashes (117 and 150 ms). A coarse background texture with $150\ \mu m$ spatial scale was used. **c** | MI populations (*mean $\pm$ s.e.m*) of OFF-RGCs for all regions saccades and flashes and RF excluded saccades. A coarse background texture with $150\ \mu m$ spatial scale was used. (Reproduced from Idrees et al. (2020b))

must be another component of suppression that acts from the very center of the RF: the central component of suppression.

The suppression persistence for later Δt_{flash} is not led by the GCS either. Thus, the lasting suppression must be addressed to another component that acts from beyond the RF center and not as far as the GCS: the surround component of suppression.

RGCs types are more suppressed by saccades of their opposite polarity   Since the CCS should act extremely local, one could hypothesize that the given suppression is due to saturating effects induced by the RGCs saccade induced responses.

To investigate this option RGC responses to luminance-step paradigm and all its possible stimulus' combinations (i.e., *On saccade On flash, On saccade Off flash, Off saccade On flash, Off saccade Off flash*) have been explored (Fig. 3.5).

If it was true that the CCS was mediated by saturating effects, what would be most expected should have been a more pronounced suppression for contrast steps and flashes of the same polarity (i.e., *On saccade On flash, Off saccade Off flash*).

Both ON-RGCs and OFF-RGCs show a greater suppression in the "crossover case" though (i.e., *On saccade Off flash, Off saccade On flash*). RGC types are thus more suppressed by saccades (i.e., steps) of their opposite polarity.

If saturating effects are not the cause of the CCS something else must bring to suppression, and this mechanism should act very locally. The emerging hypothesis (Idrees et al., 2020b)
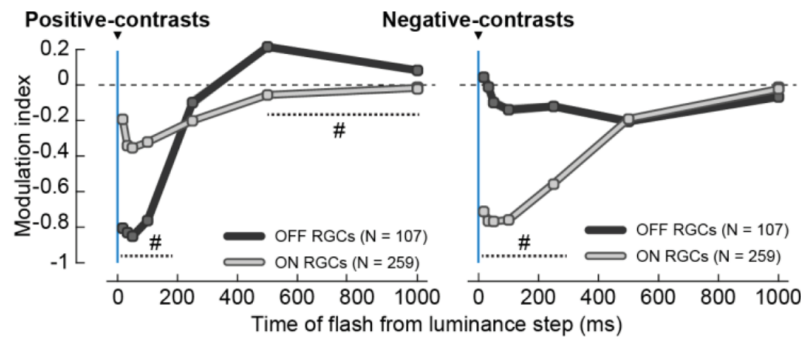
FIGURE 3.5: **Differences in suppression for luminance steps and flashes of same polarity or opposite polarity**. **Left** | MI populations (*mean ± s.e.m*) of ON and OFF RGCs for probe flashes (same polarity of the cell) following positive-contrast luminance steps (*blue line*). **Right** | MI populations (*mean ± s.e.m*) of ON and OFF RGCs for probe flashes (same polarity of the cell) following negative-contrast luminance steps. Probe flashes were presented after 17,33,50,100,250,500,1000 and 2000 ms after the onset of the luminance step. (Reproduced from Idrees et al. (2020b)).

is that the CCS is mediated by the downstream processing pathways of the retina (Section 2.1.3). The presence of a saccade in the RF center could cause imperceptible changes in the evolution of the cone response that are suddenly grasped and magnified by the downstream pathways to be then reflected onto RGCs responses.

3.2.2 Retinal saccadic suppression: certainties and hypotheses

Retinal saccadic suppression is most likely due to three different spatial components of suppression (Fig. 3.6). These three components have different strengths and action timings.

1. The global component of suppression (GCS) is fairly fast ($\simeq 350ms$ recovery) and weak, it acts from the periphery of the RGC receptive field and it does not act on OFF RGCs. Its underlying mechanisms are most likely to be found in the role of GABAergic WACs.

2. The central component of suppression (CCS) is very fast ($\simeq 200ms$ recovery) and strong too, it acts from the very center of the RGC receptive field. Its role is symmetric for what regards ON and OFF RGCs and it is likely due to downstream nonlinear retinal processing.

3. The surround component of suppression (SCS) is very slow ($\simeq 1s$ recovery) and strong, it acts only onto ON RGCs. Its action place goes beyond the very center of the RF, but it does not reach the periphery of the RGC receptive field. It remains unclear where this component comes from. Our hypothesis is that the SCS has its origins in the lateral interconnection of photoreceptors in the OPL mediated by the HCs network.
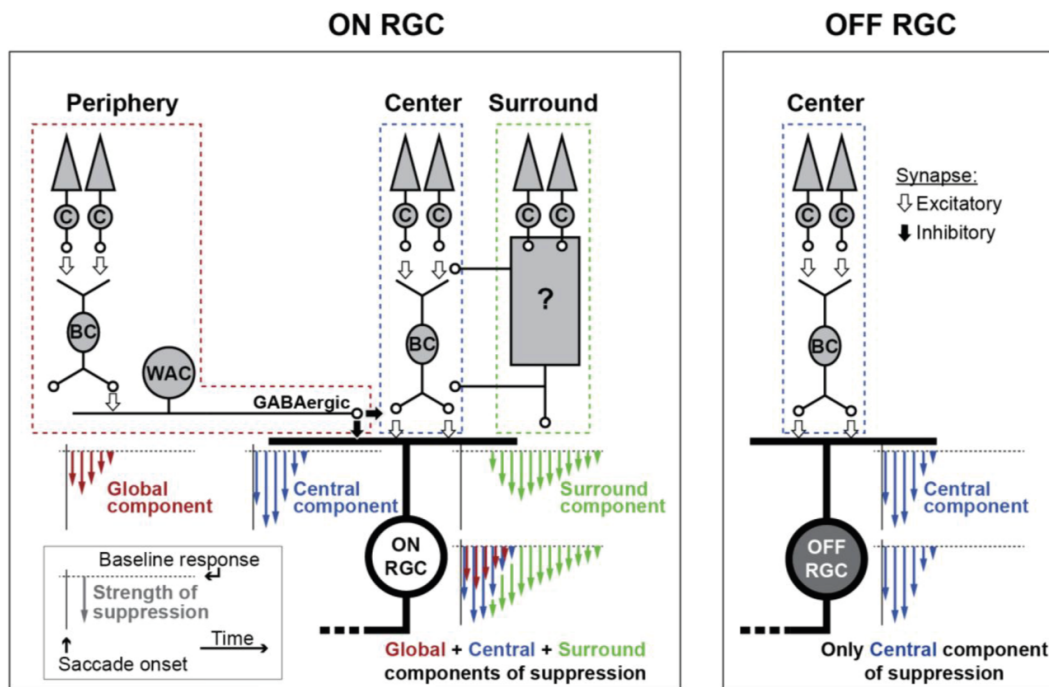
FIGURE 3.6: **The three spatial origins of retinal saccadic suppression**. ON RGCs (**left**) get suppressed by three components of suppression, each of them has its timing and strength. The central component acts from the cell's receptive field center, it is strong and short-lived. The global component acts from the periphery of the cell and is mediated by GABAergic inhibition via wide field amacrine cells. The global component's temporal profile is similar to the one of the central component, the central component is much stronger than the global component though (*blu and red arrows in the schematic*). The surround component of suppression is long-lasting and delayed if compared to the other two (*green arrows*). It might originate from the cell's immediate surround. OFF RGCs (**right**) get suppressed by only the central component of suppression. Length of arrows represent suppression strength; spread of the *arrows* show the temporal profile of suppression.(Reproduced from Idrees et al. (2020b)).

Chapter 4

Retina modelling: a supporting tool

We have seen how much the retina, in its $200\mu m$ thickness, is complex and how it is able to extract essential features from the visual scene. We have also seen how one of the foundations of visual stability, the saccadic suppression, starts already at the retinal level (Idrees et al., 2020a).

But do we really understand every single mechanism that underlies a given cellular behavior, such as those seen in Chapter 2? Are we really sure, for example, about the mechanisms underlying retinal saccadic suppression seen in Chapter 3 (see 3.2.1)?

The interpretation of specific cell behaviors and the hypothesis on the underlying mechanisms is one of the most challenging steps of research. Moreover, by changing the boundary conditions (i.e., stimuli presented, experimental protocols etc.), are we sure that cell behaviors remain consistent with those previously found?

The innumerable facets of experimental protocols make the number of potential cell behaviors exponentially increasing.

4.1 The interpretation of cellular behaviors can be facilitated by predictive models

The interpretation of certain cellular behaviors can be aided by the creation of a descriptive model. A model, moreover, could even predict new cellular behaviors and support the exploration of all those facets of experimental protocols that, in reality, would lead to a very large expenditure of time.

Many models have sharpened the understanding of how single retina's cell types respond and how they contribute to larger neural networks.

Single-compartment models, for example, integrate electrophysiological recordings and biophysical principles to mechanistically understand neuronal properties (i.e., biophysical models). Almost all retinal cell types have been simulated in this way (PRs[1], BCs[2], HCs[3], ACs[4], RGCs[5]).

Mixing more single-compartments models together, using synapse blocks models too, could lead to mechanistically detailed models. These models, however, would be computationally expansive to run.

Many other proposed models[6] are based on deep learning algorithms. They yield excellent performances in reproducing cells' responses to different sets of presented stimuli. In addition, they are not as computationally expensive as biophysical models. Nonetheless, they

---

[1] Kamiyama, Ogura, and Usui, 1996; Kourennyi et al., 2004; Publio, Oliveira, and Roque, 2006.

[2] Usui et al., 1996a.

[3] Aoyama, Kamiyama, and Usui, 2005; Usui et al., 1996b; Shirahata, 2008.

[4] Steffen et al., 2003; Shirahata, 2011.

[5] Fohlmeister and Miller, 1997; Fohlmeister, Coleman, and Miller, 1990; Kameneva, Meffin, and Burkitt, 2011; Guo et al., 2012.

[6] Kim et al., 2020; McIntosh et al., 2016; Tanaka et al., 2019.

are all characterized by a massive number of parameters that make their biological interpretation very hard.

A middle ground between biophysical models and those based on deep learning is represented by block-structured models. These are usually phenomenological models that do not attempt to reconstruct biophysical aspects of real cells, they provide functional characteristics of individual neurons and neural networks. Using a cascade of linear and nonlinear temporal filter elements, block-structured models can recreate retina's neural responses to simple stimuli. Block-structured models have been used to model outer retinal neurons[7] or even the entire retinal network (Wohrer and Kornprobst, 2009).

   We wondered if we could build a model of the retina aimed at recreating retinal saccadic suppression's effects (Chapter 3, 3.2.1) to better interpret them or even show potential new ones.

4.2   The temporal model: a phenomenological model to simulate retinal ganglion cells responses

Among some of the proposed phenomenological models, to interpret and derive predictions about retinal saccadic suppression, we chose to modify and extend an already existing model of the retina. This model has been built by Drinnenberg et al. (2018) to qualitatively describe pharmacologically induced effects on RGCs responses. From now on we will refer to this model as the *temporal model*.

The temporal model can give qualitative predictions of various retina's cell types responses and it consists of three main processing compartments:

   1. The outer retina: it simulates cones' processing of the stimulus and horizontal cells' influence.

   2. The inner retina: it simulates BCs in their various forms.

   3. The RGCs layer: it models different RGC types' responses.

4.2.1   The outer retina

The outer retina block is intended to simulate the response of the cones. The evolution of this response depends on the stimulus presented and on the inhibitory feedback provided by HCs, which is also simulated in the outer retina block.

The simulation of the cones' response due to the external stimulus is inherited from the **DA** model (*Dynamical Adaptation model* by Clark et al. (2013)), the temporal model extends the DA model by including the modelling of the inhibitory feedback from HCs.

The Dynamical Adaptation model

In the DA model the voltage response of the cones to light stimuli is recreated via a differential equation (Eq. 4.1).

$$\tau_c \frac{dc(t)}{dt} = \alpha_c I_y(t) - [1 + \beta_c I_z(t)] c(t) \tag{4.1}$$

where:

   • $c(t) = V_c(t) - V_{c,dark}$, instantaneaus and rest potentials of the cone.

---

[7]Hateren and Snippe, 2007; Hamer et al., 2005.

- $\alpha_c, \beta_c, \tau_c$ constants, with $\alpha_c < 0$ to ensure the response to be negative (i.e., hyperpolarization) if a positive change in luminance is applied.

- $I_y(t), I_z(t)$ filtered version (Eq. 4.2, 4.3) of the incident light $I(t)$.

$$I_y(t) = \int_{-\infty}^{t} K_y(t - t')I(t')dt' \qquad \text{with:} \qquad (4.2)$$

$$K_y(t) = \frac{t^{n_y}}{n_y!\tau_y^{n_y+1}}e^{-\frac{t}{\tau_y}}\theta(t)$$

$$I_y(t) = \int_{-\infty}^{t} K_z(t - t')I(t')dt' \qquad \text{with:} \qquad (4.3)$$

$$K_z(t) = \gamma\frac{t^{n_y}}{n_y!\tau_y^{n_y+1}}e^{-\frac{t}{\tau_y}}\theta(t) + (1 - \gamma)\frac{t^{n_z}}{n_z!\tau_z^{n_z+1}}e^{-\frac{t}{\tau_z}}\theta(t)$$
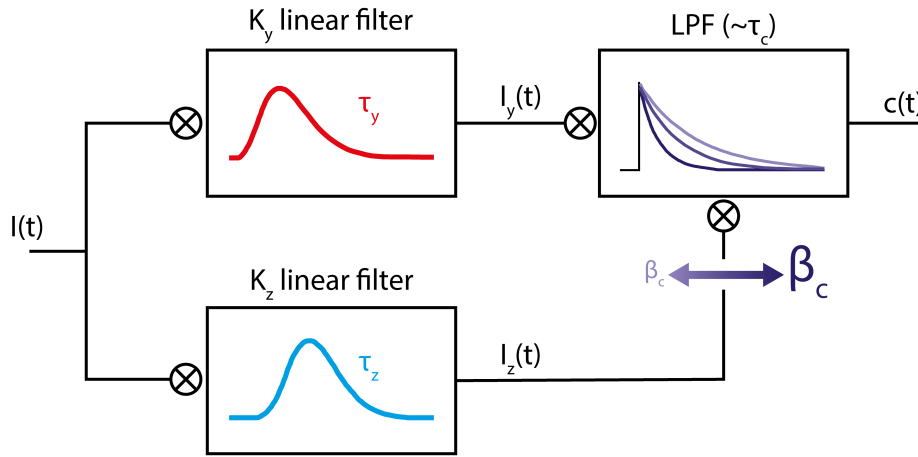
FIGURE 4.1: **Schematic of the Dynamical Adaptation (DA) model.** The stimulus $I(t)$ is convolved with the sharper K_y kernel (*red*) and the broader K_z kernel (*blue*) to produce the signals $I_y(t)$ and $I_z(t)$. The nonlinear term β_c acts on $I_z(t)$ and modulate the shape of the effective kernel (*purple*) resulting from K_y and K_z and τ_c. Smaller β_c (*light purple*) result in smaller gains (related to the area under the purple curve) and smaller time scales (related to the width of the purple curve). (Adapted from Clark et al. (2013)).

In K_y, τ_y specifies the time scale of the linear response, n_y specifies its 'rise' behavior, and θ is the Heaviside function with $\theta(t < 0) = 0$, $\theta(t > 0) = 1$.
K_z is the combination of two different components, the former fast as K_y, indeed has the same time constant τ_y, and the latter slower with a time constant τ_z. The two components are weighted complementarily (γ) to ensure to K_z a unity integral. K_y has unit integral too. The way the two kernels are designed allows having two different temporal filters in terms of timing and broadness: K_y appears sharper (Fig. 4.1, *top left*) and less delayed than K_z (Fig. 4.1, *bottom left*).
The interesting term is β_c: the gain adaptation. While setting $\beta_c = 0$ the output is a linear function of the input, highering it shows its effectiveness in terms of gain and time scale (Fig. 4.1, *top right*).
The output then will depend on the input's recent history (Eq. 4.4):

$$\frac{\tau_c}{1 + \beta_c I_z(t)}\frac{dc(t)}{dt} + c(t) = \frac{\alpha_c}{1 + \beta_c I_z(t)}I_y(t) \qquad (4.4)$$

Unlike most of the phenomenological models that use feedback non-linearities[8] to affect the input starting from the output, the DA model applies a feedforward non-linearity given by the interaction between two time scales. Although it is well documented that in biology many feedback loops are present, the feedforward DA model may still well-approximate the natural feedback behavior for a certain range of stimuli.

The DA model well describes the cone's temporal evolution in terms of peak amplitude, latency and shape. It well simulated cone responses to light flashes and steps with either a dark or light background (Fig. 4.2, a), as well as white noise flickering (Fig. 4.2, b) or natural flickering (Fig. 4.2, c).
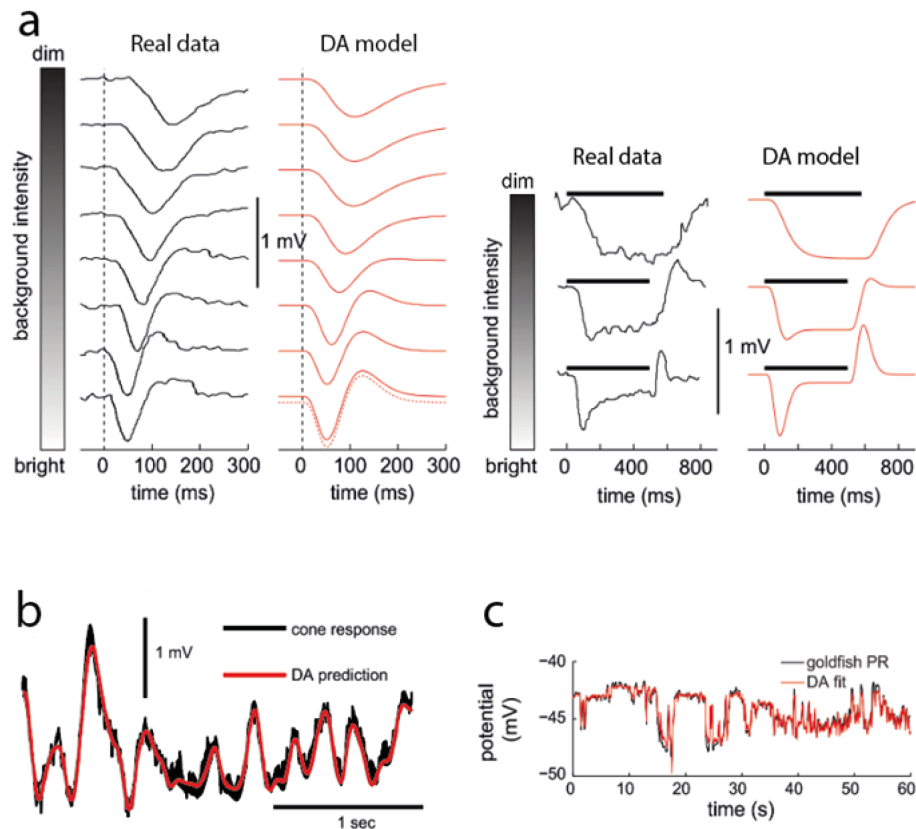
FIGURE 4.2: **The DA model can simulate cone response to different types of stimuli**. **a**| Experimental responses (*black*) and DA model predictions (*red*) for flashes (*left*) and steps (*right*) of light presented at time 0 on backgrounds of increasing intensities. Real data are extracted from Daly and Normann (1985). **b**| Comparison between salamander cone data (*black*) and DA model predictions (*red*) for white-noise flickering light stimulus. **c**| Comparison between goldfish cone response (*black*) and DA model predictions (*red*) for natural flickering light stimulus. Real data are extracted from Endeman and Kamermans (2010). (Adapted from Clark et al. (2013)).

Furthermore, the way the DA model simulates the cone response finds connections with the underlying biological mechanisms that affect cone potential.

One has to remember that although biophysical models can explain all the biological mechanisms that underlie a specific effect, the equations might be too complicated to be used to develop intuition or make predictions. As a matter of fact, sets of equations that perfectly simulate the phototransduction mechanism into cones exist, but their complexity reduces their applicability.

Many studies (Hateren, 2005) have confirmed that there is one nonlinear step that plays a dominant role in the phototransduction cascade: the cGMP (see 2.1.1). It is not the only non-linearity involved in the whole cascade. Many other feedback non-linearities come into

---

[8]Carpenter and Grossberg, 1987; Fuortes and Hodgkin, 1964; Baylor, Hodgkin, and Lamb, 1974.

play to guarantee, first of all, adaptation. Nonetheless GMP was found to be the dominant source of non-linearity.

cGMP's equations set does not stray too far from the equations of the DA model, except that cGMP's set embeds only one timescale, which is dimensionally similar to τ_y in Eq. 4.3. K_z, that has been said to be slower and broader than the more "nature like" K_y, could be the tool to simulate all the others "lighter" nonlinear terms involved in the phototransduction cascade.

The extension of the Dynamical Adaptation model

The DA model, as the authors suggested, lends itself to be used to mimic many other different effects, if slightly changed in its shape and parameters.

This is what has been done adding another block inside the DA model: the horizontal cells (Drinnenberg et al., 2018). The resulting model gave birth to the outer retina block of the temporal model.

As explained in Chapter 2 (see 2.1.2), the main purpose of the HCs in perturbing the signals in the outer retina is to give inhibitory feedback to the cones. This mechanism has been recreated in the equations adding a specific differential equation to describe HC node (Eq. 4.5) and adding in Eq. 4.1 the HC term as input (Eq. 4.6).
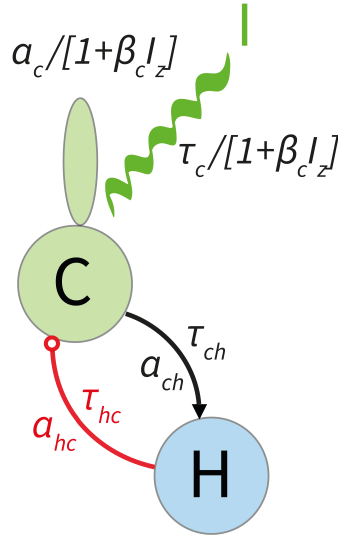
FIGURE 4.3: **Schematic of the temporal model's outer retina**. A light stimulus (I) is presented to the cone (C). The light evked response of the cone is dictated by Eq. 4.1 of the DA model. The cone node influences the HC node underneath (H) in the modes described by Eq. 4.6. The HC node gives inhibition feedback onto the cone node as described by Eq. 4.7. The inhibition feedback from HCs to cones allows to sharpen the evolution of the cone response.

$$\tau_{ch}\frac{dh(t)}{dt} = \alpha_{ch}c_y(t) - [1 + \beta_{ch}c_z(t)]\,h(t) \tag{4.5}$$

$$\tau_c\frac{dc(t)}{dt} = \alpha_c I_y(t) - [1 + \beta_c I_z(t)]\,(c(t) + \alpha_{hc}h(t)) \tag{4.6}$$

with:

- $h(t) = V_h(t) - V_{h,dark}$, instantaneaus and rest potentials of the HC.

- $\alpha_{ch}, \beta_{ch}, \tau_{ch}$ constants indicating gain, adaptation and time constant respectively.

- $c_y(t), c_z(t)$ filtered version of the cone potential $c(t)$, analogous to $I_y(t), I_z(t)$ (obtained with Eq. 4.2, 4.3).

- α_{hc} gain term that establishes the strength of the inhibition feedback from HCs to cones.

This formulation allows having a delayed inhibitory feedback affecting the cone potential from horizontal cells. The HC node receives the stimulus evoked cone potential and returns it, processed and delayed, to the same cone node (Fig. 4.3).

Eq. 4.6 can be better written (Eq. 4.7) to better see how β_c, the gain adaptation, does not act on the HCs inhibitory feedback but only on the input and the time constant τ_c.

In the temporal model the cone can have a sharper response than in the DA model. This is due to the effect of the HCs, entirely in line with the real effects described in Chapter 2(see 2.1.2).

$$\frac{\tau_c}{1 + \beta_c I_z} \frac{dc(t)}{dt} = \frac{\alpha_c}{1 + \beta_c I_z} I_y(t) - c(t) - \alpha_{hc} h(t) \tag{4.7}$$

4.2.2 The inner retina

The inner retina layer, as described in Chapter 2 (see 2.1.3), consists of a large number of different cells including manifold types of bipolar cells (BCs) and amacrine cells (ACs).

In the temporal model, the activity of the BCs in the inner retina layer is simulated with a threshold-nonlinear functional of the cone potential aimed at building six different inner retina pathways (**IRPs**, Eq. 4.8):

$$IRP_{p,k}(t) = \lfloor -1^k \left(\int_{-\infty}^{t} K_p(t - t')c(t') - \theta_{p,k} \right) \rfloor \qquad \text{with:} \tag{4.8}$$

$$\lfloor x \rfloor = 0 \quad \text{if} \quad x < 0; \qquad \lfloor x \rfloor = x \quad \text{if} \quad x \geq 0$$

$$K_1(t) = \sin\left(\frac{\pi t}{\mu}\right) \frac{1}{\sqrt{2\pi}\sigma} e^{-\frac{1}{2}\left(\frac{(t-\mu)^2}{\sigma^2}\right)} \qquad \text{with:} \quad \mu = 3ms, \quad \sigma = 1ms \tag{4.9}$$

$$K_2(t) = \frac{1}{\tau_2} e^{-\frac{t}{\tau_2}} - \frac{1}{c_2 \tau_2} e^{-\frac{1}{c_2 \tau_2}} \qquad \text{with:} \quad \tau_2 = 50ms \tag{4.10}$$

$$K_3(t) = \frac{1}{\tau_3} e^{-\frac{t}{\tau_3}} \qquad \text{with:} \quad \tau_3 = 100ms \tag{4.11}$$

$c(t)$ is the cone's output voltage, that serves as input of the inner retina block, while $\theta_{p,k}$ works as a specific threshold for each different IRP.

The k label is the ON/OFF identifier:

- $k = 1$: ON IRPs.

- $k = 0$: OFF IRPs.

The p label works as an identifier for the different time nature of the IRP:

1. $p = 1$: fast IRP (Eq. 4.9). Its kernel K_1 represented an HPF (high-pass filter) which takes the derivative of the cone potential on the order of $1ms$.

2. $p = 2$: intermediate IRP (Eq. 4.10). Its kernel K_2 is an HPF with a low cut-off frequency. The kernel allows to erase the DC component from the cone potential, leaving unchanged the rest.

3. $p = 3$: slow IRP (Eq. 4.11). Its kernel K_3 has a larger time constant (i.e., τ_3) if compared with the other two. The kernel slows down the cone response maintaining the DC component.

As could be inferred from the equations, all the combinations of the labels p and k produce six different IRPs. The sign inverting ON branch will have three temporally different IRPs, as well as the OFF branch (Fig. 4.4):

1. Fast ON IRP (Fig. 4.4, top left).

2. Intermediate ON IRP (Fig. 4.4, second from left).

3. Slow ON IRP (Fig. 4.4, third from left).

4. Fast OFF IRP (Fig. 4.4, third from right).

5. Intermediate OFF IRP (Fig. 4.4, second from right).

6. Slow OFF IRP (Fig. 4.4, top right).
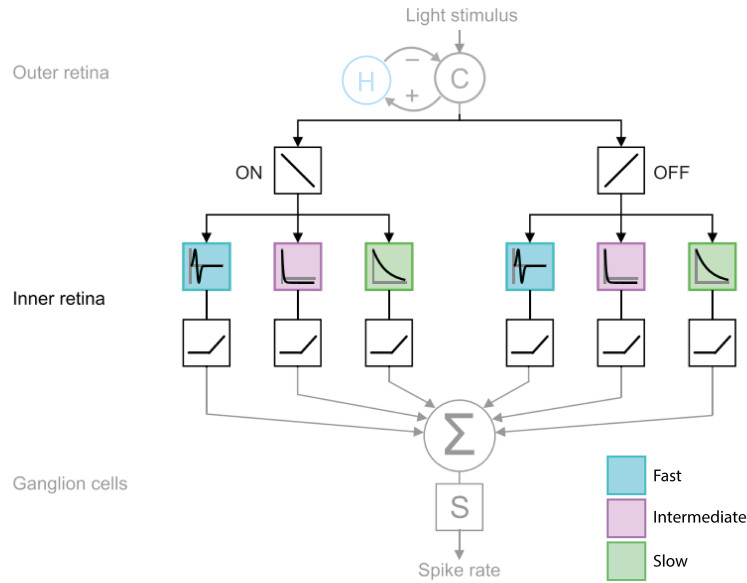
FIGURE 4.4: **Schematic of the temporal model's inner retina**. The inner retina section of the temporal model is shown not opaque. The cone's potential is split into ON (*left*) and OFF pathways (*right*). The resulting pathways of the two branches undergo filtering (*coloured boxes*) and nonlinear thresholding (*black boxes*). Three temporally different filtering blocks (i.e., fast, intermediate, slow) are used in both the two branches to simulate different bipolar cells that can extract different temporal features from the cone potential. The maths behind different pathways' definition is described by Eq. 4.8 -4.11. (Adapted from Drinnenberg et al. (2018))

4.2.3 The retinal ganglion cells layer

RGCs responses are obtained as the integration of different BCs types that synapse together in the RGC layer (i.e., IPL). Thus, in the temporal model, RGCs activity is modelled combining different IRPs.

The weighted sum of the derivative and the direct part of the resulting combination is then nonlinearly thresholded (Eq. 4.12) to finally obtain model RGCs types' firing rates (Fig. 4.5).

$$I_g(t) = \sum_{p=1}^{3} \sum_{k=0}^{1} w_{g,p,k} IRP_{p,k}(t) \tag{4.12}$$

$$RGC_g(t) = \lfloor (1 - \alpha_g) I_g(t) + \alpha_g \left(\int_{-\infty}^{t} K_g * (t - t') I_g(t') dt' \right) - \theta_g \rfloor \tag{4.13}$$

with:

- I_g: weighted combination of IRPs, $w_{g,p,k}$ weight of each $IRP_{p,k}$.

- α_g: weighting factor to declare the portion of direct or derivative part of the combination of IRPs wanted for each particular model RGC type.

- K_g: biphasic derivative filter similar to K_1 seen in Eq. 4.9.

- θ_g: nonlinear threshold aimed at turning the model RGC voltage into a firing rate (by definition larger than 0).
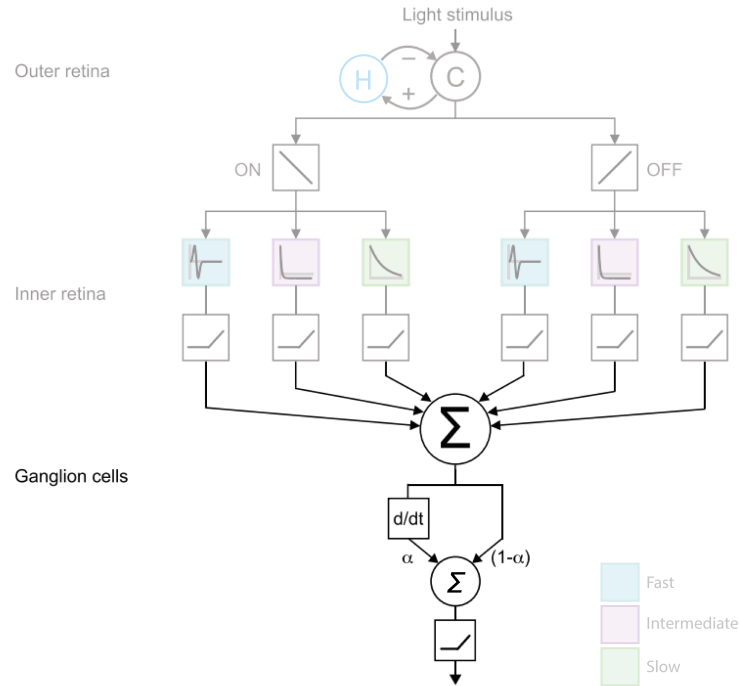
FIGURE 4.5: **Schematic of the RGCs layer of the temporal model**. The RGCs layer of the temporal model is shown not opaque. IRPs were linearly combined (Σ) and converted to a spike rate to model RGCs. Each combination of IRPs is split into its temporal direct and derivative parts. The two parts are complementarily weighted (α), combined (Σ) and nonlinear thresholded (*black box*). The maths regarding the schematic is described in equations Eq. 4.12, 4.13. (Adapted from Drinnenberg et al. (2018))

4.3 The temporal model showed up its potential

The temporal model has already been used in a study concerning the RGCs responses' perturbation induced by the lack of HCs feedback onto cones' terminals (Drinnenberg et al., 2018).

In this study mice have been injected with **PSAM** (pharmacologically selective actuator module)-expressing **AAV** (adeno-associated virus) (see C.1). It allowed to target HCs with a chloride-permeable ligand-gated ion channel.

RGCs activity was then monitored before, during and after the perfusion of a PSAM ligand, **PSEM**308 (pharmacologically selective effector molecule). The perfusion of PSEM leads to the clamp of HCs voltage at the chloride equilibrium potential.

This was done to see how HCs perturbation, in particular how the lack of inhibitory feedback from HCs onto cones' terminals, could perturb retinal output too.

Drinnenberg et al. (2018) found six main effects led by HCs perturbation (PSEM effects) on RGCs responses to a sequence of spatially uniform stimuli of different contrasts:

1. PSEM suppresses the transient part of the ON-response in transient ON-RGCs (Fig. 4.6, a *first panel*)

2. PSEM enhances the sustained part of the ON-response in sustained ON-RGCs (Fig. 4.6, a *second panel*)

3. PSEM enhances all the on-response in sustained ON-RGCs (Fig. 4.6, a *third panel*)

4. PSEM suppresses the rebound ON-response in transient OFF-RGCs (Fig. 4.6, a *fourth panel*)

5. PSEM enhances the transient part of the OFF-response in transient OFF-RGCs (Fig. 4.6, a *fifth panel*)

6. PSEM suppresses all the OFF-response in sustained OFF-RGCs (Fig. 4.6, a *sixth panel*)

In the temporal model the PSEM condition was recreated setting the value of α_{hc} equal to zero, so as not to provide the cone with the inhibitory feedback from HCs.

In the first place, the modelled lack of inhibitory feedback onto cones from HCs results in the shifting of the baseline of the cone potential (Fig. 4.6, b *1*). In addition, the cone's evolution lost the sharpness gained passing from the DA model to the temporal model.

These two apparently trivial changes in cone potential lead to significant changes downstream, at the level of the modelled RGCs (Fig. 4.6, b *3*). The temporal model captured all the six PSEM effects found in real data if it was properly set in terms of parameters and IRPs combinations' weights.
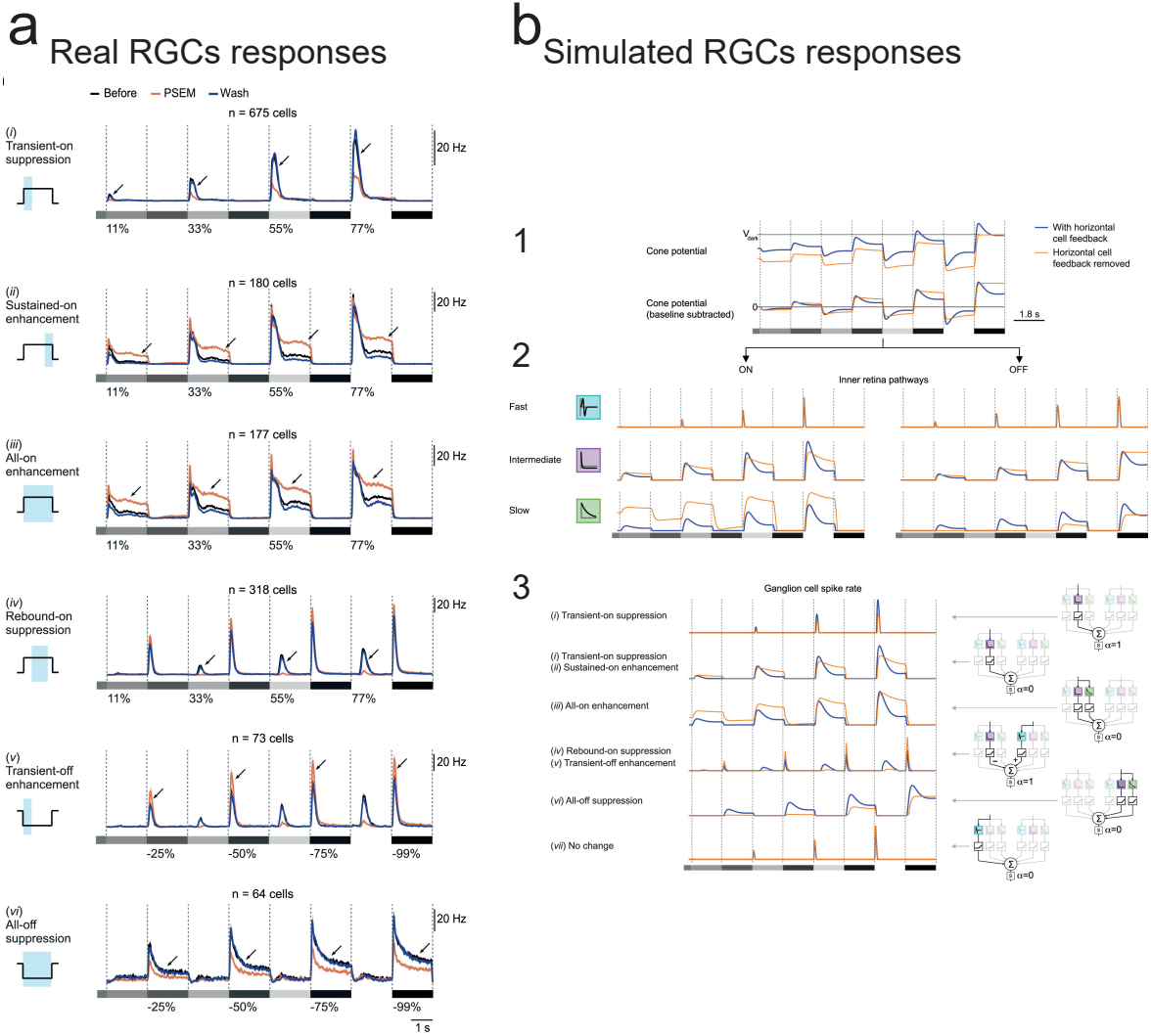
FIGURE 4.6: **The temporal model captured all the PSEM-induced effects**. **a**| Real RGCs responses. Each panel shows the spike rate of PSEM-affected cells for one of the six PSEM-induced effects (*mean ± s.e.m*). The *black line* indicates the responses before the PSEM perfusion, the *orange line* the responses during PSEM perfusion and the blue line responses after PSEM was washed out. *Gray shaded rectangles* and numbers (%), stimulus contrast; *arrows*, effects. Schematic (*left*): time window (*blue area*) in which the effect shows up. **b**| Simulated RGCs responses. *1*| simulated cone potential in presence (*blue*) and absence (*orange*) of horizontal cell feedback with (*top*) and without (*bottom*) the baseline. *2*| Trends of the six inner retina's pathways after the threshold non-linearity. *3*| Simulated RGCs' spike rates for the six PSEM-induced effects (*left*) and RGCs' building combinations of IRPs (*right*). Gray shaded rectangles (*bottom-left*) indicate the same stimulus contrast in **a**|. (Reproduced from Drinnenberg et al. (2018)).

4.4 Retinal saccadic suppression: can the temporal model help in its interpretation?

We saw how the DA model could deal with many different kinds of stimuli without losing its predictive capacity (see 4.2.1), and how its evolution embedding HCs and downstream pathways (i.e., temporal model) could qualitatively describe real RGCs responses to full field stimuli (see 4.3).

We wondered if we could use the already established temporal model to recreate, interpret and derive predictions on retinal saccadic suppression (RSS). In particular, if we can investigate the three different spatial components of suppression found by Idrees et al. (2020b) through the model.

All the components of suppression involved in retinal saccadic suppression have a robust spatial meaning related to the interconnection of adjacent or even farther "retinal processing paths" (hypothetically via networks of retinal inhibitory interneurons). The temporal model does not account for the spatial extent of the retina and for the networks of interneurons that connect its different regions. It has never been meant for this. Therefore, it may be inadequate for the purpose of modeling RSS.

Chapter 5

Retinal saccadic suppression modelling

Saccadic suppression has been found to start already at the retinal level (Idrees et al., 2020a). It is led by three specific suppression components (central, surround and global components of suppression ; CCS, SCS, GCS), each one with a specific time window of action. The origins of these three components are still not completely clear: CCS could be led by the nonlinear processing of the retina, SCS and GCS could instead be originated by the two main lateral networks of interneurons in the retina.

GCS, acting from the RF periphery, could be led by the WACs network in the IPL while hypothetically SCS, acting from the RF surround, could have its underlying mechanism in the HCs network in the OPL.

We wondered whether it would be possible to build a model that could mimic the effects of retinal saccadic suppression (RSS). In particular, if it could simulate the three different mechanisms underlying the three components of suppression and derive predictions about their functioning.

5.1 The need for a new model

We wondered if it was possible to adapt the temporal model in a way it could incorporate lateral networks of interneurons (i.e., HCs network and WACs network). In addition, we wondered if the model could give predictions about RGCs responses to non-full field stimuli, such as those used to probe GCS by Idrees et al. (2020b).

Therefore, we built a new model, which inherits a lot from the temporal model, embedding in it the two lateral networks of interneurons to predict their function in RSS.

1. The first interneurons network to be incorporated in the model was the HCs network. It has been documented that HCs are connected to each other via gap junctions in the OPL (Janssen-Bienhold et al., 2001). Gap junctions are electrical synapses and as such, they are involved in a very fast signal exchange.
   Therefore, we modelled the network of horizontal cells as a bridge between different portions of the outer retina, capable of transmitting signals very fast.

2. The second network of interneurons embedded in the model was the WACs network. As described in Chapter 2 (see 2.1.4), WACs widely spread in the INL and synapse with each other and with other cell types in the IPL.
   Thus, we modelled the network of WACs as a bridge that could interlink different portions of the inner retina.

5.2 Horizontal cells network modelling: toward the simulation of the surround component of suppression

HCs network, the hypothesized source of the SCS, spreads widely throughout the entire retina and allows every single cone to be aware of what is happening nearby.

How HCs bind each other, in terms of chemical and spatial aspects, is still not fully understood. Due to the connection between HCs and cones (see 2.1.2), the cones can also be indirectly connected to each other.

Initially, we recreated the HCs network adding a spatial component to the well-established temporal model. From now on we will refer to this extension of the temporal model as *spatial model*. We then reduced the complexity of the spatial model by introducing a simpler model we call *asymmetric model*.

5.2.1 Horizontal cells network modelling through the spatial model

The spatial model's formulation (Bucci et al., 2019) is similar to the temporal model's one: cones receive light from the outside world in the same way. Each cone has its HC node underneath and the inner retina layers process the information they were provided with, in the same manner as we saw in the previous chapter (see 4.2).

The outer retina is simulated as a $[nxm]$ *matrix* of modelled cones.

The HCs network is modelled in this way: every HC node belonging to a modelled cone is connected to the HC node of the adjacent cones, thus HC nodes affect each other (Fig. 5.1, a *left*). Cones nodes above are affected as well, due to inhibition feedback from their HC nodes below.

To make things easier, one may think about this $[nxm]$ pattern reduced in dimensions and narrow the cones' $2D$ *matrix* into a $[1xm]$ *vector* of cones. Now each cone will be influenced via HCs network by its left and right neighbour (Fig. 5.1, a *right*).

For sake of simplicity, we can look at a system of only 3 cones, each one receiving light from the outside world and each one connected with its HC node (Fig. 5.1, b). Adjacent HC nodes are linked together to influence and being influenced by the cones they do not belong to. But how do they influence each other?

To compute the horizontal cell's node potential, the voltage difference between the same node and its neighbors is taken into account. Specifically, the horizontal cell node potential is led by its Laplacian (Eq. 5.2) and a gain term α_{hh}.

α_{hh} controls the spatial extent of the HCs network action on cones, monitoring the decay of a spatial exponential. The pure interconnection between HC nodes does not involve any time constant, in this way the signal transfer is instantaneous, in line with gap junctions' timescale.

τ_{ch} controls the transition of the light evoked potential from cones to HCs, thus it controls the reaction time of HCs to light. The value of τ_{ch} is assumed to be very small in order to allow the modeling of a quasi-instantaneous reception of light by HCs.

Together with the modelled HCs network, we added two more delaying blocks to the model, in between the HC node and the cone node (Fig. 5.1, b). They control the timing and the smoothness of the inhibitory feedback from HCs onto cones separately:

- the first node, whose time constant is τ_{hc1} leads the feedback timing for $t \to 0$ (Eq. 5.3).

- the second node, whose time constant is τ_{hc2} leads the feedback timing for $t \to \infty$ (Eq. 5.4).
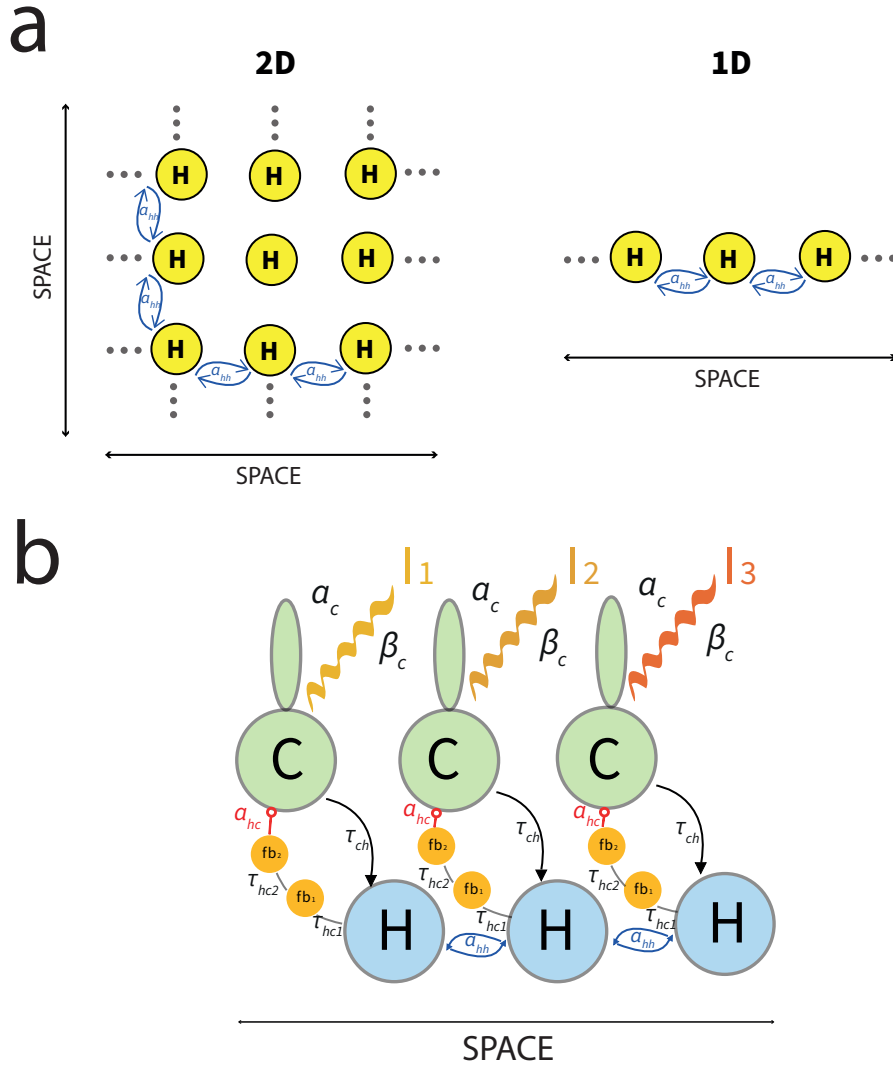
FIGURE 5.1: **Schematic of the spatial model's outer retina**. **a**| *Left*: the HCs layer in the INL is modelled by a 2*D* [*nxm*] *matrix* of HC nodes. Each HC node is influenced by and influences the adjacent HC nodes via the interconnection term's gain α_{hh} (*blue arrows*). The way each HC node is influenced depends on its Laplacian (Eq. 5.2). *Right*: simplification of the 2*D matrix* into a 1*D* [1*xm*] *vector* of HC nodes. The parameters remain the same, now each HC is influenced only by its two neighbours though. **b**| Further simplification of **a** (*right*), connections with the cones' nodes above are shown. The vector of HC nodes collapses in a 1*D* [1*x3*] *vector* of HCs, connected upstream with the cone nodes that receive light from the outside world. HC nodes are interconnected via the usual α_{hh} term (*blue arrows*). HC nodes give inhibition feedback to cone nodes via two smoothing and delaying filters (fb_1, fb_2).

$$\tau_c \frac{dc(x,t)}{dt} = \alpha_c I_y(x,t) - [1 + \beta_c I_z(x,t)] \left(c(x,t) + \alpha_{hc} h(x,t) \right) \tag{5.1}$$

$$\tau_{ch} \frac{dh(x,t)}{dt} = \alpha_{ch} c(x,t) - h(x,t) + \alpha_{hh} \Delta h(x,t) \quad \text{with:} \tag{5.2}$$

$$\Delta h(x,t) = \alpha_{hh}[(h(x_{i+1},t) - h(x_i,t)) + (h(x_{i-1},t) - h(x_i,t))]$$

$$\tau_{hc1} \frac{dfb_1}{dt} = h(t) - fb_1 \tag{5.3}$$

$$\tau_{hc2} \frac{dfb_2}{dt} = fb_1 - fb_2 \tag{5.4}$$

The delay of horizontal cells' feedback onto cones, considering $\tau_{ch} \ll \tau_{hc1}, \tau_{hc2}$, is roughly

given by the geometric mean of the two values τ_{hc1} and τ_{hc2} ($\tau_{eff} = \sqrt[3]{\tau_{ch}\tau_{hc1}\tau_{hc2}} \simeq \sqrt{\tau_{hc1}\tau_{hc2}}$).
The way the spatial model is formulated would allow not only seeing how horizontal cells deal with the perturbation of their cones but also of many cones nearby. This is due to the network they create with the interconnection term added (i.e., α_{hh}).
The HCs interconnection mechanism appears to be simple if we think about an array of only three cones, nonetheless it is not with a $[1xm]$ *vector* of cones or a $[nxm]$ *matrix* of cones.
In the $[nxm]$ *matrix* case, the spatial model, with its large number of differential equations to solve (i.e., a pair of ODEs for each modelled cone), proves to be really complex. Although it could be very accurate in modelling the HCs network, we wondered if we could reduce its complexity without losing potential performance.

5.2.2 Horizontal cells network modelling through the asymmetric model

We reduced the spatial models's complexity reducing the number of modelled nodes. We assumed the photoreceptors layer of the spatial model as divided into two main compartments:

1. The *center compartment* (**CC**): it includes all the modelled cones that belong to the virtual RF center of the downstream model RGC.

2. The *surround compartment* (**SC**): it includes all the modelled cones that belong to the virtual RF surround of the downstream model RGC.

We essentially split the $[nxm]$ spatial model's *matrix* of cones into two compartments, each one with its set of cones. These two sets could differ in number.
All the CC cones and the SC cones share the same formulation (i.e., the temporal model one).
We assumed that all the cones within the same compartment respond the same way. Therefore, by presenting a different stimulus to the CC and the SC, each cone will respond identically to all the other cones in its compartment and differently to the cones in the opposite compartment.
With this assumption all the cones within a certain compartment collapse in a single modelled cone that stays for the compartment's averaged cone.
We built the HCs network as a bridge between the two compartments at the level of the HC nodes. We connected the two compartments' cones via their respective averaged HC nodes underneath with an interconnection term similar to the spatial model's α_{hh}.
Depending on the direction (i.e., from the CC to the SC or vice-versa) the interconnection term changes in gain. The change in gain is led by the different number of cones each compartment contains. In particular, the larger the set of cones in one compartment (*i*) relative to the set of cones in the other (*ii*), the larger the gain term of the *i-ii* direction. In this way the RF center affects and is affected by the RF surround differently from how the RF surround affects and is affected by the RF center. The asymmetry between the two gains of the interconnection terms gives the name to the model: the asymmetric model (Fig. 5.2, b).

It works as the example shown in Fig. 5.2, a. Imagine to have a CC set of only one cone and a SC set of four cones. Each of the single cones has its HC node underneath and each HC node is connected to the adjacent HC nodes of the cones nearby modelling the HCs network. The HCs network's modelling, in this case, is the same used in the spatial model: the interconnection term has α_{hh} as gain.
If we apply the assumption we made above, the modelled averaged cone of the CC will see four times the influence of the averaged cone of the SC via the HCs network. Meanwhile, the averaged cone of the SC will only see once the influence given by the averaged cone of the CC.

a

b
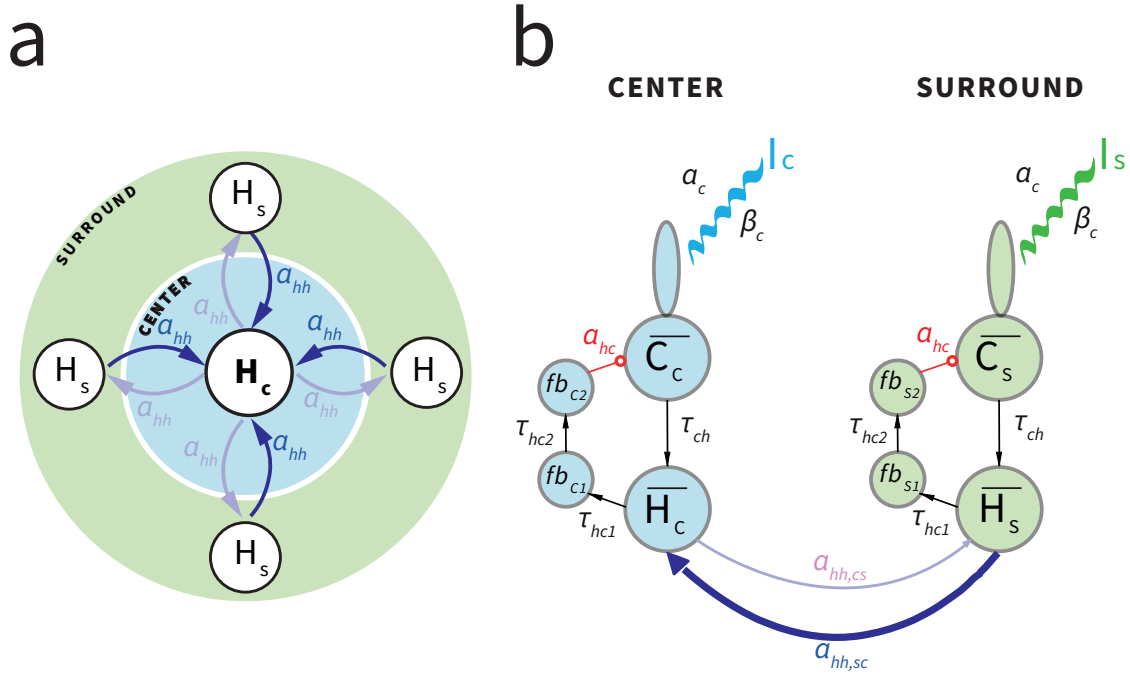
FIGURE 5.2: **Schematic of the modelling of the HCs network in the asymmetric model**. The asymmetric model is a two-compartment model: it is composed by the center and the surround compartments (CC, SC). **a|** Example of sets of cones belonging to the center (*light blue shaded circle*) and surround (*light green shaded anulus*) compartments. Each cone belonging to one of the two compartments has its HC node underneath. *White circles* represent individual HC nodes either belonging to the center compartment (H_C) or to the surround compartment (H_S). Adjacent HC nodes influence each other with the same interconnection term α_{hh} of Fig. 5.1 (*light or dark purple lines* depending on the direction). **b|** The two compartments can receive different light stimuli (I_C, I_S). Each compartment has its averaged cone node ($\overline{C_C}$, $\overline{C_S}$) and its HC node ($\overline{H_C}$, $\overline{H_S}$). The connection of HC nodes with their cone nodes is the same seen in Fig. 5.1 with the twice-delayed inhibition feedback from HCs to cones (fb_1, fb_2). The center HC node influences the surround HC node with the interconnection gain term $\alpha_{hh,cs}$ (*light purple line*). Similarly, the surround HC node influences the center HC node with the interconnection term $\alpha_{hh,sc}$ (*dark purple line*). $\alpha_{hh,cs}$ and $\alpha_{hh,sc}$ can assume different values depending on the size of the sets of cones each compartment come from. The maths underlying the scheme is described in Eq. 5.5-5.13.

The set of equations (Eq. 5.5 - 5.12) describing the asymmetric model include the entry of the new modeled HC network. We called the two asymmetric terms' gains $\alpha_{hh,cs}$ and $\alpha_{hh,sc}$:

- $\alpha_{hh,cs}$ establishes the influence strength of the CC on the SC.

- $\alpha_{hh,sc}$ establishes the influence strength of the SC on the CC.

$$\tau_c \frac{d\overline{C_C}(t)}{dt} = \alpha_c I_{C,y}(t) - [1 + \beta_c I_{C,z}(t)] \left(\overline{C_C}(t) + \alpha_{hc} fb_{C,2}(t) \right) \tag{5.5}$$

$$\tau_c \frac{d\overline{C_S}(t)}{dt} = \alpha_c I_{S,y}(t) - [1 + \beta_c I_{S,z}(t)] \left(\overline{C_S}(t) + \alpha_{hc} fb_{S,2}(t) \right) \tag{5.6}$$

$$\tau_{ch} \frac{d\overline{H_C}(t)}{dt} = \overline{C_C}(t) - \overline{H_C}(t) + \alpha_{hh,sc}(\overline{H_S}(t) - \overline{H_C}(t)) \tag{5.7}$$

$$\tau_{ch} \frac{d\overline{H_S}(t)}{dt} = \overline{C_S}(t) - \overline{H_S}(t) + \alpha_{hh,cs}(\overline{H_C}(t) - \overline{H_S}(t)) \tag{5.8}$$

$$\tau_{hc1}\frac{dfb_{C1}(t)}{dt} = \overline{H_C}(t) - fb_{C1}(t) \tag{5.9}$$

$$\tau_{hc1}\frac{dfb_{S1}(t)}{dt} = \overline{H_S}(t) - fb_{S1}(t) \tag{5.10}$$

$$\tau_{hc2}\frac{dfb_{C2}(t)}{dt} = fb_{C1}(t) - fb_{C2}(t) \tag{5.11}$$

$$\tau_{hc2}\frac{dfb_{S2}(t)}{dt} = fb_{S1}(t) - fb_{S2}(t) \tag{5.12}$$

As described before, the different infuence's strength of the RF surround onto the RF center via the HCs network is simulated through the asymmetric terms in the model (i.e., $\alpha_{hh,cs}$ and $\alpha_{hh,sc}$).
Thus, $\alpha_{hh,cs}$ and $\alpha_{hh,sc}$ could assume a spatial meaning: their ratio could simulate the relative sizes (i.e., number of cones) of the two compartments.

- $\alpha_{hh,sc}/\alpha_{hh,cs} \gg 1$ establishes a great influence of the RF surround onto the RF center. It stands for a SC larger than the CS in number of cones.

- $\alpha_{hh,sc}/\alpha_{hh,cs} > 1$ and $\alpha_{hh,sc}/\alpha_{hh,cs} \simeq 1$ ratifies a bigger influence of the RF surround onto the RF center. The cones in the SC are comparable in numbers with the ones of the CC.

- $\alpha_{hh,sc}/\alpha_{hh,cs} < 1$ would stand for a larger influence of the RF center onto the RF surround. SC number of cones would be smaller than CC number of cones. This scenario is of little interest since the RF surround is wider than the RF center (Croner and Kaplan, 1995).

In nature, the HCs network extent is really large - one HC can cover more or less 1000 μm^2 with its dendritic arbor (Behrens et al., 2019) - and takes part in the definition of the RF surround's extent. Nonetheless, the RF surround of a RGC does not extend to infinity, its size is still circumscribed. The influence of the RF surround on the RF center is therefore limited by the extent of the RF surround itself.
The asymmetric model allows to increase the modelled spatial extent of the SC to an infinite size. The ratio of $\alpha_{hh,cs}$ and $\alpha_{hh,sc}$ should therefore be limited at the upper end.
The asymmetric model has potential features to enable the simulation of the possible role of HCs network in retinal saccadic suppression without making the previous temporal model by Drinnenberg et al. (2018) too complex (i.e., spatial model).
The asymmetric model decreases the spatial model's complexity without losing the spatial extension feature introduced by the variable $\alpha_{hh,sc}/\alpha_{hh,cs}$. It also allows deriving potential predictions on model RGC responses to non-full field stimuli, making the exploration of new scenarios possible.

5.3   Wide field amacrine cells network modelling: towards the simulation of the global component of suppression

WACs network, the potential source of the global component of suppression (GCS), is widely and sparsely spread in the IPL. WACs bind bipolar cells, other WACs, and RGCs provoking a temporal sharpening effect on RGCs responses, via both inhibitory and excitatory synapses.
Since the GCS was supposed to act from the periphery of the RF of RGCs we firstly turn the surround compartment of the asymmetric model into a peripheral compartment (**PrC**). We did so by "switching off" the model HCs network seen in the previous section (see 5.2.2). We set at zero both $\alpha_{hh,cs}$ and $\alpha_{hh,sc}$. The two compartments are not connected via the HCs

network anymore, this means we can consider them quite "far" from each other. The SC turned into a PrC (Fig. 5.3, b *top*).

We embedded WACs network inside the asymmetric model as a connection bridge between the center compartment and the PrC at the level of the inner retina layer.

The extension sees the introduction of a new model BC type (i.e., a new IRP) and the model WAC block (i.e., a new filtering block). We tested the model WACs network potentiality in recreating the effects of the GCS on a new model RGC type (i.e., a new combination of IRPs).

5.3.1   Wide field amacrine cells network modeling: processing blocks

To simulate WACs network, we added two other filtering blocks to the model's processing chain.

1. The first block is aimed at building a new type of BC from the cone potential $c(t)$ (i.e., a new IRP, Eq. 5.13). The new IRP can extract specific temporal features from the cone potential upstream. The definition of the new IRP is similar to all other IRPs of the temporal model; however it has different temporal properties.
   The new IRP is composed of two processing subblocks following the usual ON/OFF branches split (k label) and a block that removes the baseline (Fig. 5.3, a *top*). The first subblock consists of a smoothing filter (K_{smooth}) with a time constant τ (Eq. 5.14). The second subblock consists of a threshold non-linearity (θ_k, Eq. 5.13).

$$IRP_{new,k}(t) = \lfloor -1^k \left(\int_{-\infty}^{t} K_{smooth}(t - t')c(t') - \theta_k \right) \rfloor \qquad \text{with:} \qquad (5.13)$$

$$\lfloor x \rfloor = 0 \quad \text{if} \quad x < 0; \qquad \lfloor x \rfloor = x \quad \text{if} \quad x \geq 0$$

$$K_{smooth}(t) = \frac{1}{\tau}e^{-\frac{t}{\tau}} - \frac{1}{c_2\tau}e^{-\frac{1}{c_2\tau}} \qquad (5.14)$$

2. The second block actually simulates WACs and consists of a derivative filter (K_{WAC}, Eq. 5.15) followed by a nonlinear thresholding (θ, Eq. 5.15), a *bottom*). The derivative filter could rapidly detect changes in the signal output of the first block and sharpen its response. The sharpening effect provided by the WACs block is in line with WACs real effect in nature (Franke et al., 2017).

$$IRP_{afterWAC}(t) = \lfloor \left(\int_{-\infty}^{t} K_{WAC}(t - t')IRP_{new}(t') - \theta \right) \rfloor \qquad \text{with:} \qquad (5.15)$$

$$\lfloor x \rfloor = 0 \quad \text{if} \quad x < 0; \qquad \lfloor x \rfloor = x \quad \text{if} \quad x \geq 0$$

$$K_{WAC}(t) = \sin\left(\frac{\pi t}{\mu} \right) \frac{1}{\sqrt{2\pi\sigma}}e^{-\frac{1}{2}\left(\frac{(t-\mu)^2}{\sigma^2} \right)} \qquad \text{with:} \quad \mu = 3ms, \quad \sigma = 1ms \qquad (5.16)$$

5.3.2   Wide field amacrine cells network role in the global component of suppression: a new retinal ganglion cell type to derive predictions

To derive predictions about the WACs network involvement in RSS we tested the model WACs network described in the previous section by looking at the responses of a new model RGC type. Since GCS primarily affects transient ON-RGCs (Idrees et al., 2020b), the RGC type we modeled was a transient ON-RGC (**nRGC**).

A new combination of IRPs was created to build the nRGC, whose responses must highlight the effects of GCS (i.e., timing and strength of suppression) mediated by the model WACs
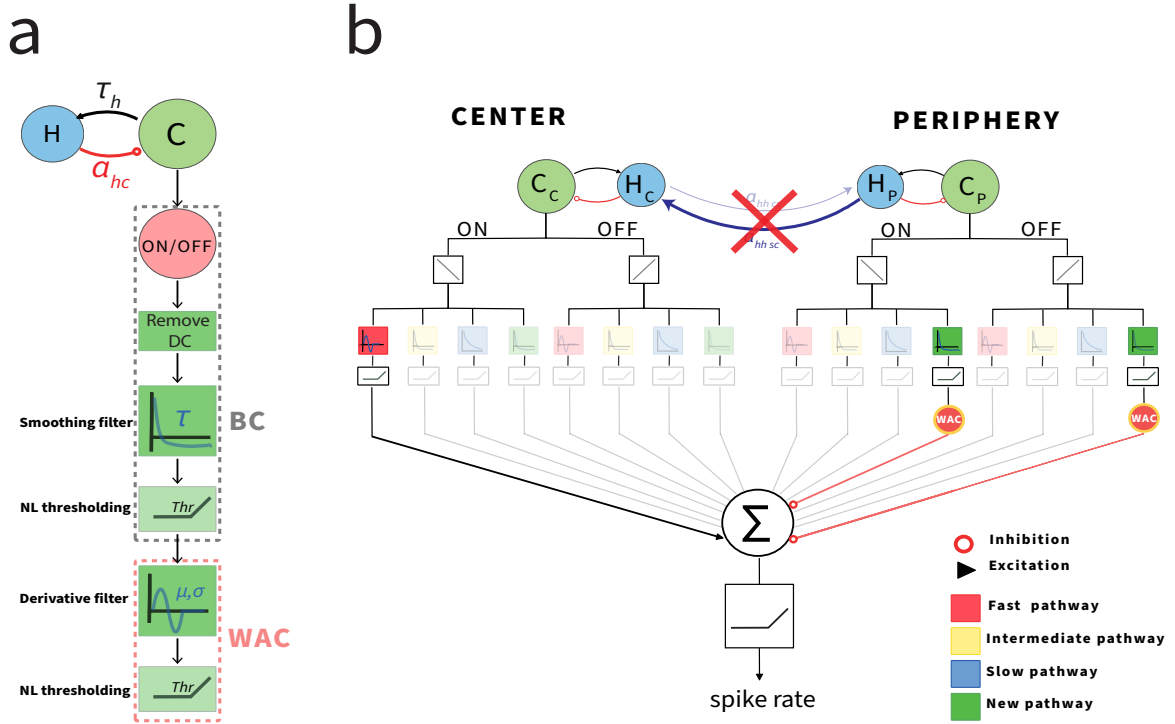
FIGURE 5.3: **Schematic of the modelling of WACs network in the asymmetric model**. **a**| The new IRP. The construction of the new pathway in the inner retina sees the succession of two filtering blocks: the first aimed at modelling a new BC type (*gray dashed line*) and the second aimed at recreating WACs network (*red dashed line*). BC block is composed by the usual ON/OFF split (*k* label Eq. 5.13), a block that removes the DC component, a smoothing filter (K_{smooth}, Eq. 5.14) with a time constant τ and a threshold non linearity (θ_k, Eq. 5.13). WACs block is composed by a first derivative filter (K_{WAC}, Eq. 5.16) and a threshold non linearity (θ, Eq. 5.15). **b**| The new modelled RGC. The surround compartment of the asymmetric model turned into a peripheral compartment (PrC) "switching off" the HCs network (*red cross*). A new RGC (transient ON cell) was modelled combining IRPs from both the center compartment and the PrC. The new combination is composed by the excitation (*black line*) of the fastON pathway from the CC (*red box*) and the inhibition (*red lines*) from both the new IRPs (ON and OFF) seen in **a** of the PrC (*green boxes*). The combination is non-linearly tresholded (*withe box, bottom*) and gives shape to the spike rate of the new modelled transient ON-RGC.

.

network.

The nRGC is built from a combination of IRPs of both the CC and the PrC of the asymmetric model (Fig. 5.3, b). In particular the new combination uses excitation from the fast-ON IRP of the CC (Eq. 4.8, 4.9), together with the inhibition from the PrC ON and OFF new IRPs (Eq. 5.13). The two peripheral compartment IRPs integrate at the RGCs level via the model WACs block.

In the experiments, what is measured is the FR of RGCs. Therefore, to relate model RGC responses to real RGC responses, the RGC model voltage is turned into a FR. Since firing rates must be larger than zero, a thresholding nonlinearity needs to be applied. Thus, the resulting IRPs combination must be thresholded at 0, to properly describe the experimental RGCs response (Fig. 5.3, b *bottom*; Eq. 4.13).

Chapter 6

The asymmetric model on retinal saccadic suppression

We wanted to probe the ability of the asymmetric model in recreating the modulation of the RGCs responses to saccade-like stimuli, as reported by Idrees et al. (2020a).

In particular, we wondered if it was possible to derive insights into the potential mechanism used by WACs in mediating the global component of suppression (Idrees et al., 2020b). In addition, we wanted to explore the possibility of the engagement of the HCs network in retinal saccadic suppression (i.e., as mediator of the surround component of suppression).

To do this we "interrogated" the asymmetric model by means of a set of stimuli, similar to the ones used by Idrees et al. (2020b), that could elicit retinal saccadic suppression (RSS). We adjusted the outer retina block parameters by fitting them against real data. We used the modulation index - the same used by Idrees et al. (2020a) - to analyze model RGC responses and derive predictions about the response behavior of real RGCs.

6.1 Recreating response behavior of real retinal gnglion cells: how to "ask" the asymmetric model for predictions

Idrees et al. (2020b) distinguished the three different spatial components of RSS analyzing RGCs responses to simple stimuli (see 3.2.1). The aim of the asymmetric model is to recreate that suppression of RGCs responses, holding the model's level of complexity low.

To investigate if the asymmetric model was capable of recreating the results reported by Idrees et al. (2020b) or even predicting HCs network involvement in saccadic suppression, we tested it with a simple stimulus protocol. We call this protocol *saccade&flash*.

6.1.1 The saccade&flash protocol

The protocol was built along the lines of what Idrees et al. (2020b) used. It is coded as a time-varying 2 elements vector whose former element is addressed to the asymmetric model's center compartment (CC), the latter to the surround/peripheral compartment (SC/PrC). A flash is presented with a varying delay (i.e., Δt_{flash}) from the onset of the saccade, modelled as a step. The flash could be either bright or dark (± 0.43 Michelson Contrast, **MC**), as well as the saccade (± 0.33 MC).

We explored all the possible combinations between saccadees and flashes: the opposite (i.e., OFF saccade ON flash, ON saccade OFF flash) and similar (i.e., ON saccade ON flash, OFF saccade OFF flash) contrast polarities and their respective occurrence in the center or surround/peripheral compartments. All the possible alternatives are shown in Fig. 6.1, each combination with its full name, abbreviation, and the acronym (which will be used from here on).
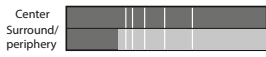
Complete Name	Schematic	Abbreviation	Acronym
a			
Full field ON saccade / Full field ON flash	Center / Surround/ periphery	ff-ON ff-ON	ff 1st
Full field ON saccade / Full field OFF flash	Center / Surround/ periphery	ff-ON ff-OFF	ff 2nd
Full field OFF saccade / Full field ON flash	Center / Surround/ periphery	ff-OFF ff-ON	ff 3rd
Full field OFF saccade / Full field OFF flash	Center / Surround/ periphery	ff-OFF ff-OFF	ff 4th
b			
Surround/peripheral-only ON saccade / Full field ON flash	Center / Surround/ periphery	nff-ON ff-ON	nff 1st
Surround/peripheral-only ON saccade / Full field OFF flash	Center / Surround/ periphery	nff-ON ff-OFF	nff 2nd
Surround/peripheral-only OFF saccade / Full field ON flash	Center / Surround/ periphery	nff-OFF ff-ON	nff 3rd
Surround/peripheral-only OFF saccade / Full field OFF flash	Center / Surround/ periphery	nff-OFF ff-OFF	nff 4th
c			
Surround/peripheral-only ON saccade / Center-only ON flash	Center / Surround/ periphery	nff-ON nff-ON	nff 5th
Surround/peripheral-only ON saccade / Center-only OFF flash	Center / Surround/ periphery	nff-ON nff-OFF	nff 6th
Surround/peripheral-only OFF saccade / Center-only ON flash	Center / Surround/ periphery	nff-OFF nff-ON	nff 7th
Surround/peripheral-only OFF saccade / Center-only OFF flash	Center / Surround/ periphery	nff-OFF nff-OFF	nff 8th

FIGURE 6.1: **All the saccade&flash protocol alternatives**. Saccade&flash is built as a time-varying 2 element vector in which the temporal evolution of the first element is supposed to be delivered to the center compartment of the model, while the temporal evolution of the second element to the surround/peripheral compartment of the model. Saccade&flash provides many different combinations of saccade-like stimuli changing the stimulus presented to the two compartments and the polarity of the contrast changes (i.e., of steps and flashes). The stimulus might be full-field (**a**) or non-full field (**b,c**). **b** and **c** differentiate for the presence of the flash in two or one compartment respectively. For **a**,**b** and **c** : first column, stimulus' combination full name; second column, stimulus' combination schematic (*darker, OFF or brighter, ON bars* indicate saccades, *white, ON or black, OFF rectangles* indicate flashes at different Δt_{flash}); third column, stimulus' combination abbreviation (*nff : non-full field; ff: full field*); fourth column, stimulus' combination acronym.

6.2   Fitting the parameter set of the outer retina

The ready-made outer retina parameter set of the temporal model (Drinnenberg et al., 2018) is not suitable since the asymmetric model embeds the twice-delayed inhibitory feedback (Eq. 5.9-5.12). The outer retina parameter set therefore needs to be fitted against real data to correctly describe the evolution of the cone potential. We fitted the set with the cones patch-clamp recordings (Szikra et al., 2014) used to fit the temporal model.

Since cones recordings for spatially not-uniform stimuli were not available, we were not able to fit the values of $\alpha_{hh,cs}$ and $\alpha_{hh,sc}$. These parameters are therefore unconstrained by the data and we set them by hand.

We constrained some of the parameters to not fall in absurd conditions such as negative time constants: we forced every time constant to be greater than zero and we bound γ (Eq. 4.3) in the $[0, 1]$ domain. We obtained a new set of parameters that fit well real cone responses (see D.1 for more details, Fig. 6.2).
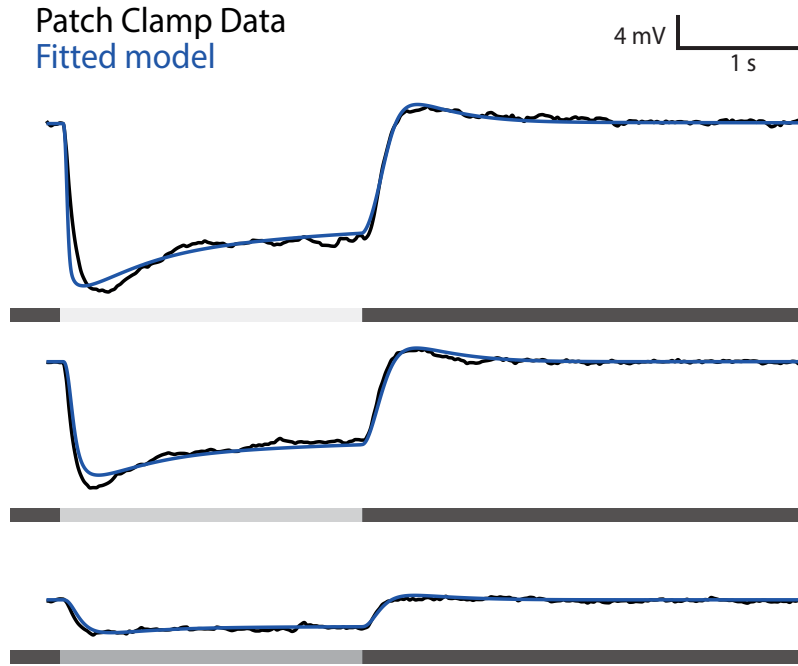
FIGURE 6.2: **The fit of the outer retina set of parameters**. The outer retina segment of the asymmetric model (twice delayed feedback from HCs to cones) was fitted on patch-clamp recordings of cones responses to different contrast changes. The model (*blue lines*) can capture the dynamics of cone light evoked responses (*black traces*) across three decades of light intensities (*shaded grey areas*). Patch-clamp recordings come from Szikra et al. (2014).

6.3 Wide field amacrine cells network modelling: validation as mediator of the global component of suppression

As it was introduced in Chapter 5 (see 5.3.1), to embed wide field amacrine cells (WACs) into the model we worked on the construction of a new IRP, a WAC simulating block, and a new "intercompartments" IRPs combination (nRGC).

In this section, the potential and operation of the new extensions will be presented in detail. We will put attention on the exact action timing of the global component of suppression found by Idrees et al. (2020b) and its reproduction using the model. We will investigate how model results change as a function of the set of parameters used, in particular how they change varying τ (i.e., the time constant of K_{smooth}, Eq. 5.14).

Before probing the new model RGC on the saccade&flash protocol, we made sure nRGC behaved as a normal transient ON-cell. To do this we used the same stimulus Drinnenberg et al. (2018) used to validate the temporal model: full field light steps of increasing contrast.
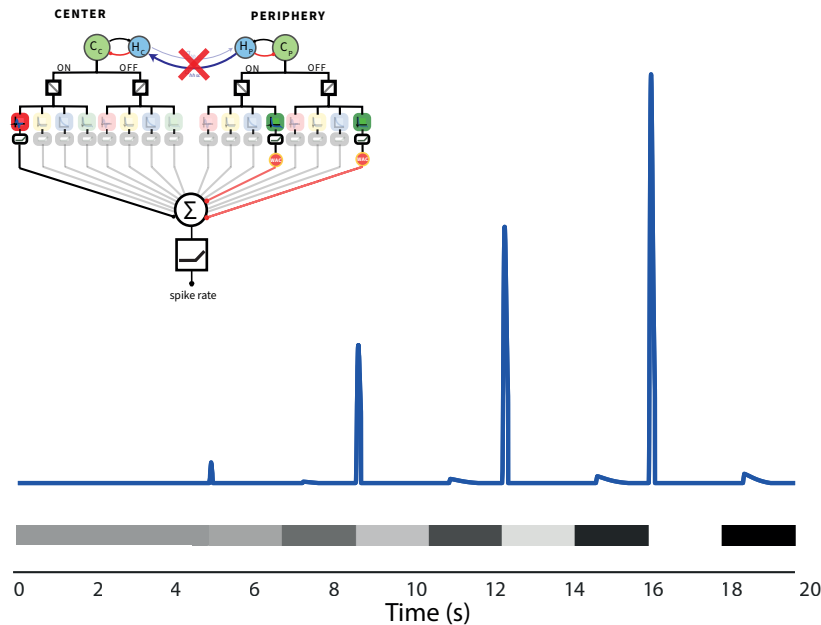
FIGURE 6.3: **The responses of the new model RGC are coherent with its nature**. Test of the asymmetric model and the new model RGC with the stimulus used by Drinnenberg et al. (2018) to validate the temporal model. The new simulated transient ON-RGC (i.e., combinations of IRPs, *top-left*), respects its "nature". As a matter of fact, it responds transiently to positive contrast changes (*grey shaded rectangles in the bottom*).

6.3.1 How to recreate the timing of the global component of suppression by means of the model: the details of the new inner retina pathway and the new model ganglion cell

The global component of suppression (GCS) acts from the periphery of the RF, this means that the given suppression must come from the asymmetric model's peripheral compartment (PrC). GCS effects are obtained using both the new IRPs of the PrC and the WAC block (see 5.3.1).

The new IRPs of the PrC (i.e., one for the ON branch and one for the OFF branch) serve as inhibitory inputs to the nRGC. They integrate in the model ganglion cells layer with the fast-ON IRP of the center compartment (CC), the excitatory input of the nRGC.

Various model RGCs alternatives have been considered in trying to recreate the GCS timing,

they all yielded a poorer match with real data. At first *(i)* we tried to build a simple intercompartmental combination between the fast-ON IRP of the CC and the intermediate ON/OFF IRPs of the PrC. This was done since the intermediate IRP is delayed compared to the fast IRP, this would yield the timing of suppression delayed and hopefully similar in effects to the GCS. Unfortunately, it did not. Next *(ii)*, we attempted to create an intercompartmental combination between IRPs of the CC and delayed versions of the IRPs from the PrC (i.e., using a delaying block in between the IRPs of the CC and the integrating GCL). This yielded a delay in the onset of suppression due to the inhibition given by the delayed saccade response of the PrC; it did not lead to the required modulation of suppression though.

These two different approaches were therefore discarded. GCS effects were better modelled using the new IRP and the new model RGC described at the beginning of this section.

To see how GCS effects are recreated by the model, we will take as example the nRGC responses to nff 3rd stimulus (Fig. 6.4).

The different temporal evolution of the stimulus presented to the two compartments leads to different IRPs responses downstream. The IRPs evolution also changes by varying the time of the flash from the onset of the saccade (i.e., Δt_{flash}). This change has repercussions on IRPs combination at the GCL and therefore on the time course of nRGC.

The new IRPs of the PrC are built through the processing chain seen in the previous chapter (see 5.3.1). Such processing chain leads to the creation of two parallel BCs responses - for the ON and OFF branches - : one of them embeds the response to the saccade, the other is zeroed instead (Fig. 6.4, e *left*).

In particular, the branch of the same polarity as the saccade keeps on capturing its presence. In addition, the captured saccade response in the "non-zeroed" branch is slightly delayed by the previously applied smoothing filter (Fig. 6.4, second green box *left*). The induced delay recreates the functional principle behind GCS action timing. The introduced delay represents the distinguishing feature of the new type of BC. It is indeed this feature that permits to achieve a targeted modulation of RGCs suppression through the WACs block.

The two parallel BCs responses pass through the WAC block: BC response's variations are captured by the derivative filter (Fig. 6.4, fourth green box *left*) and set all positive by a threshold NL (Fig. 6.4, g *left*). The WAC block aligns in time the saccade response evolution of the inhibitory new IRPs of the PrC with the excitatory fast-ON IRP of the CC (Fig. 6.4, e *right*).

The three involved IRPs combine in the GCL to build the new model RGC. Depending on Δt_{flash}, the interaction between IRPs changes (Fig. 6.4, h).

In particular, the inhibition given by the new IRPs of the PrC decreases for later Δt_{flash}. Larger Δt_{flash} allow the same responses to the saccade to complete their evolution and zero their contribution (Fig. 6.4, g *right*). Earlier Δt_{flash} do not allow the response to the saccade to flatten at zero due to the forthcoming flash.

The resulting model RGC voltage (i.e., IRPs combination) must be then turn into a model RGC firing rate to properly describe experimental RGCs responses. The resulting FR of nRGC shows to be lower for earlier Δt_{flash} (Fig. 6.4, i).

Responses of nRGC to nff 7th stimulus are analogous to the just described ones, the only difference is the lack of the flash responses in the new IRPs of the PrC. The missing flash response does not affect the decay evolution of the response to the saccade. The PrC new IRPs are thus still capable of modulating the inhibition on the CC fast-ON IRP.

Responses to nff 1st and 5th are, once again, similar to the ones described above. This time the "active" branch is the ON branch, the PrC new IRP of the OFF branch is zeroed (for more information and illustration see D.7).
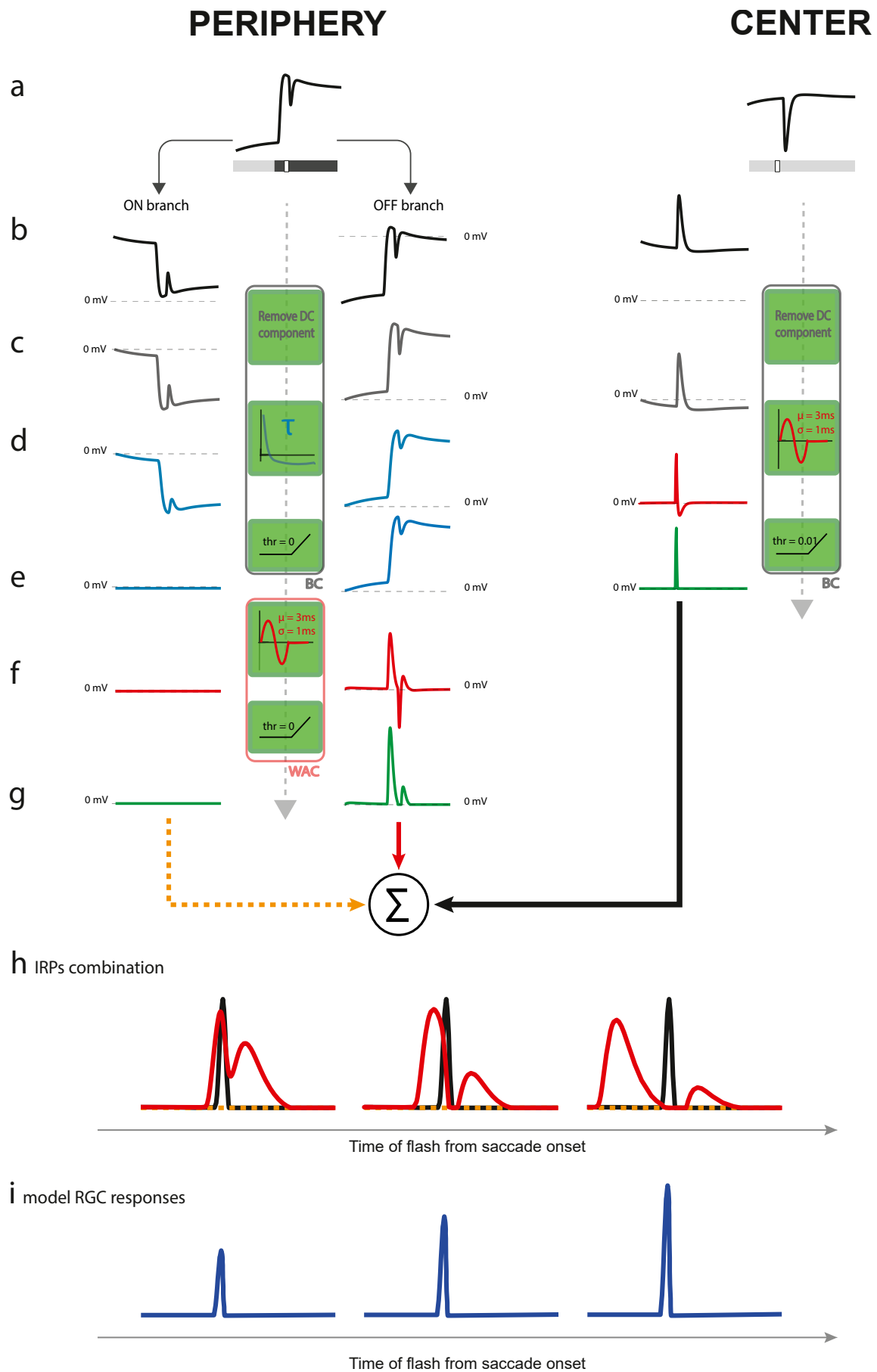
FIGURE 6.4: **GCS timing recreation by means of the model.** The figure shows the creation of the nRGC and how its responses change as a function of Δt_{flash}. *Left*, PrC new IRPs responses to nff 3rd with $\Delta t_{flash} = 500ms$. *Right*, CC fast-ON IRP response to nff 3rd with $\Delta t_{flash} = 500ms$. *Green boxes*, processing blocks. **a**| The modelled outer retina reacts to nff 3rd. The PrC cone reacts both to the saccade and the flash (*black line's* first positive bump and first negative bump). The CC cone reacts only to the flash (*black line's* negative bump). **b**| The potential of the cones of the two compartments is split into the ON and the OFF branches, both of them are cleaned from their baseline (**c**). **d**| *Left*: the responses of the two branches are smoothed with an exponantial kernel with a time constant τ (K_{smooth}, Eq. 5.14) and then nonlinearly thresholded (**e**). The branch opposite in polarity to the presented saccade flattens at zero (**e**, *left*). *Right*: the response of the ON branch is passed through a derivative filter (K_1, Eq. 4.9) and then nonlinearly thresholded (**e**). **f**, **g** | The WACs block. A temporally coarse version of the branch derivatives is obtained via a derivative kernel (K_{WAC}, Eq. 5.16). The resulting response is once again nonlinearly thresholded to avoid negative values. The two peripheral IRPs and the center fast-ON IRP combine together to build the new model RGC (*orange*, *red* and *black arrows*). **h**| The three pathways are shown overlapped to highlight how they combine together in terms of timing. From *left* to *right* increasing Δt_{flash} are used (100, 200 and 500ms). **i**| The resulting new model RGC. From *left* to *right* increasing Δt_{flash} are used (100, 200 and 500ms). Responses to flashes with smaller Δt_{flash} are suppressed.

6.3.2   Global component of suppression: how the model captured the effects

The action timing of the GCS has been found to be one of its main features. The asymmetric model controls the suppression timing of nRGC responses with both the new IRP smoothing filter parameter (i.e., τ) and the WAC block (i.e., μ and σ). To match real GCS timing, one has to act on the asymmetric model by changing these two different features.

We used the MI (Idrees et al., 2020a), to analyze model RGC responses and compare them to real RGCs response behavior. We focused on the main GCS feature (i.e., timing) to fit the model against real data: we changed the smoothing filter time constant τ to achieve the same real data's suppression timing in the model.

What we expected by changing τ was a change in the covered window of suppression. The larger τ, the broader the suppression profile. This would be due to the delay earned by the PrC new IRPs, in respect to the CC fast-ON IRP, during their construction (Fig. 6.4, second green box *left*).

To compare real RGCs suppression profiles (Fig. 2.3) with model predictions we tested the asymmetric model with the same recreated stimuli (nff 1st, nff 3rd, ff 1st and ff 3rd). To simulate the blocking of WACs done in real experiments (i.e., using *SR95531*) we blocked the modelled WACs block in the model.

Since the experimental data were collected from texture displacements protocols, no clear distinction in MI profiles was available between saccades of ON and OFF polarity. To be in line with the experimental data, we then observed the MI profile of the model averaged responses to pairs of stimuli (nff 1st- nff 3rd and ff 1st-ff 3rd).

Global component of suppression timing as the key to fit the model against real data

The GCS acts for earlier times of flash from saccade onset (i.e., until $\Delta t_{flash} \simeq 400ms$). The GCS action timing is constrained and is the key to fit the model RGCs suppression against real RGCs suppression.

To do so we introduced a new suppression index aimed at analyzing how much more suppression focuses on certain time windows than on others. We called it *suppression strength* (*SS*) and it estimates the relative percentage of suppression in various time windows from the saccade onset. It is calculated from the interpolated MI profile over time (Eq. 6.1). $SS < 0$ asserts presence of enhancement in the time window, while $SS > 0$ asserts suppression.

$$SS\Big|_{t_1}^{t_2} = \left(\frac{\int_{t_1}^{t_2} MI dt}{\int_0^{t_f} \mid MI \mid dt} * \frac{1}{t_1 - t_2} \right) * 100 \tag{6.1}$$

With:

- t_1,t_2: extremes of the observation time window.

- t_f: largest Δt_{flash} used.

We calculated SS values from Idrees et al. (2020b) data to fit SS values coming from model simulation tuning τ. (Table 6.1 , Fig. 6.5, a). Model SS values over time windows were calculated as a function of τ.

TABLE 6.1: *SS* values for real data by Idrees et al. (2020b). *SS* values are reported for 7 time windows of obsservation over the entire MI profile. We fitted the model through time windows with non-negligible *SS* values (*green*) . We discarded time windows with negligible or unreliable *SS* values (*red*).

Time window of observation after saccade onset (ms)						
0-100	100-200	200-300	300-400	400-500	500-1000	1000-2000
38	32	11	0.3	-6.3	-7.5	-4.7

SS(%) is in the leftmost label column for the bottom row.

The interpolation (see D.3 for more details) of the real MI profile (Fig. 3.3), and thus SS calculation, was not reliable for larger Δt_{flash} (i.e., $\Delta t_{flash} > 300ms$). This is due to the use, in experiments, of only one probe flash with a great Δt_{flash} (i.e., $500ms$). Thus, we used real data's SS values of only earlier time windows to fit the model suppression profile (i.e., $0 - 100ms, 100 - 200ms, 200 - 300ms$).

We looked for the values of τ that could guarantee a match with real SS values for the different windows of time (Fig. 6.5, c). We found three different likely values for τ: one for each time window considered for the fit (Table 6.2).

TABLE 6.2: τ estimate on real SS values.

Time window (ms)	τ estimate (ms)	Real data's SS (%)
0-100	105	38
100-200	279	79
200-300	79	11

The ultimate value of τ was chosen as conservatively as possible in order to preserve the SS values calculated from real data's MI profile. In fact, we opted for the average of the three values obtained from the fit weighted by their relative SS values obtained from Idrees et al. (2020b) data.

With the fixed value of tau (i.e. $170ms$) we carried out the comparison of the MI profiles coming from real data with the MI profiles derived from model simulations.
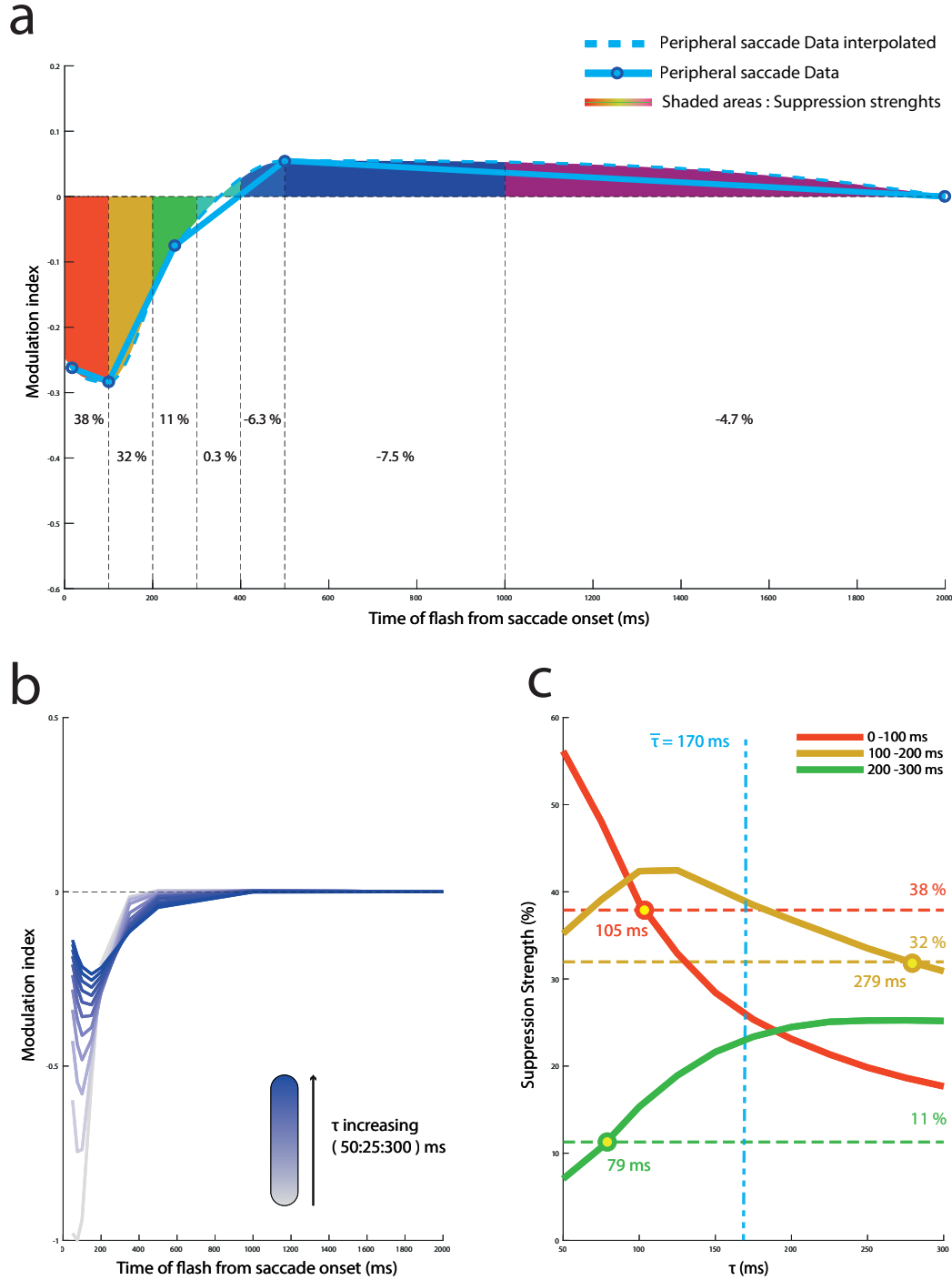
FIGURE 6.5: **The correct GCS timing by means of the model.** **a**| *SS* values of real data. *SS* values (Eq. 6.1) of real RGCs responses to peripheral saccades (Idrees et al., 2020b, *solid light blue line*) were calculated on the interpolated MI profile (*dashed light blue line*). The percentage of the total suppression was calculated in seven different time windows from the onset of the saccade (i.e., $0 - 100ms$, *red shaded area*; $100 - 200ms$, *orange shaded area*; $200 - 300ms$, *green shaded area*; $300 - 400ms$, *cyan shaded area*; $400 - 500ms$, *light blue shaded area*; $500 - 1000ms$, *blue shaded area*; $1000 - 2000ms$, *purple shaded area*). Bottom numbers % indicate the *SS* values of the above-shaded areas. **b**| MI profiles (*blue scale solid lines*) for the nRGC responses varying τ (Eq. 5.14). nRGC responses are intended as the average of the responses to nff 1st and nff 3rd. The darker the blue, the higher the value of the time constant τ (τ varied from 50 to 300 ms in increments of 25 ms). Higher smoothing powers (i.e., higher values of τ leads to weaker MI profile peaks and broader MI profiles. **c**| *SS* values (*y-axis*) in different windows of time for the nRGC, as a function of τ (*x-axis*). Only three windows of time have been reported: $0 - 100ms$, *red solid line*; $100 - 200ms$, *orange solid line*; $200 - 300ms$, *green solid line*. *Horizontal dashed lines* indicate real data *SS* values for each of the three windows of time (colours match **a**). *Yellow spots* stand for the match in *SS* between model and data for each considered window of time ($0 - 100ms$, match for $\tau = 105ms$; $100 - 200ms$, match for $\tau = 279ms$; $200 - 300ms$, match for $\tau = 79ms$). The *vertical light blue dashed line* indicates the weighted averaged value of the time constant τ that best preserves all the three matches (i.e., $\tau = 170ms$).

6.3.3   Global component of suppression timing in real data is captured by the model

Real data MI profiles' timing is captured by the model, except for three slight differences. The model predicted *(i)* a little longer lasting suppression in the peripheral-only saccade case and *(ii)* a little shorter lasting suppression in the full-field saccade case. Moreover *(iii)* it predicted the flattening of the suppression profile in the absence of WACs, instead of the slight enhancement of the earlier flash induced responses shown by data.
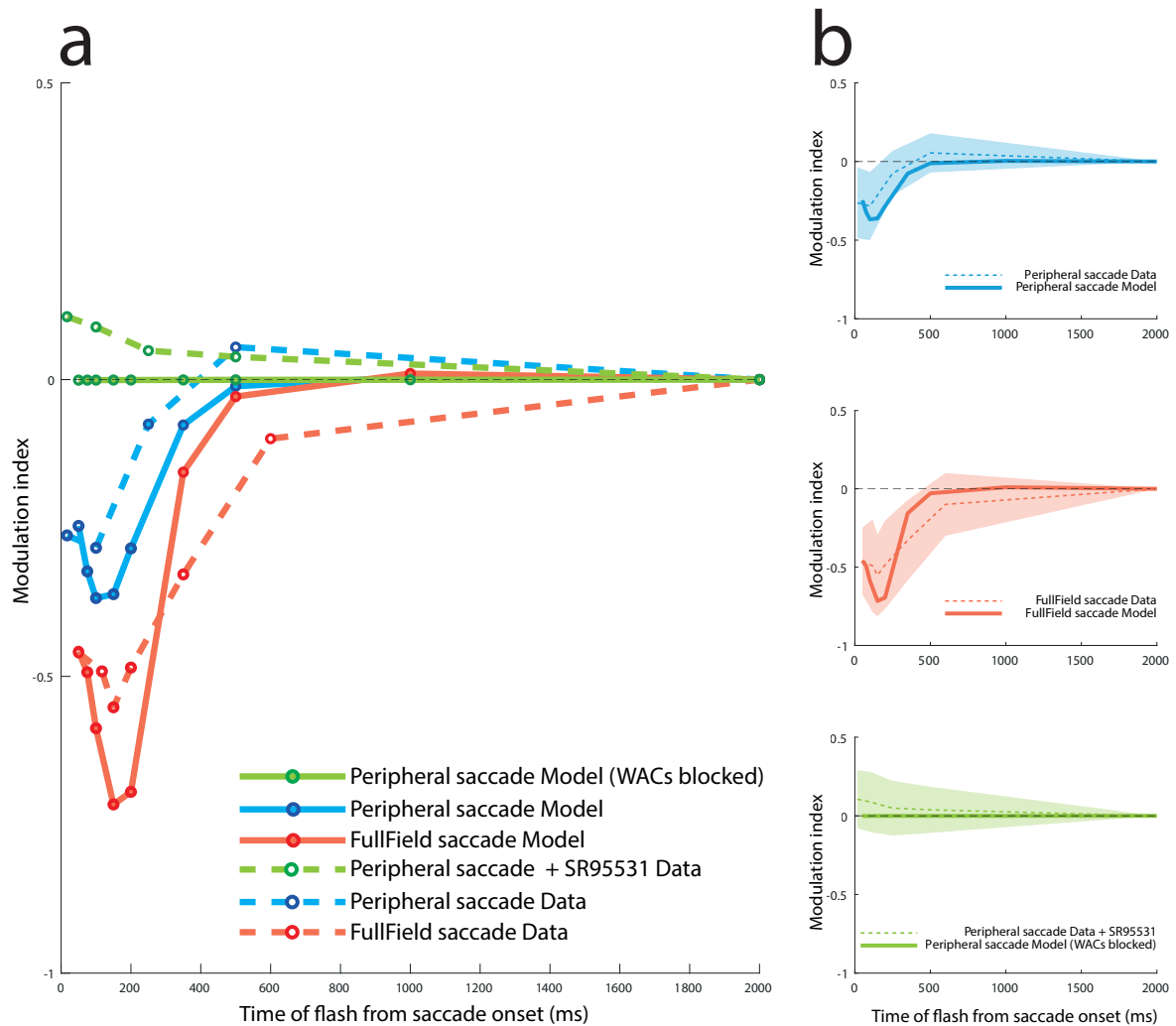
FIGURE 6.6: **Validation of the simulated WACs network**. **a** | Comparison between MI profiles calculated from real data reported by Idrees et al. (2020b) (*dashed lines*) and MI profiles coming from simulated nRGC (*solid lines*). Real data re-plotted from Fig. 3.3 *top* (saccade: texture displacement): *green dashed line*, peripheral saccade + SR95531; *blue dashed line*, peripheral saccade without pharmacology; *red dashed line*, full field saccade without pharmacology. Simulated data show the responses' suppression of nRGC to nff 1st and nff 3rd averaged. τ of the smoothing filter K_{smooth} is set at 170*ms* (Fig. 6.5, c). *Green solid line*, peripheral saccade and block of the modelled WACs network; *blue solid line*, peripheral saccade without blocking the WACs network; *red solid line*, full field saccade without blocking WACs network. The asymmetric model captures the timing of suppression expressed by real data. The difference in suppression's power between the peripheral saccade and the full field saccade is captured by the model. In addition the modelled lack of all the components of suppression (*green solid line*) predicted the lack of suppression also in the simulated responses. **b** | Decomposition of **a**, *shaded areas* indicate the standard deviation (*std*) of real data's MI's profiles. The three different suppression profiles predicted by the asymmetric model (i.e., the three conditions recreated) fall within the *std* expressed by real data.

The first slightly wrong prediction is given by the chosen value of τ. The greater difference between the data and the model could be seen in the $200 - 300ms$ time window, indeed the value of τ chosen is very far from the one that would have guaranteed the fit within

that time range (i.e., 170*ms* vs 79*ms*). Nevertheless, the suppression profile predicted by the model falls within the standard deviation range of real data (Fig. 6.6, b *top*).

The second difference is not a failed prediction actually: real data's suppression profile for full field saccades is influenced by the surround component of suppression (SCS) too. The SCS is not embedded in this formulation of the asymmetric model since it is built to only simulate the functioning of GCS. It is therefore legitimate to accept a mismatch in timing of suppression in the full field saccade case, especially if the model predicted a lack of suppression for later Δt_{flash} (i.e., in the SCS action timing).

The slight enhancement shown by real data if WACs were blocked is not captured by the model. Nonetheless, the model predicted the full lack of suppression when all the three different components of suppression were not supposed to act. In addition, its predicted suppression profile falls within the standard deviation range of real data (Fig. 6.6, b *bottom*). The GCS strength of suppression shown in real data is not fully captured by the model. Real data shows lower suppression peaks than the ones the asymmetric model predicted. Nevertheless, the difference in suppression between the peripheral-only case and the full field case shown by real data seems to be preserved by the model. The full-field case provokes greater suppression of responses for earlier delays both in real data and in the model (Fig. 6.6, a). This proves, once again (Idrees et al., 2020a), that the model already embeds the CCS. This is given by the model's nonlinear processing steps downstream from the cone response.

The fact that for recreating the right GCS timing it was necessary to adjust the smoothing power (i.e., τ) of the newly introduced model BC is food for thought. It is in fact essential that the new model BC extracts particular features from the temporal evolution of the upstream cone in the RF periphery. These features (i.e., the right timing of the decay of the saccade response) are then passed to the RF center through the fast WACs network.

It is therefore possible to assume that the WACs, in order to ensure the correct timing of suppression in the RF center, selectively synapse certain types of BCs. Such bipolar cell types would appear to be sustained BCs of both ON and OFF polarities.

6.4   Horizontal cells network as mediator of the surround component of suppression: model and experiments

Real RGC responses showed retinal saccadic suppression (RSS) for later Δt_{flash} (Idrees et al., 2020a). This effect is led by the surround component of suppression (SCS, see 3.2.1) whose bases hypothetically reside in the spread HCs network in the OPL.

To see if HCs network could be involved in RSS, we built a simple model that could simulate the role of HCs network in the retina, the asymmetric model (see 5.2.2). With the asymmetric model we wondered if we could develop intuitions about the potential involvement of HCs network as mediators of SCS.

To do so we "interrogated" the model with the saccade&flash protocol in two conditions:

1. HCs network activated (*CTRL condition*).

2. HCs network inactivated (*PSEM condition*).

Since we hypothesized the HCs network as the source of the SCS we expected no suppression of RGC responses in the PSEM condition.

In addition, we wondered if we could simulate SCS strength as a function of the size of the receptive field surround size. To do so we presented to the model the saccade&flash protocol varying the modelled influence strength of the RF surround onto the RF center (i.e. varying $\alpha_{hh,cs}/\alpha_{hh,sc}$, see 5.2.2). Given the definition of center-surround antagonism seen in Chapter 2 (see 2.2) we expected the SCS to be stronger for higher RF surround's influences. To make predictions about the response behavior of real RGCs we used the MI (Idrees et al., 2020a) on model RGC responses. We used the temporal model's modelled RGCs introduced in Drinnenberg et al. (2018) without adding the nRGC described in Chapter 5 (see 5.3.2). It was not added to the prediction's tools since it was built to show the GCS effects, not the desired SCS ones.

In addition, to evaluate the potential role of HCs network in RSS, we built a new experimental protocol (see 6.4.2). We ran both pharmacological and control experiments on mice to see if the HCs could mediate the SCS and to compare model's predictions with real data.

6.4.1   The role of horizontal cells in the surround component of suppression: the predictions of the asymmetric model

Before testing the asymmetric model with the saccade&flash protocol we made sure the PSEM condition caused the same effects Drinnenberg et al. (2018) found. We presented to the asymmetric model once again the light steps of increasing contrast stimulus. We added the nRGC described in the previous section just to verify that its response would not be changed in the PSEM condition. For all the other modelled RGCs we looked for the same temporal model predictions (see 4.3, Fig. 4.6).

All the modelled cells of the temporal model continued giving the same predictions on the "increasing contrast steps" stimulus if simulated with the asymmetric model (Fig. 6.7). The nRGC does not predict any PSEM effect, it is in line with what we hypothesized.

Confident that the asymmetric model continued to predict PSEM effects for full field stimuli, we tested the model with saccade&flash protocol. We were most interested in the nff 1st-4th stimuli since they would potentially permit to isolate only the SCS, leaving the GCS and the CCS silent.

Model predictions declare that the HCs network showed its impact in four *(i,ii,iii,iv)* different model RGC types, using two different stimuli (nff 1st, nff 4th). In addition, the model predicted that the strength of the HCs network in the influence of the RF surround on the RF center changes as a function of the relative size between the two *(v)*.

Cone Potential (baseline removed)

Ganglion Cell spike rate
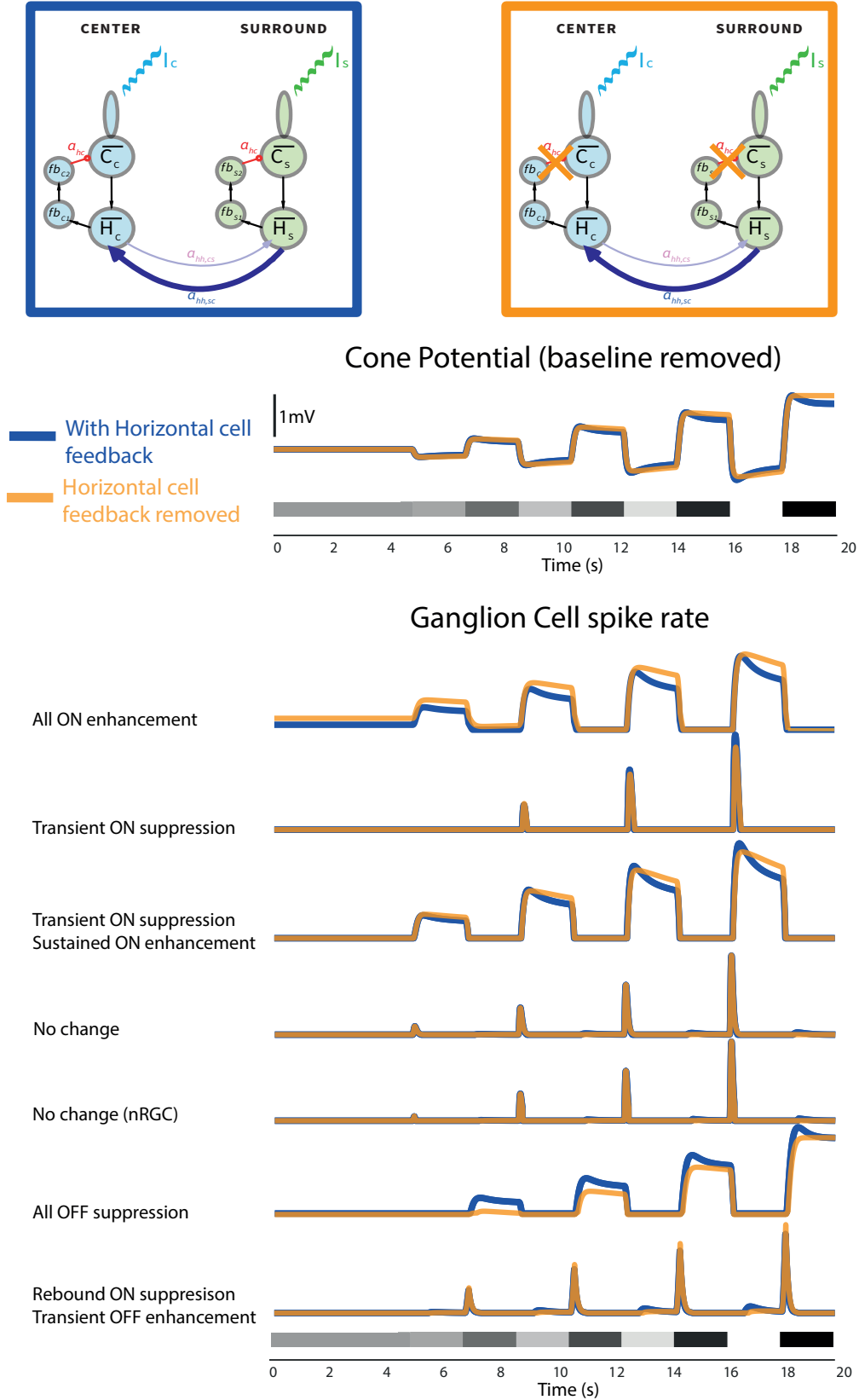
FIGURE 6.7: **The asymmetric model keeps capturing PSEM effects on RGCs responses to full field stimuli**. The asymmetric model has been tested with the same stimulus used by Drinnenberg et al. (2018) to validate the temporal model. The image is made along the lines of Fig. 4.6, IRPs have been omitted in this case. **Top**| simulated cone potential without baseline in presence (*blue*) and absence (*orange*) of horizontal cell feedback, schematics of the asymmetric model's outer retina in the two conditions are shown at the *very top* of the figure. **Bottom**| Asymmetric model's simulated RGCs spike rates for the six PSEM-induced effects found by Drinnenberg et al. (2018) , the new model RGC was added too (5th row). The nRGC, as expected, does not show any PSEM induced effect. The other six cells that had already been simulated with the temporal model show the exact same behaviors if simulated with the asymmetric model (1st,2nd,3rd,4th,6th,7th rows). *Gray shaded rectangles* indicate stimulus contrast changes.

***(i):* HCs network guarantees suppression of later responses to nff 1st in sustained ON-RGCs**   The simulate blocking of the HCs network seems to avoid the suppression of sustained ON-RGCs responses shown by the CTRL condition for later Δt_{flash} (stimulus presented: nff 1st).

This effect is present in all the three sustained ON model RGCs derived from three different combinations of IRPs (Drinnenberg et al., 2018, Fig. 4.6). We will call these three model RGCs 1st, 2nd and 3rd RGC.

All the three modelled RGCs showed a non-negligible suppression of the responses for later Δt_{flash}. In the PSEM condition, this suppression disappears.

The CTRL induced change of baseline in the cone response (which is missing in the PSEM condition, Fig. 6.8, a *right*) due to the surround saccade, causes the modulation of the model RGC responses downstream. The closer the surround compartment's (SC) saccade response steady-state, the greater the center compartment's (CC) induced change of baseline. This causes greater modulations of responses for larger Δt_{flash} and smaller for earlier Δt_{flash}.

The nff 1st stimulus provokes opposite changes in the baselines of the cone nodes of the CC and the SC. Before the hyperpolarization caused by the flash, the saccade causes a strong hyperpolarization in the SC cone and a slight depolarization in the CC cone (Fig. 6.8, a *left*). Flash induced responses for later Δt_{flash} start from a higher baseline value and can't reach as large negative values as responses to earlier Δt_{flash} or PSEM responses.

Since 1st, 2nd and 3rd RGCs are combinations of slow and intermediate IRPs (Fig. 4.6), model RGC flash induced responses reflect cone evolution's amplitude and their responses to later Δt_{flash} are smaller than for earlier Δt_{flash} or for the PSEM (Fig. 6.8, c).

It seems that the network of HCs leads to RGCs adaptation to luminance. A lasting saccade of the same polarity of the flash on the SC causes, via the network of HCs, a lower amplitude of center compartment's RGC responses to the flash. As if the center had memory of an unseen stimulus.

This memory increases its power if the saccade-like stimulus on the surround is shown for a long time before the center receives the flash (i.e., for larger Δt_{flash}).

FIGURE 6.8: **PSEM deletes flash induced responses' modulation of suppression in sustained ON cells**. Modulation of flash induced responses' suppression in the 1st modelled RGC.

Valid for **a,b,c** : *solid lines* show responses of model cells of the center compartment (CC) to surround-only ON saccade + full field ON flash ("test case"). Dashed lines show responses of model cells of the CC to surround-only ON saccade without any flash ("baseline case"). For all the colour scales, the darker the color, the closer the flash to the saccade onset (Δt_{flash}: $100, 200, 400, 600, 800, 1000, 2000 ms$). For **a,b,c** *left* panels present CTRL condition, right panels present PSEM condition.

a| Schematic of the presented stimulus (*top*). Model CTRL cone evolution changes with different Δt_{flash} (*red scale solid lines*). The CTRL condition shows a change in the baseline due to the presence of a saccade in the surround (depolarization). The PSEM cone does not feel the presence of the surround saccade as a result of the lack of inhibition feedback from modelled HCs onto cones. Thus the PSEM cone evolution is flat except for the flash induced response.

b| Single simulated ON sustained RGC responses to the test case (*blue scale solid lines*) with superimposed responses to the baseline case (*blue scale dashed lines*).

c| Overlapped flash induced responses (*testCase − baselineCase*) of the simulated ON sustained RGC to different Δt_{flash} (*purple scale solid lines*). Modulation of suppression, as a function of the time of flash from saccade onset, for the CTRL condition (*solid black line*) and the PSEM condition (*solid orange line*). *Grey bar* indicates saccades onset, *white rectangles* indicate times of flash.

The CTRL condition shows suppression for later Δt_{flash} if compared to the PSEM condition. Little changes in the cone responses (**a**) leads to magnified effect downstream. ($\alpha_{hh,sc}/\alpha_{hh,cs} = 3 * 10^3$)

(ii): HCs network guarantees enhancement of later responses to nff 4th in transient OFF-RGCs   The lack of the HCs network causes the flattening of the suppression profile shown by model transient OFF-RGC in response to nff 4th.

This effect is present in one model transient OFF-RGC derived from a combination of IRPs (Drinnenberg et al., 2018). We will call this model RGCs 4th RGC.

The 4th RGC showed a non-negligible enhancement of the responses for later Δt_{flash}. In the PSEM condition, this enhancement disappears.

This time the OFF saccade in the SC causes a slight hyperpolarization on the CC cone in the CTRL condition. The evolution of the PSEM cone baseline is not affected by any saccade induced changes (Fig. 6.9, a *right*).

The change of Δt_{flash} results in indetectable variations at the CTRL cone level, they are captured and amplified by IRPs which mirror the magnified variations to RGCs. RGCs responses appear, thus, modulated in amplitude as a function of Δt_{flash}.

The 4th RGC is a combination of fast and intermediate IRPs, as such it can detect the above-mentioned variations. RGCs responses to later Δt_{flash} appear to be enhanced in the CTRL condition, if compared to responses to earlier Δt_{flash} or PSEM responses (Fig. 6.9, c).
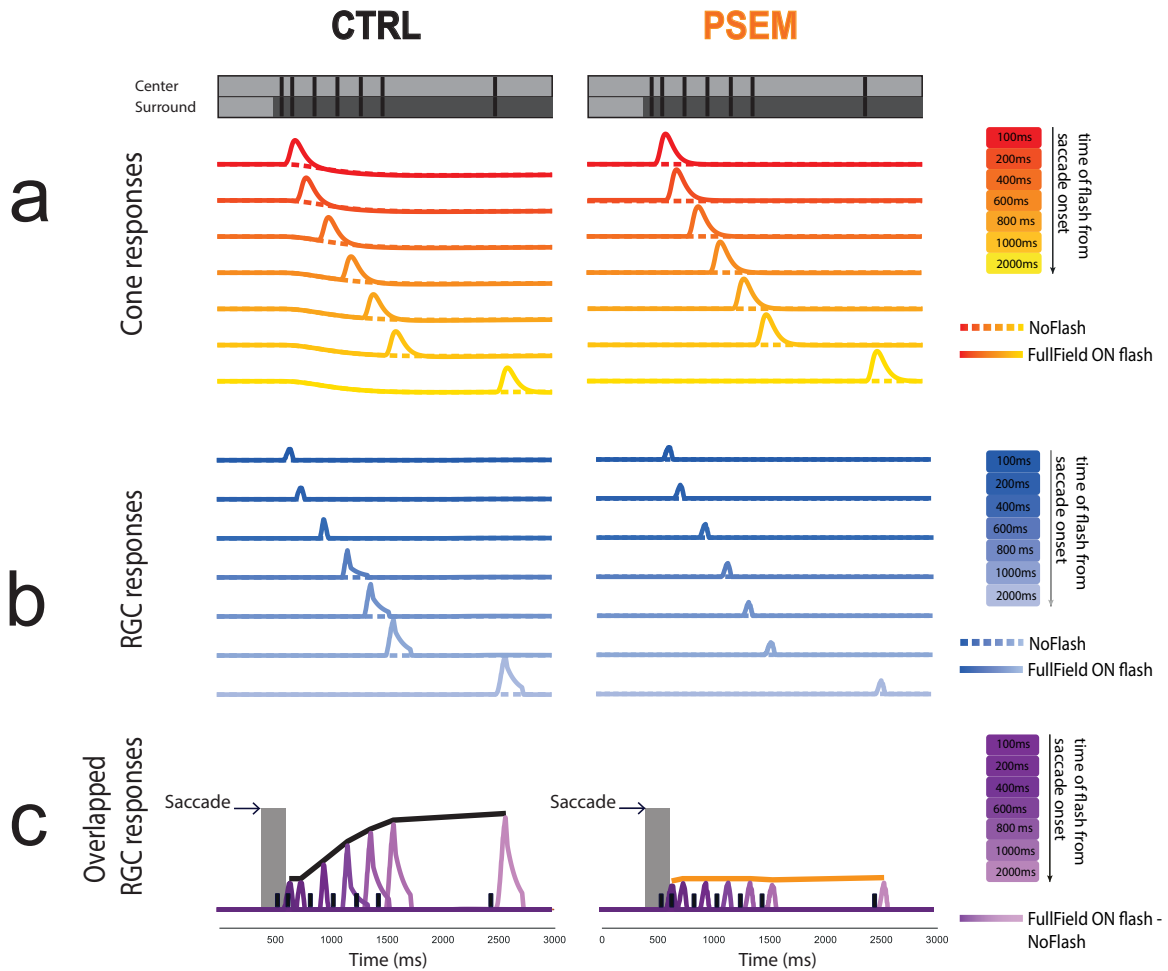
It seems that the network of HCs increases center RGCs responsiveness. A surround stimulus of the same polarity of the flash causes, via the network of HCs, a higher responsiveness of CC RGC responses to the flash. As if the center were already prepared to receive a stimulus of the same polarity. The responsiveness increases by enlarging the lag between the surround saccade-like stimulus and the flash (i.e., for larger Δt_{flash}).
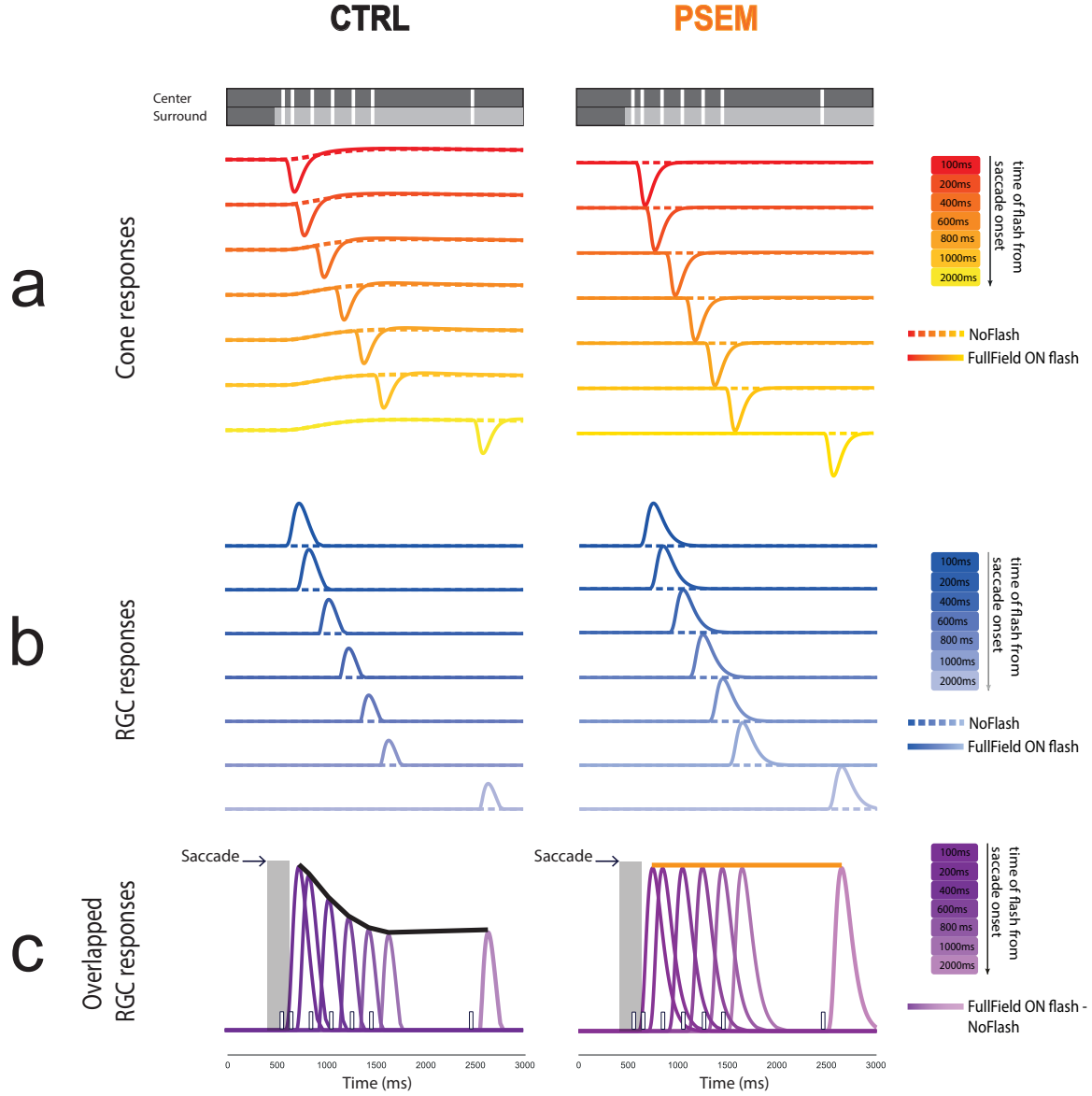
FIGURE 6.9: **PSEM deletes flash induced responses' suppression in transient OFF cells**. Modulation of flash induced responses' suppression in the 4th modelled RGC (i.e., transient OFF-RGC). Same as Fig. 6.8 with a different stimulus presented (schematic in **a**, *top*): *solid lines* show responses to surround-only OFF saccade + full field OFF flashe ("test case"), dashed lines to surround-only OFF saccade without any flash presented ("baseline case"). **a**| The CTRL condition shows a change in the baseline due to the presence of a saccade in the surround (hyperpolarization). The PSEM cone does not show any changes over different Δt_{flash}, the PSEM condition does not allow the center cone to perceive the saccade on the surround. **b**| Simulated transient OFF-RGCs responses to the test and baseline cases (*blue scale solid and dashed lines*). **c**| The flash induced responses (*testCase − baselineCase, purple scale solid lines*) are enhanced for later Δt_{flash} in the CTRL condition (*solid black line*), while they are unmodulated in the PSEM condition (*solid orange line*). ($\alpha_{hh,sc}/\alpha_{hh,cs} = 3 * 10^3$)

(iii): HCs network guarantees suppression of later responses to nff 4th in sustained OFF-RGCs The network of HCs (i.e., CTRL condition) leads to suppression of sustained OFF-RGCs later flash-induced responses to nff 4th. The blocking of the HCs network (i.e., PSEM condition) leads to lack of modulation of model RGCs responses.

This effect is present in one of the model sustained OFF-RGC (Drinnenberg et al., 2018), we will refer to this model RGC as 5th RGC.

The results are analogous to the *(i)* effect, this time sustained cells of the OFF polarity, instead of ON polarity, are involved. The working mechanism is the same seen in *(i)*: a saccade of the same polarity of the forthcoming flash causes a sort of adaptation to the same flash. Interestingly, the cone response has the same evolution of *(ii)* since the stimulus shown is still nff 4th (Fig. 6.10, a). But this time the modulation of the model RGC responses downstream is diametrically opposite to that seen in *(ii)* (Fig. 6.10, c). Same changes in the cone evolution are captured and processed differently by sustained and transient model RGCs.

FIGURE 6.10: **PSEM deletes flash induced responses' modulation of suppression in sustained OFF cells**. Modulation of flash induced responses' suppression in the 5th modelled RGC (i.e sustained OFF-RGC), the stimulus presented is surround-only OFF saccade + full field OFF flash (**a**, *top*).
Same as Fig. 6.8 - 6.9: *solid lines* show responses to surround-only OFF saccade + full field OFF flash ("test case"), dashed lines to surround-only OFF saccade without any flash presented ("baseline case").
a| The CTRL condition shows the very same evolution seen in Fig. 6.9, the presented stimulus is the same indeed. The PSEM cone does not does not show any changes over different times of flash from saccade onset.
b| Simulated sustained OFF-RGCs responses to the test and baseline cases (*blue scale solid* and *dashed lines*). Although the cone responses are the same of figure Fig. 6.9 a, the different model processing parameters give rise to completely different RGC evolution (Fig. 6.9, b vs Fig. 6.10, b).
c| The flash induced responses (*testCase − baselineCase, purple scale solid lines*) are suppressed for later Δt_{flash} in the CTRL condition (*solid black line*), while they are unmodulated in the PSEM condition (*solid orange line*). ($\alpha_{hh,sc} / \alpha_{hh,cs} = 3 * 10^3$)

The saccade in the surround leads to greater adaptation the longer it is shown before the flash onset (i.e., for later Δt_{flash}), this adaptation results in weaker but more abrupt responses to flashes in the CTRL. The lack of HCs network (i.e., PSEM condition) does not permit light adaptation, thus the RGCs responses are not modulated.

(iv): **HCs feedback onto cones guarantees delayed suppression of responses to ff 1st in transient ON-RGCs**   Inhibitory feedback from HCs onto cones (i.e., CTRL condition) causes a slight suppression of RGC responses for *600-1000ms* Δt_{flash}. The lack of inhibitory feedback onto cones (i.e., PSEM condition) makes the slight suppression vanishing (Fig. 6.11, c).
This effect is present in one of the model RGC by Drinnenberg et al. (2018), we will call this model RGC 6th RGC.
The ff 1st stimulus, since it is full field, does not engage the effect of the HCs network in the model. For this reason, the only effect given by the lack of HCs is the lack of inhibitory feedback onto cones.

The local inhibition feedback from HCs plays a dominant role: it sharpens the evolution of the saccade response (Fig. 6.11, a); this reflects in the modulation of the subsequent superimposed flash induced response (Fig. 6.11, b). The lack of inhibition feedback from HCs (i.e., PSEM condition) does not allow the onset of modulation of the flash-induced responses during the recovery phase of the saccade-induced response.
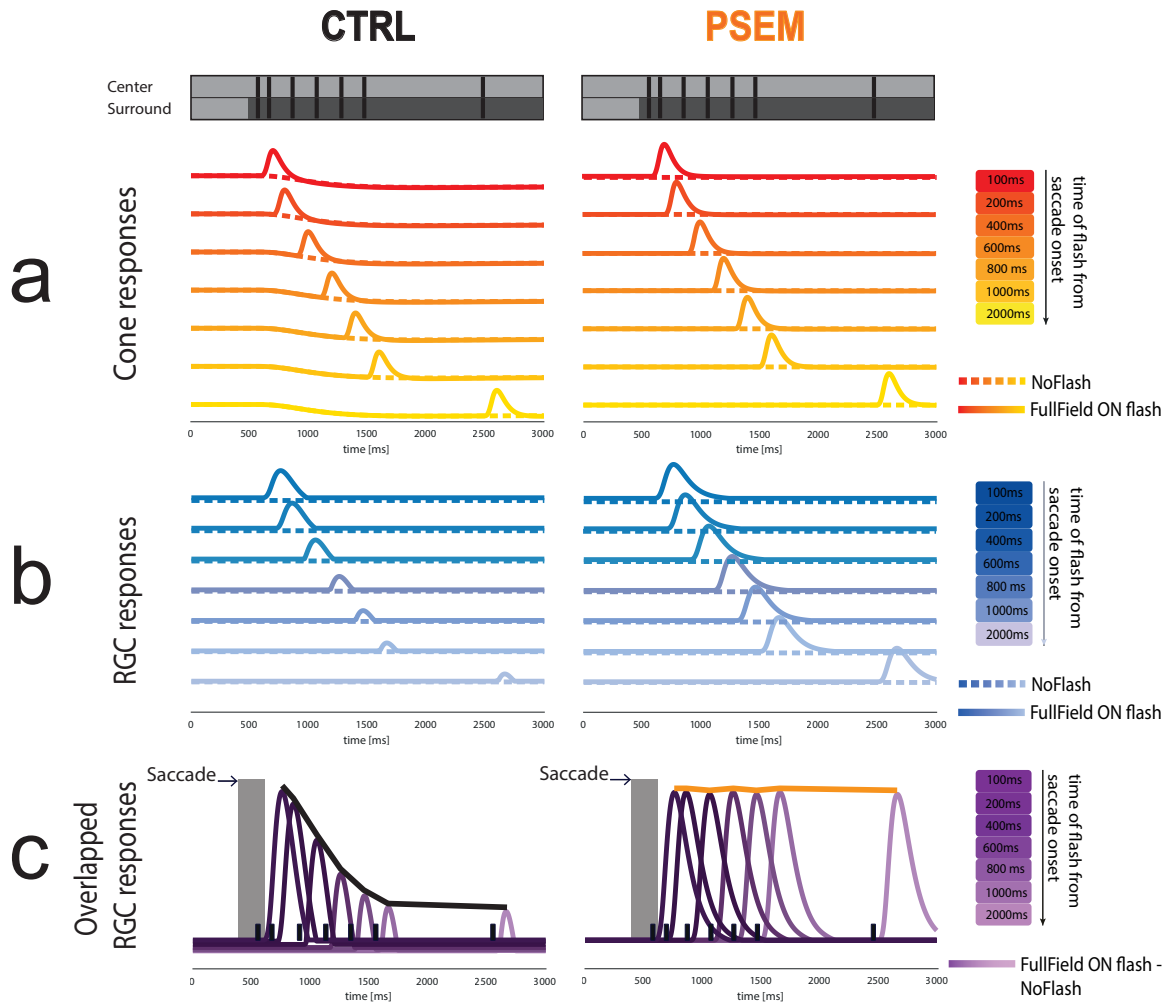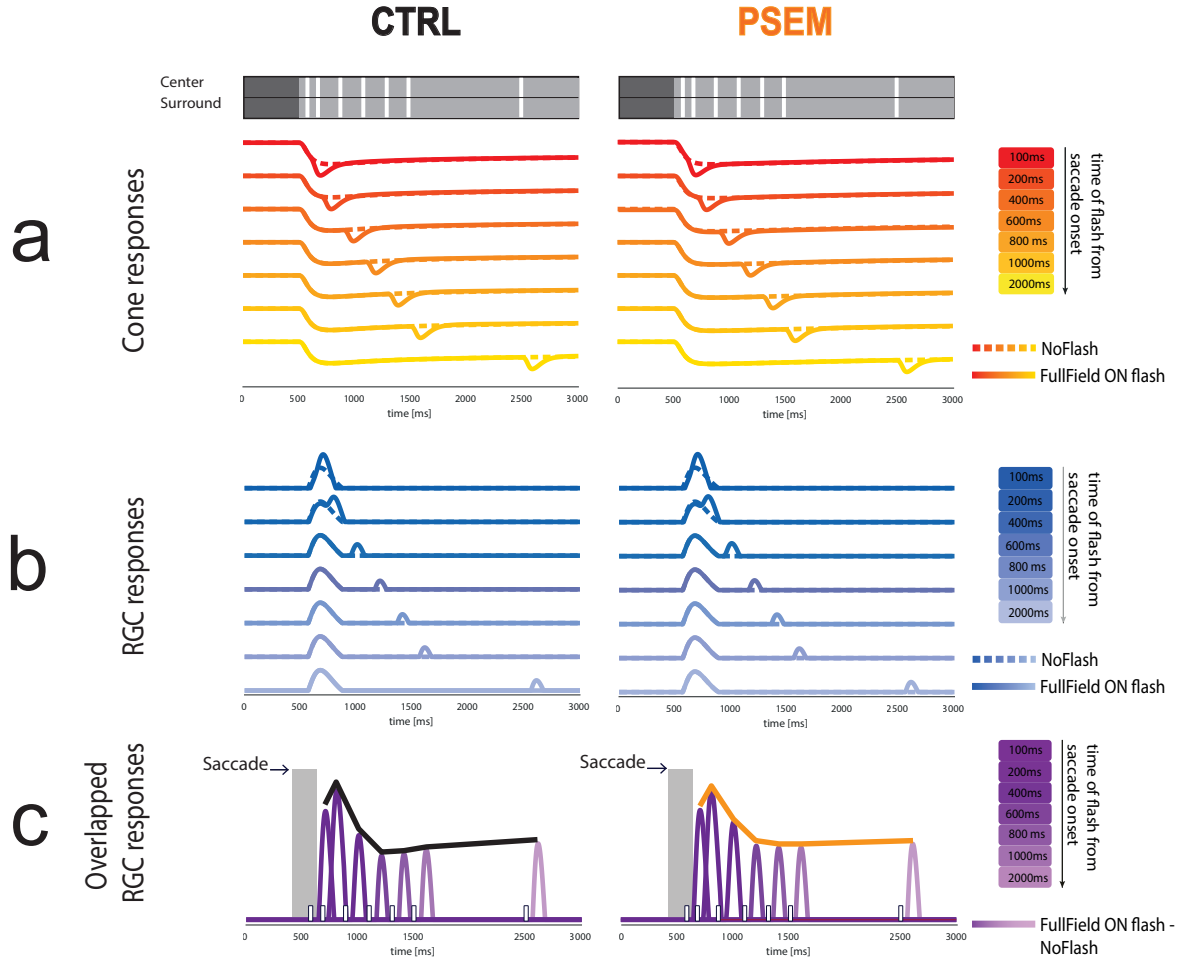
FIGURE 6.11: **PSEM deletes flash induced responses' delayed suppression in transient ON cells**. Modulation of flash induced responses' suppression in the 6th modelled RGC (i.e., transient ON-RGC), the stimulus presented is a full field ON saccade + full field ON flash (**a**, *top*).
Same as Fig. 6.8 - 6.10: *solid lines* show responses to full field ON saccade + full field ON flash ("test case"), dashed lines to full field ON saccade without any flash presented ("baseline case").
a| The CTRL condition shows a higher recovery rate if compared to the PSEM condition, this is due to the presence of the inhibition feedback from HCs onto cones.
b| Simulated transient ON-RGCs responses to the test and baseline cases (*blue scale solid* and *dashed lines*). The dissimilarities across the different responses to the flashes are hard to see, this is due to the superimposition (*blue scale solid lines*) of the flash induced response and the saccade induced response (*blue scale dashed lines*).
c| The flash induced responses (*testCase − baselineCase*, *purple scale solid lines*) show an initial enhancement in both the CTRL and PSEM condition ($\Delta t_{flash} = 100, 200, 400ms$). Nevertheless the responses appear to be suppressed for later Δt_{flash} (i.e., 600, 800 ms) in the CTRL condition (*solid black line*), while they are unmodulated in the PSEM condition (*solid orange line*). ($\alpha_{hh,sc}/\alpha_{hh,cs} = 3 * 10^3$)

***(v)*: HCs network strength in modulating RGC responses depends on the relative size between the RF center and surround** HCs network strength in modulating the downstream responses of RGCs varies by changing the modelled relative size of the RF surround and the RF center.

As explained in 5.2.2, we modeled the relative variation in size between RF surround and RF center by changing the ratio of gain terms that establish the intercompartmental connection (i.e., changing $\alpha_{hh,sc}/\alpha_{hh,cs}$).

We used five different ratio's values increasing it from 0.3 to $3 * 10^6$, thus starting from a modelled little more numerous center compartment's set of cones and ending with a significantly more numerous surround compartment's set of cones.

HCs network power in the modulation of 1st, 2nd, 3rd, 4th and 5th RGCs responses changes by varying $\alpha_{hh,sc}/\alpha_{hh,cs}$. Specifically in *(i)*, *(ii)* and *(iii)* the increase of RF surround size (i.e.,

the increase of the ratio) leads to stronger modulations of RGCs responses (Fig. 6.12). What is of particular interest is that the upper limit of the RF surround influence onto the RF center (6.2) is captured by the model. The influence of the surround compartment onto the center compartment is superiorly bound. It is as if only a part of the cells in the RF surround could have a role in influencing the RF center via the modelled HCs network.
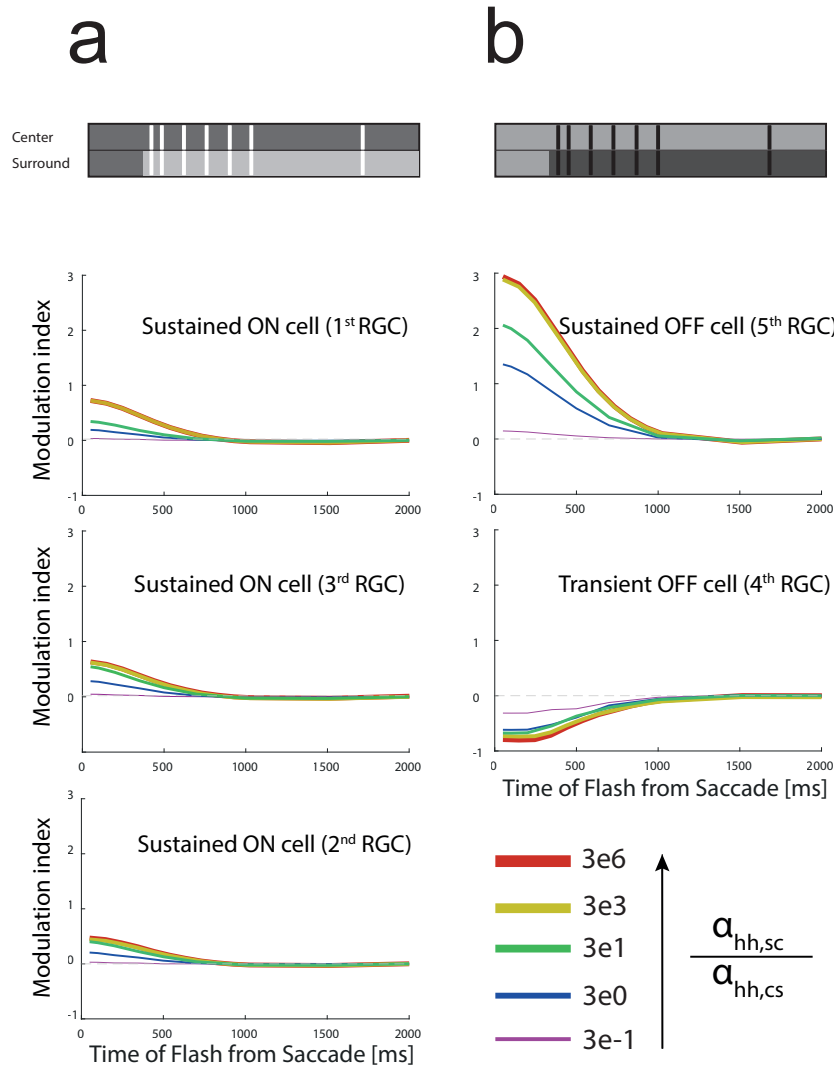
FIGURE 6.12: **The suppression profile of the model RGCs changes varying the surround influence's strength onto the center compartment**. MI profiles of modelled RGCs responses to surround-only ON saccade + full field ON flash (schematic, **a** *top*) and surround-only OFF saccade + full field OFF flash (schematic, **b** *top*). $\alpha_{hh,sc}/\alpha_{hh,cs}$ varies across simulations of the model (0.3, *purple*; 3, *blue*; 30, *green*; $3*10^3$, *yellow*; $3*10^6$, *red*).
The effect of the SC onto the CC RGCs responses modulates according to the SC size (i.e., according to $\alpha_{hh,sc}/\alpha_{hh,cs}$, Fig. 5.2, a). In particular, the larger the modelled RF surround (i.e., the larger $\alpha_{hh,sc}/\alpha_{hh,cs}$), the stronger the effects seen in Fig. 6.8 -6.10, c. However, the increase in the effects is not infinite: no particular changes could be noticed changing $\alpha_{hh,sc}/\alpha_{hh,cs}$ from $3*10^3$ to $3*10^6$ (*yellow* and *red lines*). Some cells show saturation of modulation effects even for smaller values of $\alpha_{hh,sc}/\alpha_{hh,cs}$ (i.e., 3, *green lines* in 2nd, 3rd and 4th RGCs).

The presence of the flash in the RF surround does not influence the modulation effects on responses of the RF center   We wondered if the HCs network would lead to the same effects in modulation of responses (*(i)*, *(ii)*, *(iii)*) if no flashes were presented to the SC (i.e., nff 5th and nff 8th stimuli).

The model's predictions were the same described in the previous sections: the presence or not of a flash in the surround too does not influence the amount and the timing of suppression led by the HCs network (Fig. 6.13). Model RGC in the CC have their flash induced responses suppressed just as to the previous cases.
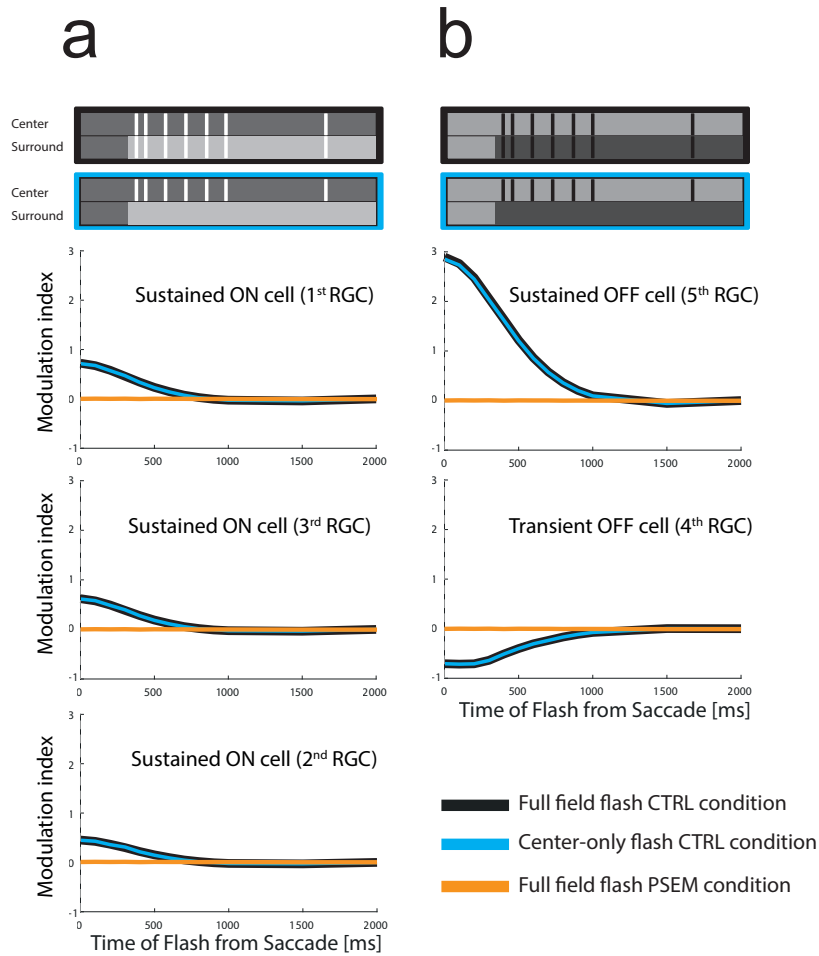
FIGURE 6.13: **Presenting or not the flash on the surround compartment does not change the modulation of RGCs responses in the center. a**| *Top*: schematic of the two stimuli presented to the model: surround-only ON saccade + full field ON flash (*black rectangle*) and surround-only ON saccade + center-only ON flash (*light blue rectangle*). MI profiles of three (1st, 2nd, 3rd) modelled sustained ON-RGCs in the CC to full field ON flashes (*solid black lines*), center-only ON flashes (*solid light blue lines*) and PSEM condition (*solid orange lines*). The presence or not of the flash on the surround compartment does not affect the MI profile.
b| *Top*: schematic of the two stimuli presented: surround-only OFF saccade + full field OFF flash (*black rectangle*) and surround-only OFF saccade + center-only OFF flash (*light blue rectangle*). MI profiles of modelled sustained OFF-RGCs (4th, 5th) and transient OFF-RGCs in the CC to full field OFF flashes (*solid black lines*), center-only OFF flashes (*solid light blue lines*) and PSEM condition (*solid orange lines*). As in **a**, presenting or not the flash on the surround compartment does not affect the modulation of responses. ($\alpha_{hh,sc}/\alpha_{hh,cs} = 3 * 10^3$)

6.4.2   The role of horizontal cells in retinal saccadic suppression: experiments. Was the model right?

HCs network involvement in retinal saccadic suppression (effects *(i)*, *(ii)*, *(iii)*) and HCs network varying strength depending on the size of the RF surround (effect *(v)*) have been predicted by the asymmetric model.

To validate these predictions, we ran real experiments. We designed a new experimental protocol that could highlight HCs network engagement in RSS and could allow analyzing the RF surround influence onto the RF center depending on their relative size.

To see if the HCs network was actually involved in RSS, we ran pharmacological experiments on mice with chemogenetically perturbed HCs.

To highlight the influence of the RF surround onto the RF center depending on their sizes we built a new light stimulation protocol, we called it *circular saccade suppression protocol* (**CSS**).

How to elicit a varying influence's strength of horizontal cells in retinal saccadic suppression: the light stimulation protocol

CSS is a two-compartment stimulus, it consists in a background rectangle with a superimposed annulus in the middle, the non-overlapping part constitutes one compartment (compartment S) while the central annulus forms the other compartment (compartment C). We will refer to compartment C as *stimulus center compartment* and compartment S as *stimulus surround compartment*.

The stimulus center compartment can change its size throughout the protocol (i.e., the central annulus can assume three different diameters), thus the stimulus surround compartment changes its size too. The change in relative size of the two compartments leads to the inclusion of different numbers of cells in the same compartments over the trials of the protocol. The bigger the size of the stimulus center compartment the smaller the number of cells sitting in the stimulus surround compartment. Thus, the smaller the influence of the whole surround compartment on the center compartment.

In this way we wanted to bring to reality different simulated $\alpha_{hh,sc}$, $\alpha_{hh,cs}$ ratios: smaller sizes of the stimulus center compartment stay for smaller $\alpha_{hh,sc}/\alpha_{hh,cs}$, greater sizes of the stimulus surround compartment stand for greater $\alpha_{hh,sc}/\alpha_{hh,cs}$.

We treated the two compartments as separated: the saccade-like stimulus (i.e., step), either bright or dark, was presented in the stimulus surround compartment only. The flash, bright or dark as well, was presented in both the compartments simultaneously with different delays from the surround saccade onset (i.e., Δt_{flash}) (see A.2 for more details) (Fig. 6.14).

The varying influence's strength of horizontal cells in retinal saccadic suppression: experimental results and comparison with model predictions

To evaluate the HCs network engagement in retinal saccadic suppression predicted by the model, we ran CSS on isolated retinas of 3 wild type (WT) mice and 3 PSAM-injected mice (see C.1 for more details) and recorded the ganglion cell activity. We based the comparison of real data and model predictions on the MI profile (Idrees et al., 2020a).

We ran 6 experiments (11 CTRL configurations, 5 PSEM configurations). RGCs spiking activity was recorded with HD-MEA (see A.4 for more details), it was then spike sorted to identify all the units and their firing rates (see D.5 for more details).

All the sorted cells were filtered based on their responses' quality (see B.3 for more details). We isolated cells that were sitting on the stimulus center compartment for all the three different sizes of the central annulus (see C.1 for more details) and divide them in four cell types (transient ON-RGCs, sustained ON-RGCs, transient OFF-RGCs, sustained OFF-RGCs) to target the desired effects separately (see B.2 for more details). For each cell type obtained, we
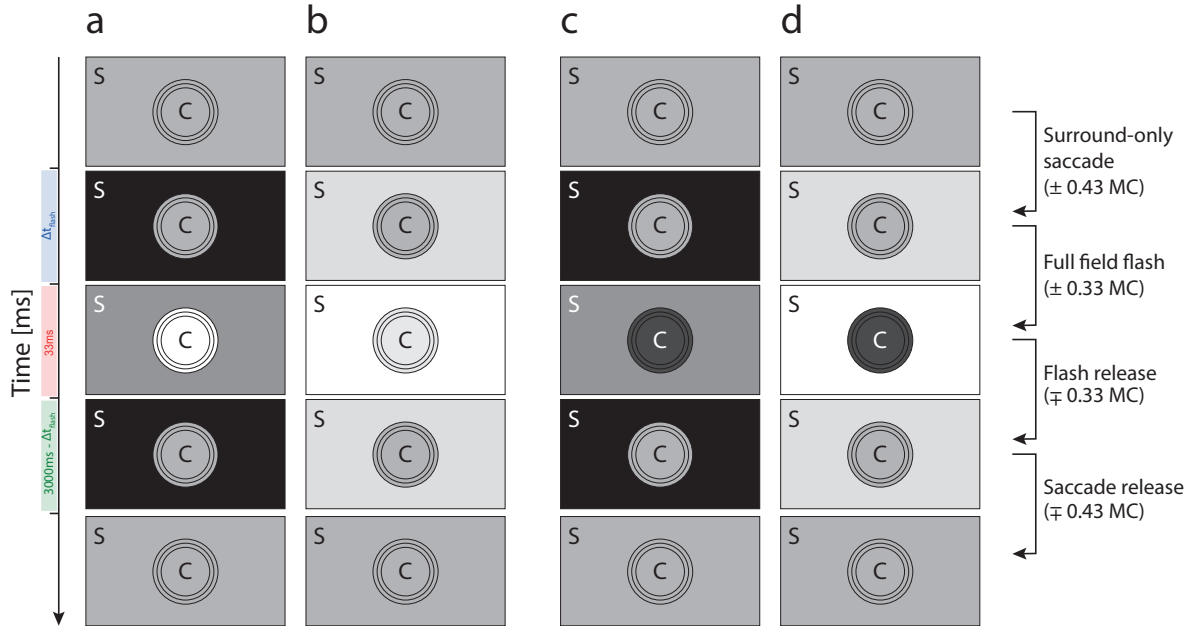
FIGURE 6.14: **The circular saccade suppression protocol**. The circular saccade suppression protocol is a light stimulation protocol in which the stimulus is multicompartmental. In particular the stimulus is divided in two main compartments : the stimulus center compartment (C) and the stimulus surround compartment (S). The stimulus center compartment is an annulus whose diameter changes across trials (diameter : $500, 600, 700\mu m$). The stimulus surround compartment is obtained by the non-overlapping area of a rectangle and the stimulus center compartment. The two compartments are treated separately and have a different temporal evolutions (time line *extreme left*).

Both C and S start from the same luminance level (i.e., grey: first row **a**, **b**, **c**, **d**). S changes its luminance's value toward darker or brighter values (i.e., $\pm 0.43MC$: second row **a**, **b**, **c**, **d**). This change is aimed at simulating the saccade. Across trials $100, 300, 600, 800, 1000$ or $2000ms$ after the saccade both S and C change their luminance level simultaneously toward darker or brighter values (i.e., $\pm 0.33MC$: third row **a**, **b**, **c**, **d**). This change in contrast establishes the presentation of the flash. The flash is released after $33ms$ (fourth row **a**, **b**, **c**, **d**), both C and S regain the previous luminance levels. $3s$ after the first change in contrast of the stimulus surround compartment the same compartment resets its initial luminance level (fifth row **a**, **b**, **c**, **d**). Different stimulus combinations, depending on the positive or negative change in contrast of both the simulated saccades and flashes, can be designed. **a**| Surround-only OFF saccade + full field ON flash. **b**| Surround-only ON saccade + full field ON flash. **c**| Surround-only OFF saccade + full field OFF flash. **d**| Surround-only ON saccade + full field OFF flash.

then observed the cellular responses to different combinations of the CSS. We thus obtained multiple cell datasets categorized according to polarity, latency, position and responsiveness to the stimulus. These datasets were then subject to further subdivision through the elimination of their outliers. We then observed both the original datasets without the outliers, and new datasets consisting only of the previously discarded outliers. Details about the sizes and the construction of such datasets are provided in Appendix D.4.

The results we found are reported as follows. In the 1st paragraph of the next section proofs of PSAM infection effectiveness are shown. The influence of the stimulus surround compartment size in the suppression of the responses of RGC belonging to the stimulus center compartment will be treated in the 2nd paragraph, together with the comparison with model predictions. The change of the stimulus center compartment size should not lead to differences in suppression of responses of RGCs belonging to the stimulus surround compartment. We anyway verified it and it will be treated in the 3rd paragraph.

HCs network engagement in RSS will be evaluated in the 4th paragraph. It will be evaluated at different stimulus center compartment's sizes for RGCs belonging to the center compartment. For RGCs sitting on the stimulus surround compartment, responses in CTRL and PSEM conditions are compared as averaged over different stimulus center compartment's sizes.

Below we do not report all the results obtained but only the most significant ones. For more information and illustrations of the results see D.7.

Chemogenetic channel targeted to horizontal cells. To enable observations about possible effects of the HCs network in saccadic suppression, we first ensured that PSAM injection had been effective and targeted HCs. If so, perfusion of PSEM during the experimental protocol would have resulted in the blockade of the inhibitory feedback from HCs onto cones. Injecting the mice intravenously with AAV Ef1a-DIO-PSAM coated with the PHP.B capsid (Deverman et al., 2016) led to retina-wide expression of PSAM in horizontal cells (Fig. 6.15, see C.2 for more details).
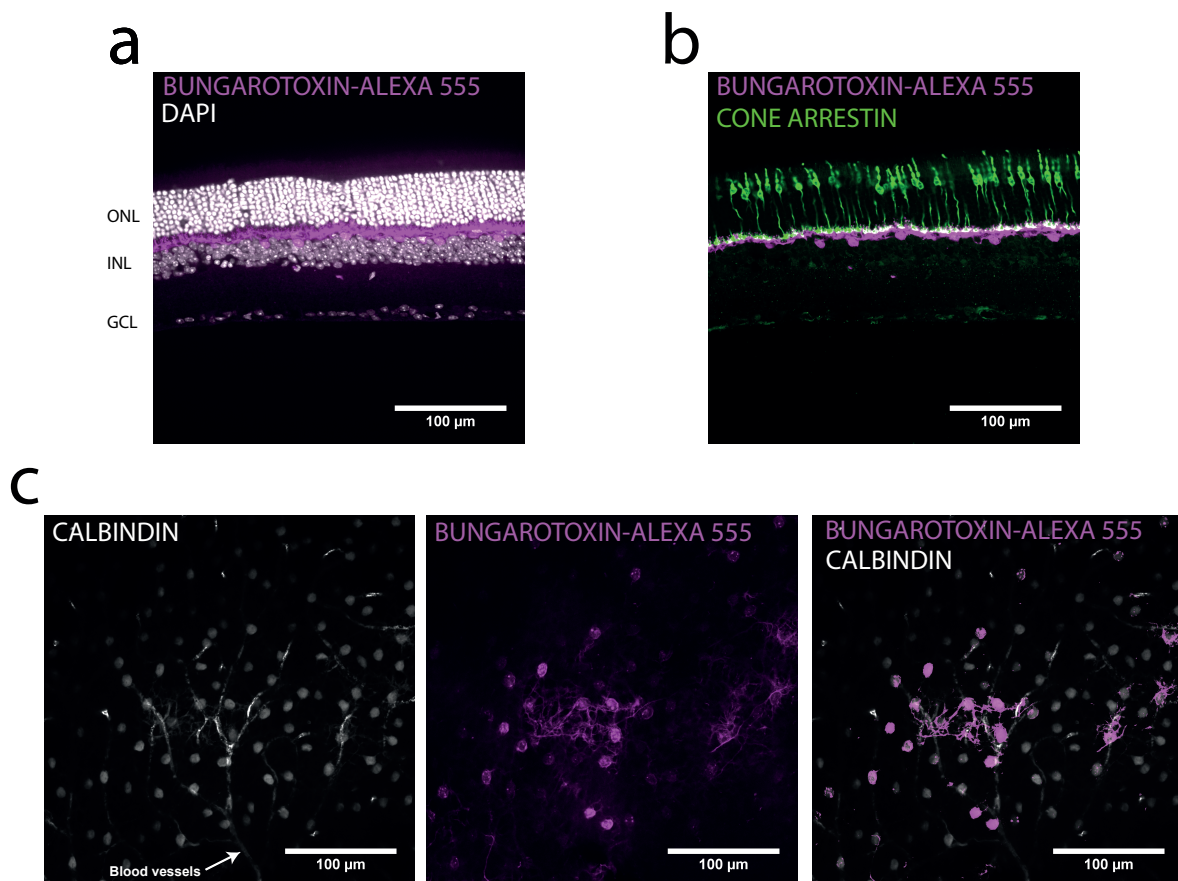
FIGURE 6.15: **Chemogenetic channel PSAM targeted to HCs. a-c**| Confocal images of retinas of Gja10-Cre mice systematically injected with AAV Ef1a-DIO-PSAM. PSAM was labelled with bungarotoxin-Alexa 555 (*magenta*). **a**| Retinal section: nuclei were labelled with dapi (*white*), PSAM is positioned between the INL and the ONL, where HCs cell bodies and network are supposed to be. **b**| Cones are labelled with cone arrestin antibody (*green*). PSAM is positioned in correspondence with cones' terminals, the same site in which HCs bind cones to provide them with inhibitory feedback. **c**| *Left*, HCs labelled with calbindin antibody (*white*); *central*, PSAM labelled with bungarotoxin-Alexa 555; *right*: left and central overlapped. PSAM targeted specifically HCs cell bodies.

Different numbers of cells in the stimulus surround compartment cause distinct suppression profiles in cells belonging to the stimulus center compartment depending on the cell nature and the stimulus shown. What we expected to see, increasing the number of cells targeted with the saccade in the stimulus surround compartment, was a stronger modulation of the responses of the cells sitting in the stimulus center compartment. Such modulation of responses could be either suppression or enhancement, what we expected, however, was an increase in the effect for larger surround compartments.

This was what we had initially hypothesized and what the model had predicted about the different influences of RF surround on the RF center.

Data show that different influences of RF surround on the RF center (i.e., modelled as different sizes of the stimulus center compartment) have diverse effects on the modulation of

cell responses in the stimulus center compartment (Fig. 6.16). These effects seem to depend on the cell nature and the stimulus presented to the cells. Even different subsets of cells of the same nature show different modulation of responses varying the stimulus center compartment size.

(i) There are cell natures that have their responses more suppressed if the cells presented with the saccade in the potential RF surround are small in numbers (i.e., increasing stimulus center compartment size).

(ii) Other cell natures show the opposite behavior: they seem to be more suppressed if more cells in their potential RF surround have been targeted by the saccade.

(iii) Other cell natures do not even seem to have their responses suppressed by the saccade on the surround, their responses are enhanced for earlier Δt_{flash} though. In particular, they may appear to be more enhanced the larger the size of the surround.

The *(i)* behavior contrasts with what we had hypothesized: what we expected was a greater modulation of responses for larger stimulus surround compartment sizes. However, the MI profiles show suppression of responses for earlier Δt_{flash}, consistent with Idrees et al. (2020b) results.

On the other hand, the *(ii)* behavior seems to be in line with what we had presumed to be the effect of a larger number of cells potentially belonging to the RF surround.

The *(iii)* behavior is not in line with the results reported by Idrees et al. (2020b) but seems to show in part the same effects predicted by the model (see Fig. 6.12).

In particular, the *(i)* effect is shown by a subset of sustained ON-RGC (39 cells) presented with a CSS combination analogous to nff 1st (Fig. 6.16, a *1st panel*).

The *(ii)* effect is shown by sustained ON-RGC (33 cells) and transient ON-RGC (6 cells) responses to CSS combination analogous to nff 3rd (Fig. 6.16, a *2nd panel*, b *2nd panel*). A behavior similar to the *(ii)* effect is also shown by the noisy dataset of transient ON-RGC (23 cells) if presented with a CSS combination similar to nff 1st (Fig. 6.16, b *1st panel*).

The *(iii)* effect could be partially seen in a subset of sustained ON-RGC (20 cells) presented with CSS combination like nff 1st (Fig. 6.16, a *3rd panel*). In addition, very small sustained OFF-RGCs datasets (4 and 7 cells) show behaviors similar to the *(iii)* effect if presented with CSS combinations analogous to nff 2nd and nff 4th (Fig. 6.16, c).

Interestingly in sustained ON-cells, at least on average, is that same-polarity and opposite-polarity saccades and flashes lead to contrary results to the ones highlighted by Idrees et al. (2020b) (see 3.2.1). Flash induced responses, in presence of a saccade of the same polarity, seem to be more suppressed than in presence of a saccade of the opposite polarity (Fig. 6.16, a *1st* and *2nd panels*).

This effect could be led by the HCs network and the HCs inhibitory feedback onto cones. The presence of the saccade in the RF surround is forwarded to the RF center via the HCs network. The HCs, however, forward it to the RF center cones as opposite in polarity (i.e., via inhibition feedback) to how they perceived it from the surround. Thus, the RF center could see, indirectly, the contrary situation of the RF surround, and this could lead to results opposite to the ones obtained with full field stimuli (Idrees et al., 2020b).

All the observations made so far are based on very small datasets of cells. All these datasets also show large variability; for this reason, it is perhaps more correct to speak of speculations rather than observations. It is also complex to try to identify a precise cellular behavior given the noisiness of the datasets. It would be rash to draw conclusions given the smallness of the datasets and their large variability.
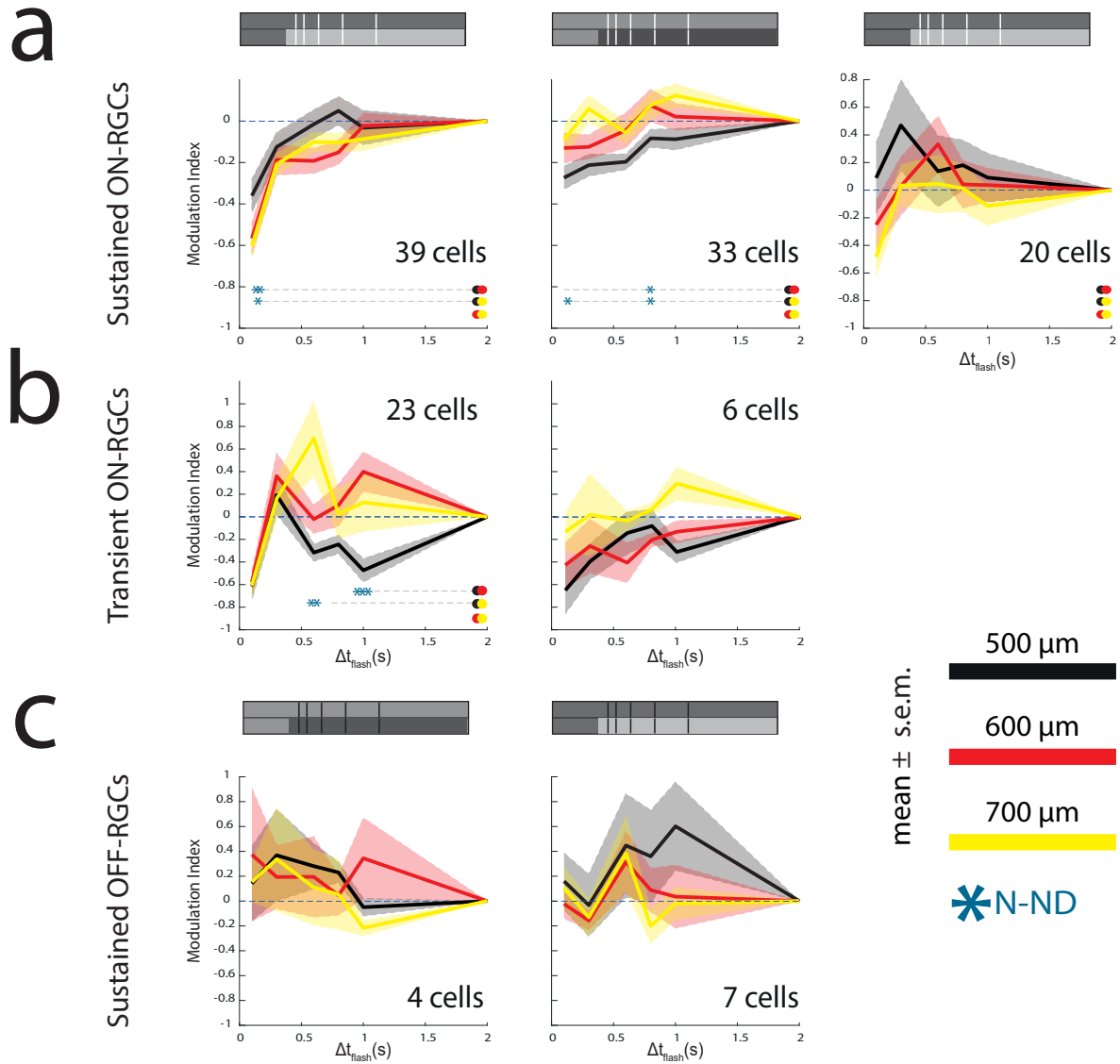
FIGURE 6.16: **The influence of the surround size on cells sitting in the center**. Saccade-like stimuli covering different portions of the RF surround nonunivocally influence RGC responses. The modulation of cell responses depends on the stimulus presented and the cell type.

Valid for **a,b,c**: population MI (mean $\pm$ *s.e.m.*) of different RGC types and different combinations of CSS (*grey scale schematics*). Different populations of MI are plotted depending on the stimulus center compartment diameter used over CSS's trials (*black*, $500\mu m$; *red*, $600\mu m$; *yellow*, $700\mu m$). *Blue* asterisks indicate statistical significance ($*p < .05$, $**p < .01$, $***p < .001$, see B.5 for more details) among various combinations of MI populations (populations come from non-normal distributions).

a | Population MI of subsets of sustained ON-cells responsive to different combinations of CSS: original dataset erased from outliers (39 and 33 cells, *first* and *second panels*), only the outliers of the original dataset (20 cells, *third panel*). **b** | Population MI of subsets of transient ON-cells responsive to different combinations of CSS: original dataset (23 cells, *first panel*), original dataset erased from outliers (6 cells, *second panel*). **c** | Population MI of subsets of sustained OFF-cells responsive to different combinations of CSS: original dataset erased from outliers (4 cells, *first panel*), original dataset (7 cells, *second panel*).

For more details about the datasets see D.4.

The suppression of responses of RGCs sitting in the stimulus surround compartment is not affected by the change of the stimulus center compartment's size.   All the cells sitting in the stimulus surround compartment received both the saccade and the flash in the CSS. As such, they were presented with the same full-field stimulus Idrees et al. (2020b) used. Therefore, we expected to find similar results to the one previously reported.

In addition, RGCs sitting in the stimulus surround compartment should not be affected by changing the stimulus center compartment size since they saw the saccade firsthand. We verified this assumption by looking at the lack of difference between MI profiles over the three different stimulus center compartment sizes presented.

All the cell natures' suppressions of responses seem not to be affected by changing the stimulus center compartment size. In addition, many of the results reported by Idrees et al. (2020b) have been recreated with CSS.

In particular, all the cell natures show suppression of responses for earlier Δt_{flash} (Fig. 6.17, a *1st* and *2nd panels*, b ,c, d). Saccades of opposite polarity to flashes cause more suppressed flash-induced responses for same Δt_{flash} ranges (Fig. 6.17, a *1st* and *2nd panels*, b, c).

Interestingly, using a CSS combination analogous to nff 1st, transient ON-RGCs responses seem to be slightly suppressed for a very precise range of Δt_{flash} (i.e., 300-800 ms), after having been enhanced for very earlier Δt_{flash} (Fig. 6.17, b *1st panel*). This behavior is somehow similar to the *(iv)* effect predicted by the asymmetric model (see 6.10), in which the CTRL condition had its responses firstly enhanced and then suppressed for a specific range of Δt_{flash}.

Of particular interest is the presence of a specific subset of sustained ON-RGCs whose responses to CSS combinations like nff 1st are not suppressed by the saccade. On the contrary, they seem to be enhanced (Fig. 6.17, a *3rd panel*). This behavior is similar to the *(iii)* effect described for part of the sustained ON-RGCs sitting in the stimulus center compartment (see previous paragraph). It could be food for thought about the existence of a counter-current variety of sustained ON-RGCs. Their responses indeed could be enhanced instead of suppressed after the onset of the saccade.

Again, the cell datasets have a small size and high variability. On average, we can assert that the suppression of cell responses in the surround is not affected by the change of center size. Still, on average we can claim to have recreated Idrees et al. (2020b) results and speculate on the existence of a counter current cell type. Nevertheless, the variability of the datasets does not allow to make any final statement.
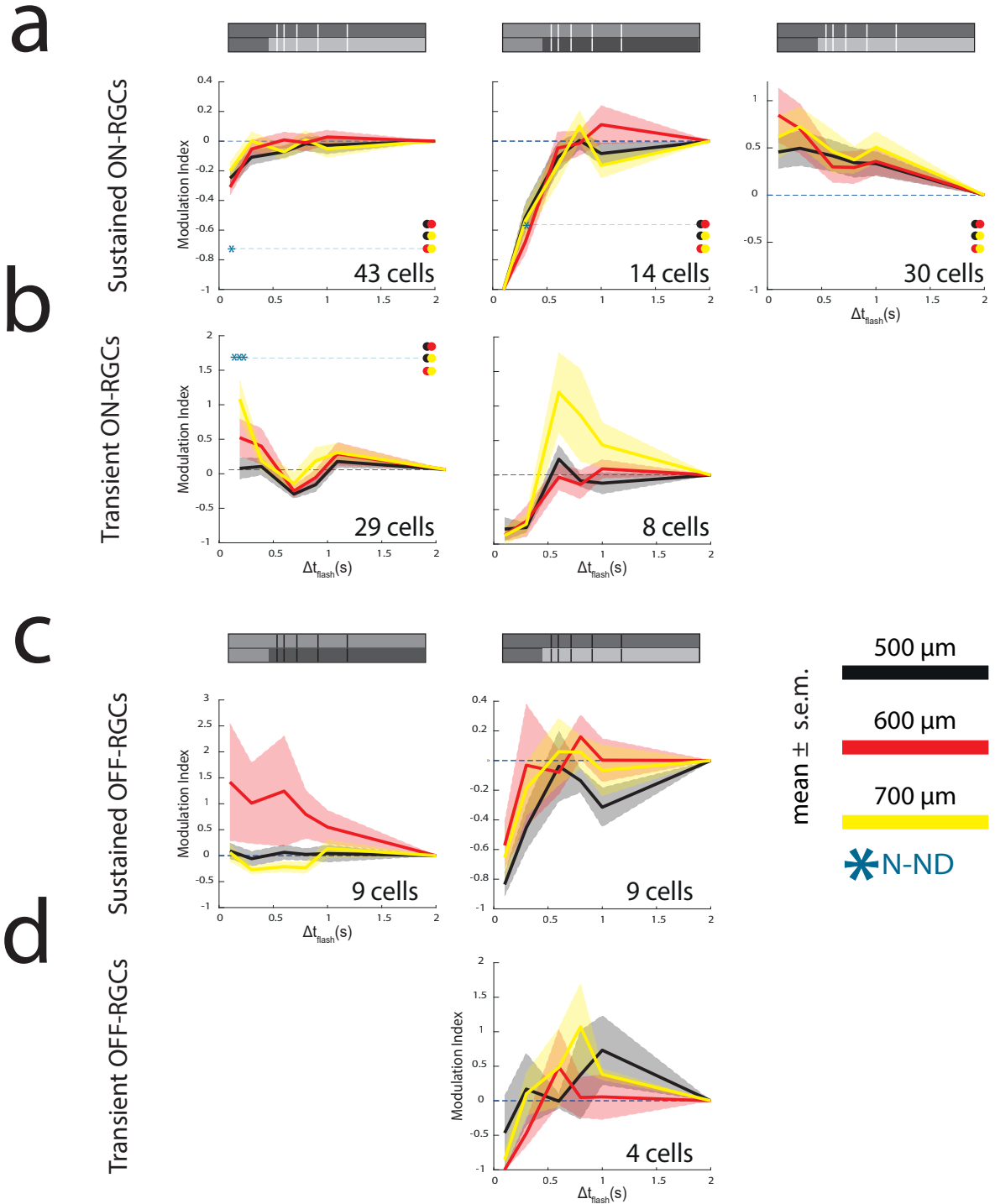
FIGURE 6.17: **The influence of the surround size on cells sitting in the center**. We recreated some of the results reported by Idrees et al. (2020b) about the RGC responses' suppression to full field saccade-like stimuli. We also present the possibility of the existence of a counter current type of sustained ON-cells. They, in the presence of saccade-like stimuli, would behave contrary to what is reported by Idrees et al. (2020b). Their responses are indeed enhanced for early Δt_{flash} (**a**, *third panel*). Valid for **a**, **b**, **c**, **d**: same as Fig. 6.16.
a | Population MI of subsets of sustained ON-cells responsive to different combinations of CSS: original dataset erased from outliers (43 and 14 cells, *first* and *second panels*), only the outliers of the original dataset (30 cells, *third panel*). **b** | Population MI of subsets of transient ON-cells responsive to different combinations of CSS: original dataset (29 and 8 cells, *first* panel and *second panels*). **c** | Population MI of subsets of sustained OFF-cells responsive to different combinations of CSS: original dataset (9 and 9 cells, *first* and *second panels*). **d** | Population MI of subset of transient OFF-cells, they were responsive for only one combination of the CSS: original dataset (4 cells). For more details about the datasets see D.4.

HCs network role in retinal saccadic suppression seems to vary over cell natures and presented stimuli.   We wanted to explore the possibility that the HCs network had a role in retinal saccadic suppression (RSS), particularly if it were the foundation of the surround component of suppression. If it were so, the suppression of responses to later Δt_{flash} shown by Idrees et al. (2020b) would vanish with the HCs network blocked.

To explore this possibility in the first place we built the asymmetric model. It predicted the engagement of the HCs network in RSS. Indeed, by simulating the blocking of such a network, the modulation of RGC responses vanished in all the model RGC types (see Fig. 6.12). Second, to see if the predicted engagement was real, we ran real experiments blocking HCs feedback onto cones.

Suppression profiles of real RGCs responses show a different behavior from the predicted one. Indeed, the pharmacologically induced blocking of the HCs inhibition feedback onto cones (i.e., via PSEM perfusion, see A.2 for more details) did not lead to consistent changes in MI profiles over different cell types (Fig. 6.18, 6.19).

In most of the cases, the smallness of the sizes of the datasets of cells perfused by PSEM does not allow to even consider the likely induced changes in RGCs behavior as effects.

In different types of RGCs sitting in the stimulus center compartment, blocking inhibitory feedback from HCs leads to inconsistent effects as the stimulus center compartment's size varies *(i)*. Other RGCs types, blocking HCs, seem to have their responses suppressed *(ii)*, unmodulated *(iii)* or even enhanced *(iv)* if compared to the CTRL condition. These multiple potential effects seem to depend also on the presented stimulus.

In particular, sustained OFF-RGCs belonging to the stimulus center compartment show the *(i)* effect (Fig. 6.18, b).

The *(ii)* effect is shown by sustained ON-cells in the stimulus center compartment, indeed PSEM seems to lead to greater suppression of responses than in the CTRL condition for CSS combinations analogous to nff 3rd (Fig. 6.18, a *second row*). Transient OFF-RGCs in the stimulus surround compartment seem to show the same behavior (if presented with CSS analogous to nff 2nd). RGCs in the CTRL condition have their responses less suppressed than in the PSEM condition (Fig. 6.19, d).

Blocking the HCs network does not lead to any change in responses modulation (i.e., *(iii)* effect) of sustained OFF-RGCs sitting in the stimulus surround compartment (Fig. 6.19, c). A part of sustained ON-RGCs in the stimulus surround compartment seem to have their suppression of responses unmodulated if PSEM was perfused (if the CSS combination presented is analogous to nff 1st) (Fig. 6.19, a *right*).

Speculations regarding these three first possible effects are made on very small and variable datasets. Indeed, the number of RGCs perfused by PSEM is really small. However, the results shown may give insights to look for similar effects in future experiments.

The *(iv)* effect is the only one involving datasets of slightly larger size. It is shown by sustained ON-RGCs of both the stimulus center and surround compartments (the presented CSS combination is analogous to nff 1st). The missing inhibition feedback from HCs seems to lead to the deletion of the suppression of RGC responses, in exchange for enhancement (Fig. 6.18, a *first row*; Fig. 6.19, a *left*). This could be partially in line with our hypothesis that the HCs network mediates the SCS. Nevertheless, it is anomalous that MI profile does not show any suppression, both the central and the global components of suppression should be active.

Although sustained ON-RGCs datasets were slightly larger than the ones of other cell types, their size is not large enough to allow conclusions to be drawn. However, these results, if found in future experiments, could become significant.
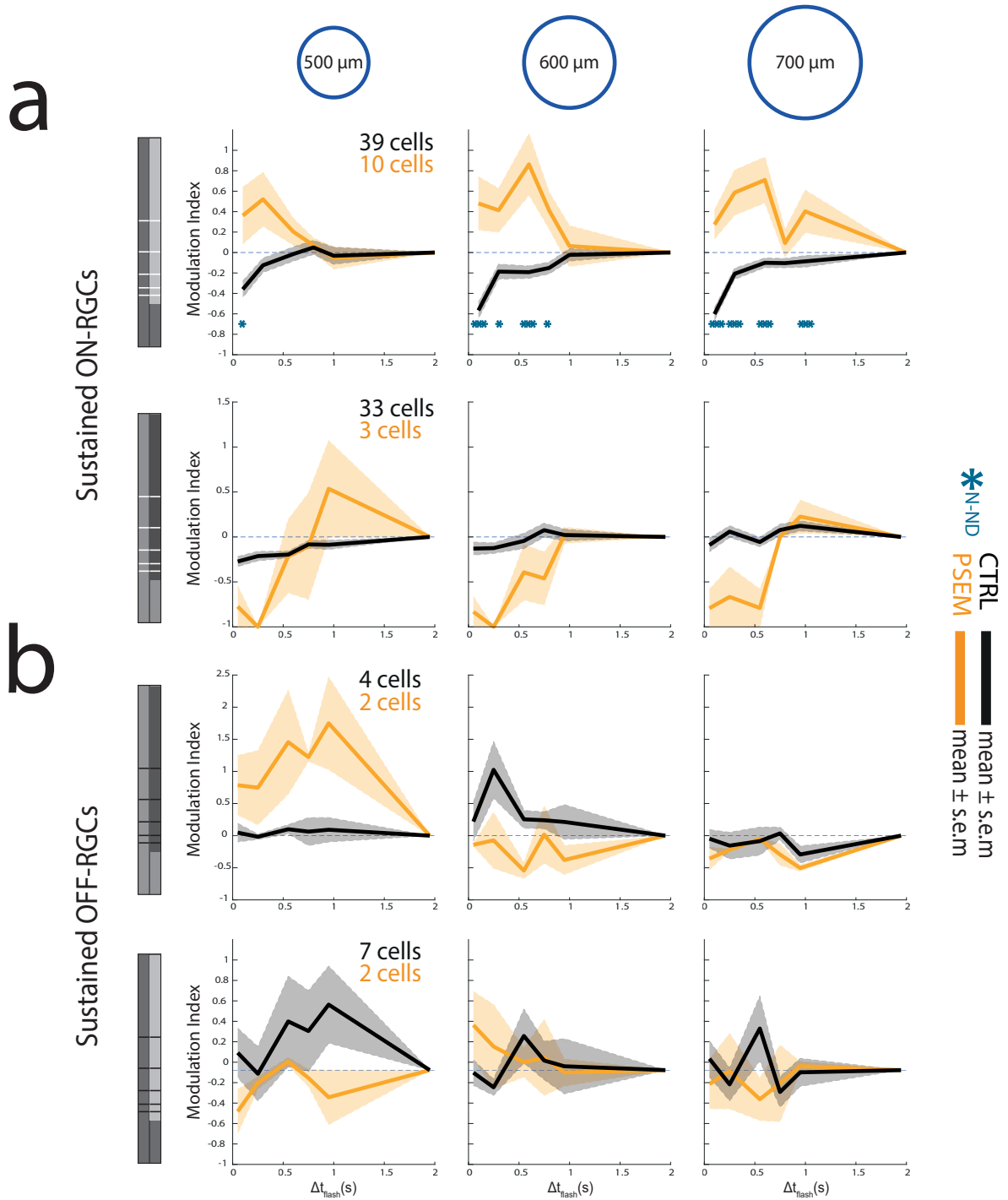
FIGURE 6.18: **HCs network does not act univocally in modulating the MI profile of cells that did not receive the saccade-like stimulus.** The effect of PSEM on the MI profiles of cells sitting in the stimulus center compartment seems not to be unique. The lack of HCs feedback onto cones seems not to affect univocally the suppression of the RGC types responses. If PSEM really has an effect it also depends on the stimulus presented. Valid for **a** and **b**: population MI (mean $\pm$ s.e.m.) of different RGC types and different combinations of CSS (grey scale schematics, *top left*) for both CTRL (*black*) and PSEM (*orange*) conditions. The *first column of panels* show MI populations when the diameter of the stimulus center compartment is equal to $500\mu m$. The *second column of panels* show MI populations for $600\mu m$ diameter while the *third columns of panels* show MI populations for $700\mu m$ diameter. *Blue* asterisks indicate statistical significance ($*p < .05$, $**p < .01$, $***p < .001$, see B.5 for more details) between CTRL condition and PSEM condition (populations come from non-normal distributions). **a** | Population MI of subsets of sustained ON-cells responsive to two combinations of CSS. For the first CSS combination (*first row*, analogous to nff 1st) 39 CTRL and 10 PSEM cells were found responsive (original dataset erased from outliers). For the second CSS combination (*second row*, analogous to nff 3rd) 33 CTRL and 3 PSEM cells have been analyzed (original dataset erased from outliers). **b** | Population MI of subsets of sustained OFF-cells responsive to two combinations of CSS. For the first CSS combination (*first row*, analogous to nff 2nd) 4 CTRL and 2 PSEM cells compose the small dataset (original dataset erased from outliers). For the second CSS combination (*second row*, analogous to nff 4th) only 7 CTRL and 2 PSEM cells were found responsive (original dataset).
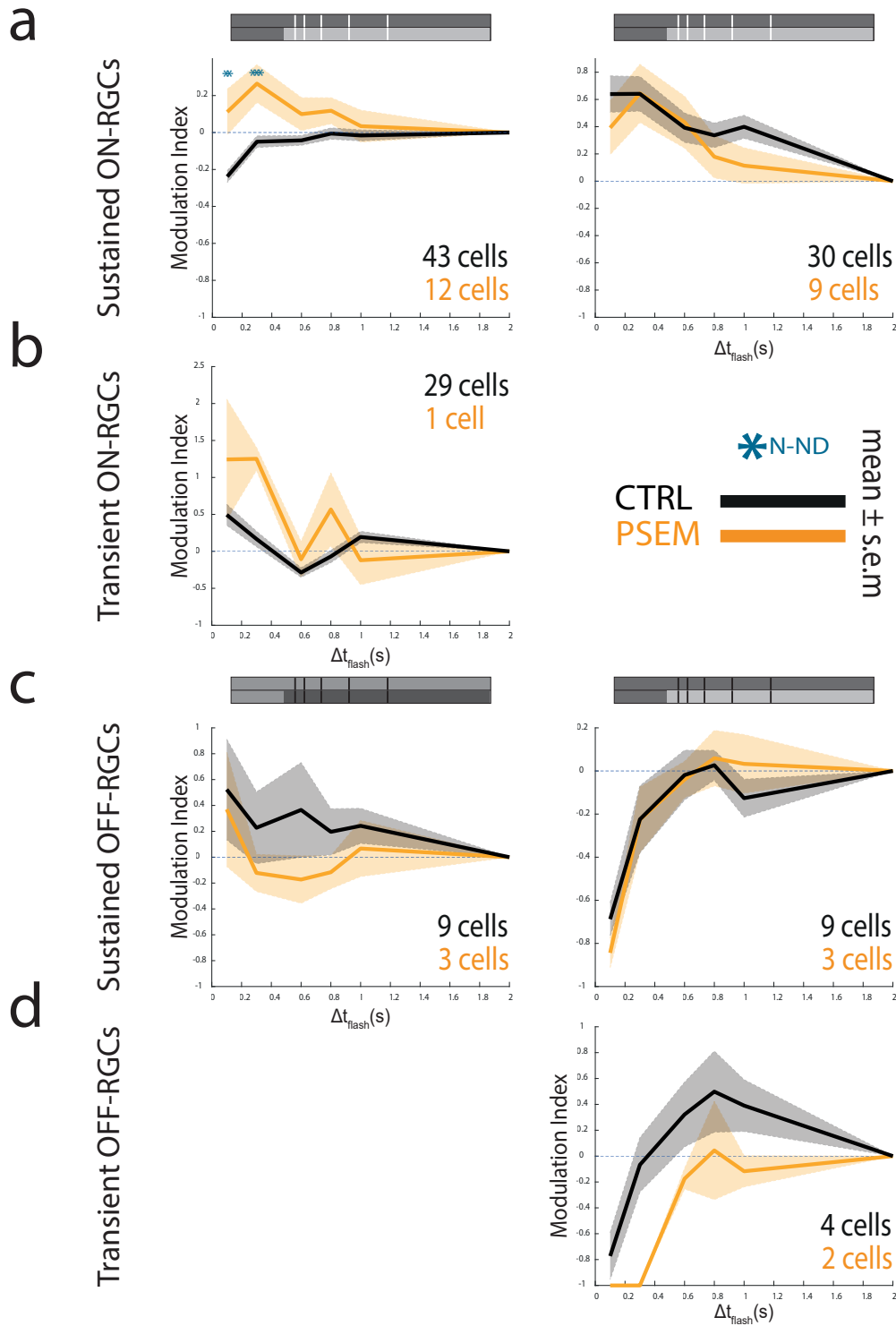
FIGURE 6.19: **HCs network does not act univocally in modulating the MI profile of cells that receive the saccade-like stimulus**. If PSEM, and thus blocking the HCs network, has an effect on suppressing cells' responses, it is not unique even if the saccade is shown full field. Different cell types in the stimulus surround compartment show indeed different modulations of their suppression profile in the PSEM condition. Same cell types, when presented with different stimuli, appear to show a different effect if the feedback of HCs onto cones is interrupted. Valid for a, b, c, d: population MI (mean $\pm$ *s.e.m.*) of different RGC types to different combinations of CSS (*grey scale schematics* on *top*) for both CTRL (*black*) and PSEM (*orange*) conditions. MI population at different stimulus center compartment sizes were averaged (see 6.17 for the reasons). *Blue* asterisks indicate statistical significance ($*p < .05, **p < .01, ***p < .001$, see B.5 for more details) between CTRL condition and PSEM condition (populations come from non-normal distributions). **a**| Population MI of two subsets of sustained ON-cells responsive to only one combination of CSS (analogous to nff 1st). The two subsets show different potential PSEM effects. At the same time, in the two different cellular subsets, PSEM appears not to change modulation of cellular responses (*second panel*) and to delete suppression for early Δt_{flash} in exchange for enhancement (*first panel*). 12 PSEM cells, sided by 43 CTRL cells (original dataset without outliers), present the first effect. 9 PSEM cells instead, contribute to show the second effect when compared with 30 CTRL cells (only outliers). **b** | Population MI of subsets of transient OFF-cells, PSEM perfused cells are too few to identify a clear effect (only 1 cell perfused with PSEM, original dataset). **c** | Population MI of sustained OFF cells to both CSS combinations analogous to nff 2n and 4th (3 cells perfused by PSEM, 9 CTRL cells; original dataset). c | PSEM seems to cause a greater suppression of transient OFF-cells. The number of CTRL and PSEM cells is too small to draw conclusions (2 PSEM cells and 4 CTRL cell; original dataset).

Chapter 7

Discussion

It is well established that saccadic movements cause a temporal window of suppression in visual sensitivity. The suppression process starts already in the retina (Idrees et al., 2020a) and it is due to three different components of suppression that originate in different locations of the receptive field (RF) of a retinal ganglion cell (RGC). The central component of suppression (CCS), the surround component of suppression (SCS) and the global component of suppression (GCS) (Idrees et al., 2020b).

The underlying mechanisms of all the three components are still not completely clear. The CCS and the GCS most likely are mediated respectively by the retina's non-linear processing chain and by the wide field amacrine cells (WACs) network. The origin of the SCS remains even less clear, its action timing could lead thinking about the involvement of the horizontal cells (HCs) network.

We built a phenomenological model of the retina inspired to an already published model (*temporal model* by Drinnenberg et al. (2018)) to recreate and predict RGCs responses' modulation to saccade-like stimuli. The new model (*asymmetric model*) can support in developing intuition on the three components of suppression:

- The CCS action is simulated by a filtering blocks' chain together with nonlinear thresholding steps.

- The SCS action is simulated through the modelling of the HCs network, built as a connective bridge between outer retina's segments of different simulated portions of the RF (see 5.2.2).

- The GCS action is simulated via the model WACs network, also built as a connective bridge between different regions of the RF, but at the inner retina's level (see 5.3.1).

We designed a new experimental protocol and ran experiments on mice's fixed retinas to evaluate the possible involvement of the HCs network in retinal saccadic suppression. We used pharmacology to externally block HCs feedback onto cones and see how RGCs responses were modulated in presence of saccade-like stimuli. We used the definition of modulation index (Idrees et al., 2020a), MI to analyze the modulation of RGCs responses. We designed a novel light stimulation protocol (i.e., CSS) to evaluate the strength of the SCS depending on the stimulus presented (see 6.4.2).

We checked if the asymmetric model had been able to derive the right predictions about the HCs network role in saccadic suppression and its strength.

Real data already collected (Idrees et al., 2020b) were used to validate the simulation of GCS effects by the model. In addition, by means of the model, we hypothesized a possible mechanism by which WACs could operate as mediators of GCS.

The functionality of the CCS was already embedded in the temporal model (Idrees et al., 2020b) and has been inherited by the asymmetric model.

7.1   Model performance discussion and future pipeline

The suppression of real RGC responses, varying the influence of the RF surround onto the RF center, is weakly captured by the model.   We evaluated how much the RF surround could influence the suppression of the responses to saccade-like stimuli. We did so by analyzing resposes of real RGCs that were sitting in the stimulus center compartment of CSS. The influence of the RF surround in the suppression of RGCs responses seems to vary depending on the stimulus presented and the nature of the cells. No unique patterns arose regarding how the RF surround influence the RF center in presence of saccade-like stimuli.

The model, on the other hand, predicted greater modulation of RGCs responses as the strength of RF surround influence increased.

By comparing the diverse suppression profiles of the real data with the predictions provided by the model, similarities can be found.

Small subsets of real cells show similar MI profile's trends when compared to model predictions. A cluster of sustained ON-RGCs and sustained OFF-RGCs seem to show modulations of RGCs responses similar to the model's ones for earlier times of flashes from saccade onset (i.e., Δt_{flash}) (see 6.4.2).

These clusters of sustained RGCs show weaker modulations of the suppression of responses by changing the RF surround influence onto the RF center. Nonetheless, in the model, the simulated change of the RF surround's influence onto the RF center led to significant changes in MI profiles. Maybe the light stimulation protocol itself was not able to emphasize enough different RF surround's influences (see 7.2).

The high variability expressed, and the very small sizes of real cells datasets do not permit to make any definitive statement about model prediction goodness. What is also true is that all the analogies, although weak, are based on small subsets of cells composed of only the outliers of the original datasets. If the model really captured these behaviors, then it predicted the suppression trends of counter current RGCs. In principle, this is not what one would expect from a predictive model. Contrary one would aspire to capture the behavior of most of the dataset, instead of a small fraction of it.

As we have seen in Chapter 6 (see 6.4.1) the model did not really predict modulation of flash induced response for earlier Δt_{flash}. It predicted the modulation of the really final flash induced responses. This different point of view changes radically the definition of the baseline response though (see B.4 for more details). In experiments, the final flash induced response (i.e., $\Delta t_{flash} = 2000ms$), is supposed to be the least influenced by the saccade. Nevertheless, in the model, it seems to be the most affected one. We used the same definition of modulation index (see B.4 for more details) for both experimental data and simulated ones. Nonetheless, the definition of the model baseline response is not in line with the experimental definition.

One could think of changing the model baseline response's definition as the flash induced response to a "preceding-saccade" flash. It would allow seeing how the saccade influences the flash induced response throughout all its course. It would show clearly that the most affected flash induced responses would be the ones to later Δt_{flash}. However, the earlier flash induced response would be still higher in amplitude than the later ones, making the predictions unchanged in the end.

Another possibility could be defining the MI as Idrees et al. (2020a) did in their research (i.e., bounding it in [-1, 1] domain) and take as the baseline response the flash induced response to a "preceding-saccade" flash. It would highlight again that the most influenced

flash induced responses would be the last ones. However, this method, in the end, would result in the same predictions our first MI definition gave.

Changing the definition of the baseline response of the model only leads to a different normalization in MI calculation. It does not change model predictions about the different suppression of responses in different time windows from the onset of the saccade.

If one can't act on MI definition, it means that something should be changed upstream. Problems could be solved by adding new modelled IRPs which could catch different features of the upstream cone temporal evolution. This possibility is still under investigation. One thing that should be done for sure is to fit the responses of the cones to saccade-like stimuli provided by the model against true recordings of photoreceptor activity (i.e., patch clamp or calcium imaging) to the same types of stimuli. This would allow to bypass the hand-setting of the two variables $\alpha_{hh,cs}$ and $\alpha_{hh,sc}$ and fit their values against real data (see 6.2). This could lead to a higher reliability of the model, at least in the outer retina segment, and could allow an eventual more targeted modification of the subsequent blocks.

HCs network might have a role in saccadic suppression according to real data, the model predicted so, but its predictions do not reflect what real data show. HCs network role in mediating the SCS has been evaluated adding pharmacology to the experimental protocol (see 6.4.2). We pharmacologically blocked the HCs inhibition feedback onto cones in chemogenetically modified mice and studied the MI's profiles comparing them with a CTRL condition.

The few cells perfused with PSEM and found responsive to CSS do not show unique effects on MI profiles. Depending on the nature of the cell and on the presented stimulus the HCs network block seems to lead to diverse effects on the modulation of the responses of RGCs when compared with the CTRL condition. Unfortunately, all the datasets of cells perfused by PSEM are too small. This makes it hard to make statements about the possible role of HCs network in retinal saccadic suppression.

The asymmetric model allowed to virtually block inhibition feedback from HCs to cones, thus blocking the likely influence of the HCs network in saccadic suppression. The model also predicted a change in the suppression of the flash induced responses of RGCs, when the HCs network was blocked. In particular, it predicted the deletion of the modulation of responses for all the model RGC types. Although this lack of supression was in line with our hypothesis that HCs network mediates the SCS, the model does not reflect real data behaviors.

Although the model seems not to predict real HCs network involvement in saccadic suppression, real data arouse interest and observations.

The most interesting likely PSEM effect is shown by sustained ON-cells presented with CSS combination analogous to nff 1st (Fig. 6.19, a *left*). PSEM perfusion seems to delete the suppression of responses shown in the CTRL condition, in change of enhancement. This is not completely in line with our predictions but still something to focus on in further experiments. Once again, the variability and the smallness of the datasets do not allow to make any final statement.

Many cells stopped responding after the perfusion of PSEM, almost all of them did not show any response after the washing out. In addition, few cells showed the PSEM effects described in Drinnenberg et al. (2018). Although we found proof of PSAM presence in the fixed tissues (Fig. 6.15), we wonder if PSEM perfusion was really effective or not.

Until there is no consistent data which prove the HCs network involvement, and how it is involved in RSS, it is difficult to speculate on a possible improvement in the

modelling of the same HCs network. The asymmetric model predicted to some degree what we expected by blocking the HCs network, what was unexpected were the manifold real RGCs behaviors.

The GCS has a precise time of action: the model captures the suppression timing and qualitatively simulates the WACs network. GCS acts from the periphery of the RF and takes part in retinal saccadic suppression for a well-defined window of time (Idrees et al., 2020b). Most likely the WACs network in the IPL is responsible for the GCS.

We modelled the WACs network to simulate the action of the GCS. We modified the asymmetric model's formulation to no longer model a set of cells from the RF surround but rather from the RF periphery. We added a new kind of model BC to the set used in Drinnenberg et al. (2018) and a new filtering block to simulate WACs network (see 5.3.1). Using an intercompartmental combination of IRPs, by driving peripheral IRPs from the WAC block, we built a new model RGC capable of showing the effects of GCS.

GCS timing of suppression shown by Idrees et al. (2020b) is qualitatively recreated by the suppression of the responses of the new model RGC introduced in the asymmetric model (see 6.3.3). The new model RGC shows different suppressions of its responses to different kind of saccade-like stimuli, consistent with what previously reported.

We observed that interaction time is the crucial feature that allows WACs to mediate GCS. By recreating the effects of GCS through the model, we hypothesized the interaction of WACs with specific types of bipolar cells. Such BC types (i.e., ON and OFF sustained BCs) capture specific temporal features of the upstream cone evolution to saccade-like stimuli. The interaction of WACs with these specific BC types, and the subsequent inhibitory input in the ganglion cell layer, allows to qualitatively obtain the right timing of suppression expressed by GCS.

Certainly this is not the only possibility, it is, however, the insight to which the model has led.

Several other possibilities could cause the specific suppression timing expressed by GCS, not the least the speed of conduction of signals through axons. The WACs, with their large dendritic arbour, could in fact not alter the signal coming from the BCs of the periphery, but only delay it differently depending on the distance of the same BCs from the RF center. If then WACs carry these signals as inhibitors on the RF center they could cause a temporal modulation of the suppression of responses.

7.2 Light stimulation protocol discussion and future pipeline

The light stimulation protocol can't really highlight different RF surround influences on the RF center. We designed and built a new light stimulation protocol (CSS, see 6.4.2) for fixed retinas. The way it was built was intended to highlight how different portions of the RF surround of a RGC could influence its responses to saccade-like stimuli. It was done via the introduction of two different stimulus compartments, whose sizes change one relative to each other. One of the two compartments described flashes, the other both steps (i.e., saccades) and flashes.

CSS does not seem to have proven effective in emphasizing different RF surround influences on RGCs responses. It could be that essentially the surround RF does not strongly affect RGCs responses. Most likely the protocol should be reviewed though.

One of the biggest problems we encountered was the low number of cells to analyze (i.e., the ones sitting in the stimulus center compartment) in order to assess how they

were differently affected by their RF surround. They were always too few, especially in pharmacological experiments.

In addition, the way we identified cells position (see B.1 for more details) was maybe not accurate enough to state whether the RF of a cell sat in either stimulus compartment. We anyway checked if cells responses were in line with their assumed location.

Other methods have been proposed to identify the RF location of RGCs (Chichilnisky, 2001) but they always led to smaller datasets due to filtering procedures.

There are two main possibilities one could start to think about to change the light stimulation protocol:

1. The first possibility is using a modified version of the stimulus Idrees et al. (2020b) used in their work (see Fig. 3.4). This time the grey mask should change from denser to sparser patterns. It would allow having a denser or sparser projection of flashes and saccades in different regions.

   Looking then at the cells which sat in the "flash-only" regions one would expect to see changes in the MI profiles according to the sparsity of the grey mask. In particular, the denser is the pattern the higher would be the modulation of the responses.

   This possibility could allow finding a higher number of cells in the "flash-only" compartments.

2. The second possibility would see an even simplified version of the CSS. The stimulus should still be divided into two compartments, this time not circular shaped though.

   One could imagine dividing the projected rectangle into two subrectangles: one showing both the saccade and the flash and the other a flash only. A vertical separation line states the division between the two compartments. After having set an initial position of the separation line, one could record the activity of a bunch of cells which sit over a given distance from the line and in the "flash-only" compartment. Moving the separation line toward the recorded cells would enlarge the "saccade and flash" compartment.

   Recording from the same bunch of cells one could expect different responses' modulations at different positions of the dividing line. In particular, the closer the line to the bunch of cells, the higher the modulation of responses.

CSS did not permit to clearly distinguish the suppression's modulation differences changing the stimulus presented to the RF surround of a cell.

Nevertheless, results showed slight changes in modulation of suppression by varying the strength of the surround influence.

The light stimulation protocol itself, together with the results it brought, served as an evaluation of the stimulus. As such it essentially led to good results, being it the first attempt. It could be now modified and improved, allowing further experimental results to be more significant and satisfactory.

Appendix A

Experimental protocol: details

A.1 Tissue preparation and perfusion

Before the sacrifice every mouse has been dark adapted (i.e., in the box) for more than 1 hour. After the sacrifice, every mouse has been deprived of both the eyes.

After having separated the retinal tissue from the whole eye it is cut in pieces of dimensions similar to the chip (i.e., $3.85x2.1mm^2$). The dissection procedure is done inside a chamber filled with RINGER solution. The ventral part of the retina has been chosen for all the experiments performed.

The piece of tissue is then moved directly to the chip and pressed with a thin membrane to allow the direct contact of RGCs and HD-MEA's electrodes. Every cut isolated retina was adapted to a light level (i.e., on the chip): in the first 2 experiments (4 configurations) it was grey adapted for more than 1 hour, in the other 4 experiments (9 configurations) it was dark adapted for more than 1 hour.

During the whole experiment, the RINGER solution is perfused into the chamber ($1.5ml/min$) to not compromise the sample's vitality.

In pharmacology experiments (i.e., using PSAM injected Gja10-Cre mice) RINGER solution has been perfused in the control condition. PSEM was bath-applied during physiological experiments with $3\mu M$ concentration (wash-in time 15 mins) and then washed out for 15 mins at a perfusion rate of $1.5ml/min$.

A.2 Light stimulation protocol

The circular saccade suppression protocol is a light stimulation protocol that is compartmentalized into 2 compartments. The 2 compartments stimulus was composed by a central annulus (center compartment, C) overlayed on a rectangle (the non-overlapping area stays for the surround compartment, S).

We used three different diameter sizes for C ($500, 600, 700\mu m$) to include different numbers of cones in the two compartments over trials, they changed in decreasing order during the protocol.

Both the two compartments start from the same grey luminance value. The compartment S changes in contrast (±0.43 MC) and maintains the "final value" for $3s$ (i.e., step contrast changes, saccade). After a varying delay - over trials - from the initial contrast change of compartment S (i.e., Δt_{flash}) an additional change in contrast affects the two compartments simultaneously (±0.33 MC) for $33ms$ (i.e., flash contrast change, probe flash).

We used $100, 300, 600, 800, 1000$ or $2000ms$ as Δt_{flash} and each Δt_{flash} was presented randomly over trials in order to avoid cells' bias.

Each stimulus combination (*ON step - ON flash, ON step - OFF flash, OFF step - OFF flash, OFF step - ON flash*) has been repeated at least 5 times for each diameter's size of the compartment C. Also the "saccade-only" combination (useful for MI calculation, see B.4) was

repeated at least 5 times for each size of the compartment C.

The duration of the whole protocol was about 20 mins minimum (using 5 repetitions).

The light stimulation was controlled via the Python software PsychoToolbox.

A.3   Stimulation setup

Fixed retinas were stimulated through an UV projector (*EKB Technology Ltd: E4500MKII - G-UV - ID7*). The light was focused on the microelectrode array by a focusing lens (*AF-S Micro NIKKOR 60mm f/2.8 ED*) and a Custom *2.5x* single-lens objective (*ThorLabs*). Stimulation area covered $3.5x2.1mm^2$ and was centered on the electrode configuration's center by moving the stage via a joystick-controlled system (*Scientifica*).

A.4   HD-MEA setup

RGCs electrical activity during physiological experiments was recorded using CMOS-based HD microelectrode arrays (Fiscella et al., 2012). The chip is composed by 26400 platinum electrodes, they cover an area of $3.85x2.1mm^2$, the interelectrode distance is $17.5\mu m$.

RGCs activity was recorded by a configurable subset of 1024 electrodes ($\simeq 1.5mm^2$). All the configurations were chosen to cover both the center and surround compartments (see A.2).

Appendix B

Analysis of RGCs responses: details

B.1 Identification of ganglion cells' position in relation to the stimulus

The position of the cells has been evaluated using the unit's "center of mass" resulting from the spike sorting algorithm (Diggelmann et al., 2018). It is calculated as the location of the maximum activity of a unit.

A receptive field radius of $50\mu m$ has been hypothesised and a circular "virtual RF" has been built using the center of mass as its centre. Only if the virtual RF fully sits inside the smaller center compartment (see A.2) used in the protocol (i.e., $500\mu m$ diameter), the cell is considered a "center belonging" cell. Similarly, a cell is considered "surround belonging" only if its "virtual RF" sits completely outside the largest center compartment used in the protocol (i.e., $700\mu m$ diameter). Cells that change location as a function of the size of the center compartment used in the protocol have not been analyzed yet.

Each "center belonging" cell underwent further review. Each one was checked manually to confirm that it did not show clear responses to the saccade. If the cell showed responses to the saccade, for even one of the three radii used for the stimulus center compartment, allocation had been wrong and therefore the cell was filtered out.

Even if stimuli that allow receptive fields' estimate exist (Chichilnisky, 2001), we decided to use the RGCs maximum activity location to avoid subjecting the cells to further filtering.

B.2 Classification of retinal ganglion cells according to their nature

RGCs have been classified according to their polarity and transiency. It was done using "Chirpsweep" stimulus which already showed potentiality in clustering cells on these features[1]. The clustering method we used is based on the evolution of the firing rate of the RGC during the Chirpsweep half square wave.

Substantially, if a cell responds to the rising phase of the half square wave it has ON polarity; contrarily, if it responds to the falling phase of the half same square wave it has OFF polarity. Depending on the temporal evolution of the response, the cells could be then classified as transient or sustained.

For identifying ON and OFF cells the spike rate, in response to the half square wave, is taken into account in this way: the spike count is evaluated for a $400ms$ window after both the rising and the falling phase of the half square wave (Idrees et al., 2020b). The ON-OFF index ($ONOFF_{idx}$) is calculated as the ratio of the difference of the two spike counts and their sum, then properly normalized in the [0,1] domain.

- $ONOFF_{idx} = 1$: pure ON cell.

---

[1]Jouty et al., 2018; Baden et al., 2016.

- $ONOFF_{idx} = 0$: pure OFF cell.

A threshold system helps in identifying the right polarity of the cell :

- $ONOFF_{idx} > 0.65$: ON cell.

- $ONOFF_{idx} < 0.35$: OFF cell.

- $0.35 \leq ONOFF_{idx} \leq 0.65$: ON-OFF cell.

To clarify if a cell is either transient or sustained another $400ms$ window is taken into account. If the cell has ON polarity the $400ms$ window starts with the rising phase of the half square wave, if the cell has OFF polarity the time window starts with the falling phase of the half square wave. The latency index (LAT_{idx}) is calculated as the ratio between the integral of the spike count of the cell in the $400ms$ window and the integral of the spike count over the rising/falling subsequent half period of the square wave. The latency index domain is [0,1]:

- $LAT_{idx} > 0.75$: transient cell.

- $LAT_{idx} \leq 0.75$: sustained cell.

B.3   Filtering procedure of cells' responses to circular saccade suppression protocol

The cells identified by the spike sorting (Diggelmann et al., 2018) have been firstly filtered looking at the quality of responses to CSS.
For each trial of CSS (see A.2) the flash induced response of every single cell has been evaluated. The spike count of the cell is evaluated in three different time windows with respect to the onset of the flash:

1. right after the flash onset (i.e., where the flash induced response is supposed to be seen, SP_1).

2. before the flash onset (i.e., where only the saccade induced response is supposed to be seen, SP_2).

3. considerably after the flash onset (i.e., where only the saccade induced response is supposed to be seen, SP_3).

The difference, in terms of spike count, of the window in between and the other twos is then calculated. The "mean spike count difference" is calculated and the resulting parameter is used to set a threshold to establish the CSS response quality.

$$\frac{\sum_{i=1}^{n} \frac{(SP_{i,2}-SP_{i,1})+(SP_{i,2}-SP_{i,3})}{2}}{n} \quad \text{, n \# of trials for a single combination of the CSS}$$

For our experiments, we set the above-mentioned threshold equal to 5.
It is sufficient that a cell responds well to the flash of a single combination of CSS to not be filtered out by the described threshold.
Every single cell that was not filtered out via the threshold just described was subjected to further filtering.
Since the preliminary filtering did not take into account that a cell might respond to only one of the three radii used in CSS (see A.2), we took care to keep only those cells that were responsive in all three trials.

In addition, we cross-checked the cellular responses to CSS with the cellular nature of the cell in question (see B.2). ON cells are supposed to respond to OFF-ON or ON-ON combinations of CSS; OFF cells are supposed to respond to ON-OFF and OFF-OFF combinations. The preliminary filtering does not take into account the cell nature so we made sure that the cells not removed by the first filtering steps were really responsive in the combinations we were interested in.

We also added an additional filtering factor: each cell must respond to the flash with the largest Δt_{flash}. This was done for the purpose of subsequent MI calculation (see B.4).

Regarding the cells subjected to PSEM perfusion instead (see A.1), they underwent an additional filtering procedure. Indeed, each cell, besides having to be responsive to each of the radii used in the trials of CSS, must be responsive both in the "before" condition (i.e., before PSEM wash-in) and in the "during" condition (i.e., during PSEM perfusion).

B.4 Modulation Index definition

MI calcuation in Idrees et al., 2020a The modulation index (MI) was built to quantify retinal saccadic suppression. It is defined as:

$$MI = \frac{R_d - R_b}{R_d + R_b}$$

where R_d is the maximum of the flash induced response at a given time from "saccade" onset and R_b is the maximum of the baseline response, both of them in terms of firing rate of RGCs.

The flash induced response (i.e., R_d) is intended as the response caused only by the probe flash at a given Δt_{flash}: usually, saccades themselves cause a neural response in RGCs and this results in a signal given by the superimposition of the saccade and flash responses. To isolate the component of the response caused by the probe flash only, the saccade-alone response is subtracted from the superimposition.

The baseline response (i.e., R_b) is intended as the flash induced response to a later Δt_{flash} for which it is reasonable to think that the presence of the saccade does not affect the flash response ($\Delta t_{flash} = 2000ms$ in experiments).

MI calcuation in our experiments and model simulations We modified Idrees et al., 2020a way of calculation of the MI. We used the same R_d and R_b definitions. We did not bound MI in $[-1, 1]$ domain but in $[-1, +\infty)$ domain:

$$MI = \frac{R_d - R_b}{R_b} - 1$$

In this way we wanted to account for the variability, in terms of response amplitude, of every single cell. From the model point of view in this way we wanted to observe the variability of responses amplitudes across different values of $\alpha_{hh,sc} / \alpha_{hh,cs}$.

In experiments, the baseline response (i.e., R_b) was taken as the flash induced response for the latest Δt_{flash} shown in all the trials ($\Delta t_{flash} = 2000ms$). The saccade-alone response was taken as the average of RGCs responses for all the trials where no flash was shown at all.

For the model simulations we used the same approach in calculating the MI. R_b was taken as the flash induced response with $\Delta t_{flash} = 2000ms$ and the saccade-only response was obtained by not including any flash in the saccade&flash protocol.

B.5　Statistical analysis

Outliers identification　For each MI population, the outliers have been identified to build two different datasets (see D.4). The first one *(i)* composed by the original dataset without the outliers and the second one *(ii)* built with only the outliers previously found.
A sample has been considered an outlier if its value was more than three scaled median absolute deviations (MAD) away from the median of the distribution.

Statistical tests　We ran statistical tests to compare MI profiles in CTRL condition for different stimulus center compartment sizes (see A.2) and to compare MI profiles of the CTRL condition with the ones of the PSEM condition.
The following statistical tests were used: nonparametric Friedman's test, two-sample t-test, Welch's test, Mann-Whitney U-test, one-sample Kolmogorov-Smirnov test, two-sample F-test for equal variances (for more information see D.7).
Statistical tests have been run only on datasets with more than nine samples.

Appendix C

Perturbation of HCs: details

C.1 Chemogenetical perturbation of horizontal cells

Gja10-Cre mouse line was used to conduct pharmacological experiments, this particular transgenic mouse line was generated by bacterial artificial chromosome (BAC)-based transgenesis. Gja10 is a gene that is specifically expressed by HCs and not by all the other cells in the retina (Siegert et al., 2012).

An adeno-associated virus (AAV), specifically the *pAAV-Ef1a-DIO$_{PSAM}$*, was injected in anaesthetized mice to express PSAM (pharmacologically selective actuator module), in Cre-expressing horizontal cells. The used channel, *PSAM L141F Y115F-GlyR*, is chloride permeable. The activation of the PSAM is induced by PSEM (pharmacologically selective effector module).

The binding of PSEM with PSAM clamps HCs to the equilibrium potential of chloride not allowing them to provide cones with inhibitory feedback.

C.2 Immunohistochemistry and quantification of retinal infection

Whole mount retinas and retinal cross sections were stained as described by Szikra et al. (2014). After having embedded the fixed retina in 3% agarose in PBS, $150 \mu m$ thick cross sections were obtained using a vibratome.

These sets of primary and secondary antibodies were used:

- Primary: rabbit anti-cone arrestin (*Millipore, AB15282, 1:200*); Secondary: donkey anti-rabbit IgG conjugated with Alexa-488 (*1:200*)

- Primary: mouse anti- calbindin (*Swant, code-300, 1:500*); Secondary: donkey anti-mouse IgG conjugated with Alexa-647 (*1:200*)

PSAM was stained with alpha-Bungarotoxin conjugated with Alexa-555 (*1:200*) and nuclei were stained with DAPI (*1:500*).

To verify PSAM expression in *Gja10-Cre* mice's retinas, confocal stacks were acquired from retinas' cross sections and wholemount pieces using a spinning disk confocal microscope (*IXplore by Olympus*) and processed by the image processing software "CellSense" (*Olympus*).

Appendix D

Other details

D.1   Fitting procedure to constrain outer retina's parameters

The parameter set of the outer retina was constrained finding the minimum distance between model predictions on cone potential and patch-clamp recordings (Szikra et al., 2014). Model predictions were compared across real cones responses to five decades of light intensities.

The whole model simulation is considered as a multivariable function, its minimum was looked for using a derivative-free method. The cost function has been so built:

$$err = \frac{\sum_{i=1}^{5}(C_M - C_D)^2}{\sum_{i=1}^{5} C_D^2}$$

Where C_M stays for model predictions about cone potential and C_D indicates real patch-clamp recordings, i varies according to the five decades of light intensities used in real experiments.

The only outer retina's parameters we constrained during the fitting procedure were time constants (i.e., they had to be above zero) and γ which had not to fall out from $[0, 1]$ domain .

The fit returned an error of $0.00842mV$. These the values of the parameters of the outer retina: $\alpha_c = -1.045 * 10^{-5}$, $\tau_c = 0.0377ms$, $\beta_c = 1.303 * 10^{-5}$, $\tau_{ch} = 8.548 * 10^{-4}ms$, $\alpha_{hc} = 0.223$, $\tau_{hc1} = 0.205ms$, $\tau_{hc2} = 0.331ms$, $\tau_y = 0.047ms$, $tau_z = 0.967ms$, $\gamma = 0.717$.

D.2   Michelson contrast

Given a change in luminance, Michelson contrast (MC) measures the relation between the spread and the sum of two luminances. It is defined as follows:

$$MC = \frac{I_{max} - I_{min}}{I_{max} + I_{min}}$$

MC is defined as always positive in its formulation. In this thesis it is also given negative values. With this we want to differentiate different polarities of the change in luminance. Positive MCs indicate changes in luminance from dark to bright while negative MCs state for transitions from bright to dark. Essentially our definition of MC is the following:

$$MC = \frac{I_{after} - I_{before}}{I_{after} + I_{before}}$$

D.3 Interpolation of Modulation Index profiles

In order to calculate suppression stength (SS) values in continuous Δt_{flash} time windows from discrete MI profiles, the same MI profile was interpolated across the range of the used Δt_{flash}.

The discrete MI profile has been interpolated with a *Shape-Preserving Piecewise Cubic Intrpolation* method. The polynomial $P(x)$ used is a piecewise cubic polynomial that preserves the shape of the data and respects monotonicity. For each $P(x_j = y_j)$, the first derivative $\frac{dP}{dx}$ is continuous.

D.4 Cells datasets

After all the filtering procedures described in B.1 - B.3, we constructed cellular datasets based on polarity, latency, location, and presented stimulus. Some of the cells that passed the filtering procedures were part of the pharmacological experiments and thus were perfused by PSEM.

In the Table D.1 we report the sizes of the multiple cellular datasets we constructed, indicating also how many of the cells belonging to the datasets were subjected to PSEM perfusion. From these cellular datasets, we obtained the MI populations which allowed further analysis of the results.

		Stimulus Center Compartment		Stimulus Surround Compartment	
		CTRL	PSEM	CTRL	PSEM
Sustained ON-cells	ON saccade ON flash	59	11	85	23
	OFF saccade ON flash	52	4	42	2
Transient ON-cells	ON saccade ON flash	23	0	29	1
	OFF saccade ON flash	15	0	8	0
Sustained OFF-cells	OFF saccade OFF flash	8	3	9	3
	ON saccade OFF flash	7	2	9	3
Transient OFF-cells	OFF saccade OFF flash	0	0	1	0
	ON saccade OFF flash	0	0	4	2

TABLE D.1: Number of cells found in real experiments. All the datasets of cells found in real experiments (CTRL and pharmacological) sorted by nature (i.e., polarity and transiency), position relative to the stimulus (center/surround stimulus compartment), resposiveness to a particular stimulus combination, condition (CTRL, *black*; PSEM, *orange*).

In order to decrease the noisiness of the MI populations the original dataset of cells found in the experiments was narrowed by removing its outliers (see B.5).

Below we report the sizes of the datasets resulting from the deletion of the outliers from the original dataset (Table D.2) and additional datasets composed only of the outliers removed from the original dataset (Table D.3).

		Stimulus Center Compartment		Stimulus Surround Compartment	
		CTRL	PSEM	CTRL	PSEM
Sustained ON-cells	ON saccade ON flash	39	10	55→43	14→12
	OFF saccade ON flash	33	3	14	0
Transient ON-cells	ON saccade ON flash	9	0	18	0
	OFF saccade ON flash	6	0	2	0
Sustained OFF-cells	OFF saccade OFF flash	4	2	7	3
	ON saccade OFF flash	4	2	5	3
Transient OFF-cells	OFF saccade OFF flash	0	0	1	0
	ON saccade OFF flash	0	0	2	2

TABLE D.2: Cells datasets without outliers. All the datasets were narrowed removing the MI populations outliers. Cells are sorted by nature (i.e., polarity and transiency), position relative to the stimulus (center/surround stimulus compartment), resposiveness to a particular stimulus combination, condition (CTRL, *black*; PSEM, *orange*). The dataset of sustained ON-cells in the stimulus surround compartment found responsive to surround-only ON saccades and full field ON flashes underwent two steps for filtering outliers.

		Stimulus Center Compartment		Stimulus Surround Compartment	
		CTRL	PSEM	CTRL	PSEM
Sustained ON-cells	ON saccade ON flash	20	1	30	9
	OFF saccade ON flash	19	1	28	2
Transient ON-cells	ON saccade ON flash	14	0	11	1
	OFF saccade ON flash	9	0	6	0
Sustained OFF-cells	OFF saccade OFF flash	4	1	2	0
	ON saccade OFF flash	3	0	4	0
Transient OFF-cells	OFF saccade OFF flash	0	0	0	0
	ON saccade OFF flash	0	0	2	0

TABLE D.3: Cells datasets with only outliers of the original datasets. All the datasets were built as complementary to those in Table D.1, they contain only the outliers of the MI populations of the original dataset. Cells are sorted by nature (i.e., polarity and transiency), position relative to the stimulus (center/surround stimulus compartment), resposiveness to a particular stimulus combination, condition (CTRL, *black*; PSEM, *orange*).

D.5   Spike sorting algorithm

The spike sorting algorithm used (Diggelmann et al., 2018) is optimized to provide excellent performance in sorting cellular units from recordings made by HD-MEA. It is based on three main steps that lead to the identification of cell units.

1. **Subdivision into local electrode groups (LEGs)**: each recording electrode is assigned to a specific group of electrodes (with a maximum of 9 electrodes). LEGs are built in such a way as to be positioned adjacent to each other in order to minimize the number of LEGs and the overlap zones.

2. **Parallel process of LEGs**.

    (a) *Spike detection*: the activity of each electrode is thresholded. This threshold is taken as 4 times the median absolute deviation (MAD) of the signal resulting from the previous thresholding of the recorded activity with its standard deviation. The spike event is detected when the signal reaches its maximum within a short time window after having exceeded the threshold. If several quasi-simultaneous spikes are detected within a single LEG, they are combined to obtain a multi-electrode waveform.

    (b) *Waveform alignment*: due to the recording sampling rate, waveforms may not be well aligned in time, a phenomenon known as registration jitter. Jitter is corrected by oversampling the waveforms, aligning them based on their cross-correlation, and then restoring them to their original recording sampling rate.

    (c) *Feature selection*: after a signal pre-whitening procedure, the waveforms are subjected to PCA.

    (d) *Clustering*: a parameter-free spike clustering method by using mean-shift clustering with a flat kernel is used. This method assigns each spike to a particular cluster which has the mean of the neighborhood of the same spike. The clustering method is defined to build templates that will later support cell-unit identification.

    (e) *Template matching*: each waveform of each spike is compared with the built templates. The highest similarity across templates is then sought using a method called Bayes optimal template matching (Franke et al., 2015).

    (f) *Cluster merging*: spikes from the same neurons could be assigned to different clusters due to the variability of the neuron. If this is the case then the clusters are merged by comparing the new templates they formed.

3. **Duplicate resolution**: each LEG has now a number of neuronal units, each one with its spike train and template. If multiple LEGs detect the same neuronal unit the LEG with maximal template's amplitude is not discarded.

D.6   Model simulations

The construction of the entire asymmetric model has been carried out in MATLAB, through which simulations have been run too. The resolution of the system of differential equations governing the evolution of the cone potential and HCs in the outer retina was accomplished with the *ode15s* routine. A stiff differential equation solver was used in order to account for abrupt changes in the stimulus presented to the model. The solution was evaluated for each time point of the stimulus evolution: from point $t = 0$ to $t = t_f$ in steps of $1ms$. The resulting accuracy is therefore $1ms$. The maximum integration step was set at $15ms$, this

value is smaller than the shortest change in contrast of the stimulus (i.e., 33*ms*, probe flash see A.2) and as such, adequate.

D.7   Supplementary figures

All supplementary figures are available at this link. The figures are organized as follows:

- *Experiments* folder:

  - CENTER cells.pdf: all MI populations derived from cells belonging to the center compartment (original dataset, dataset without outliers, dataset with only outliers). All cell natures and all CSS combinations are described in the figure through MI profile and boxplots and mean RGCs responses. Both comparison between different sizes of the center compartment and CTRL-PSEM comparison (as a function of the center compartment size) are present. We recommend to download the figure and explore it with the zoom function.

  - SURROUND cells.pdf: all MI populations derived from cells belonging to the surround compartment (original dataset, dataset without outliers, dataset with only outliers). Same contents as described above with the addition of CTRL-PSEM comparison by averaging the MI profiles resulting from the three different radii of the center compartment. We recommend to download the figure and explore it with the zoom function.

  - Sustained ON cells CENTER.pdf: differences in suppression induced by OFF and ON saccades on sustained ON cells sitting in the center compartment. The comparison between the same-polarity case and the opposite-polarity case is described for both the CTRL and PSEM conditions.

  - Raw responses Sustained ON cells SURROUND.pdf: raw responses to ON saccade and ON flash of sustained ON cells sitting in the surround compartment. The dataset without outliers and the dataset consisting only of the outliers are compared, highlighting the differences in responses of CTRL cells and cells perfused by PSEM. We recommend to download the figure and explore it with the zoom function.

  - Immunohistochemistry.pdf: additional figure at four times the zoom used in Fig. 6.15. The cell body and the dendritic arbour of a horizontal cell is highlighted in the image. For the staining procedure see Appendix C.2.

  - Statistic.pdf: description of the analysis of the MI populations in order to apply the correct statistical tests for the comparison.

- *Model* folder:

  - nRGC Construction ON&OFF saccades.pdf: dissection plots of the construction of the new type of RGC for both ON and OFF peripheral saccades and full field ON flashes. The figure is intended as supplementary and supportive to Fig. 6.4.

  - GCS validation ON&OFF saccades.pdf: deepening of Fig. 6.5, b and Fig. 6.6, a. In this case the MI profiles for both OFF and ON peripheral saccades and full field ON flashes are shown, they were not averaged.

Bibliography

[1] Jasper Akerboom et al. "Optimization of a GCaMP calcium indicator for neural activity imaging". In: *Journal of Neuroscience* 32.40 (2012), pp. 13819–13840. ISSN: 02706474. DOI: 10.1523/JNEUROSCI.2601-12.2012.

[2] Kenneth R. Alexander. "Information processing: Retinal adaptation". In: *The Curated Reference Collection in Neuroscience and Biobehavioral Psychology* October 2015 (2016), pp. 379–386. DOI: 10.1016/B978-0-12-809324-5.01403-6.

[3] Toshihiro Aoyama, Yoshimi Kamiyama, and Shiro Usui. "Simulation analysis of receptive-field size of retinal horizontal cells by ionic current model". In: *Visual Neuroscience* 22.1 (2005), pp. 65–78. ISSN: 09525238. DOI: 10.1017/S0952523805221107.

[4] Dhea Aulianida, Siani Indria Liestyasari, and Siti Rochani Ch. "Masland summary". In: *Journal of Chemical Information and Modeling* 53.9 (2019), pp. 1689–1699. ISSN: 1098-6596. arXiv: arXiv:1011.1669v3.

[5] Stephen A. Baccus et al. "A retinal circuit that computes object motion". In: *Journal of Neuroscience* 28.27 (2008), pp. 6807–6817. ISSN: 02706474. DOI: 10.1523/JNEUROSCI.4206-07.2008.

[6] Tom Baden et al. "The functional diversity of retinal ganglion cells in the mouse". In: *Nature* 529.7586 (2016), pp. 345–350. ISSN: 14764687. DOI: 10.1038/nature16468.

[7] H. B. Barlow and W. R. Levick. "The mechanism of directionally selective units in rabbit's retina." In: *The Journal of Physiology* 178.3 (1965), pp. 477–504. ISSN: 14697793. DOI: 10.1113/jphysiol.1965.sp007638.

[8] D. A. Baylor, A. L. Hodgkin, and T. D. Lamb. "Reconstruction of the electrical responses of turtle cones to flashes and steps of light". In: *The Journal of Physiology* 242.3 (1974), pp. 759–791. ISSN: 00223751. DOI: 10.1113/jphysiol.1974.sp010733.

[9] Christian Behrens et al. "Retinal horizontal cells use different synaptic sites for global feedforward and local feedback signaling". In: *bioRxiv* (2019), p. 780031. DOI: 10.1101/780031.

[10] Bin Lin and Richard H. Masland, Bin Lin, and Richard H. Masland. "Populations of Wide-Field Amacrine Cells in the Mouse Retina BIN". In: *Journal of Comparative Neurology* 346.October 2007 (2008), pp. 339–346. ISSN: 00219967. DOI: 10.1002/cne.

[11] Paola Binda and Maria Concetta Morrone. "Vision during saccadic eye movements". In: *Annual Review of Vision Science* 4 (2018), pp. 193–213. ISSN: 23744650. DOI: 10.1146/annurev-vision-091517-034317.

[12] Frank Bremmer et al. "Neural Dynamics of Saccadic Suppression". In: 29.40 (2009), pp. 12374–12383. DOI: 10.1523/JNEUROSCI.2908-09.2009.

[13] Annalisa Bucci et al. "How the coupling strength of horizontal cells effects the retinal processing of spatio-temporal light stimuli - Model and experiments". In: *Society for Neuroscience 2019 (SFN 2019), October 19-23, 2019, Chicago, Illinois* 173728 (2019), p. 694829.

[14]   David C. Burr, M. Concetta Morrone, and John Ross. "Selective suppression of the magnocellular visual pathway during saccadic eye movements". In: *Nature* 371.6497 (1994), pp. 511–513. ISSN: 00280836. DOI: 10.1038/371511a0.

[15]   Jon Cafaro, Joel Zylberberg, and Greg D. Field. "Global motion processing by populations of direction-selective retinal ganglion cells". In: *Journal of Neuroscience* 40.30 (2020), pp. 5807–5819. ISSN: 15292401. DOI: 10.1523/JNEUROSCI.0564-20.2020.

[16]   Gail A. Carpenter and Stephen Grossberg. "Adaptation and transmitter gating in vertebrate photoreceptors". In: *Advances in Psychology* 43.C (1987), pp. 273–310. ISSN: 01664115. DOI: 10.1016/S0166-4115(08)61764-1.

[17]   E. Castet et al. *'Saccadic suppression' - No need for an active extra-retinal mechanism [1] (multiple letters)*. 2001. DOI: 10.1016/s0166-2236(00)01828-2.

[18]   Le Chang, Tobias Breuninger, and Thomas Euler. "Chromatic Coding from Cone-type Unselective Circuits in the Mouse Retina". In: *Neuron* 77.3 (2013), pp. 559–571. ISSN: 08966273. DOI: 10.1016/j.neuron.2012.12.012.

[19]   Camille A. Chapot, Thomas Euler, and Timm Schubert. "How do horizontal cells 'talk' to cone photoreceptors? Different levels of complexity at the cone–horizontal cell synapse". In: *Journal of Physiology* 595.16 (2017), pp. 5495–5506. ISSN: 14697793. DOI: 10.1113/JP274177.

[20]   Taro Chaya et al. "Versatile functional roles of horizontal cells in the retinal circuit". In: *Scientific Reports* 7.1 (2017), pp. 1–15. ISSN: 20452322. DOI: 10.1038/s41598-017-05543-2.

[21]   Hui Chen, Xiaorong Liu, and Ning Tian. "Subtype-dependent postnatal development of direction- and orientation-selective retinal ganglion cells in mice". In: *Journal of Neurophysiology* 112.9 (2014), pp. 2092–2101. ISSN: 0022-3077. DOI: 10.1152/jn.00320.2014. URL: https://www.physiology.org/doi/10.1152/jn.00320.2014.

[22]   E. J. Chichilnisky. "A simple white noise analysis of neuronal light responses". In: *Network: Computation in Neural Systems* 12.2 (2001), pp. 199–213. ISSN: 0954898X. DOI: 10.1088/0954-898X/12/2/306.

[23]   Damon A. Clark et al. "Dynamical Adaptation in Photoreceptors". In: *PLoS Computational Biology* 9.11 (2013). ISSN: 1553734X. DOI: 10.1371/journal.pcbi.1003289.

[24]   Lisa J. Croner and Ehud Kaplan. "Receptive fields of P and M ganglion cells across the primate retina". In: *Vision Research* 35.1 (1995), pp. 7–24. ISSN: 00426989. DOI: 10.1016/0042-6989(94)E0066-T.

[25]   D Dacey et al. "Center surround receptive field structure of cone bipolar cells in primate retina". Vision research, vol. , pp. , . Retrieved from http://www.ncbi.nlm.nih.gov/pubmed/10837827." In: 40.14 SRC - GoogleScholar FG - 0 (2000), pp. 1801–1811.

[26]   Scott J. Daly and Richard A. Normann. "Temporal information processing in cones: Effects of light adaptation on temporal summation and modulation". In: *Vision Research* 25.9 (1985), pp. 1197–1206. ISSN: 00426989. DOI: 10.1016/0042-6989(85)90034-3.

[27]   Jonathan B. Demb et al. "Functional circuitry of the retinal ganglion cell's nonlinear receptive field". In: *Journal of Neuroscience* 19.22 (1999), pp. 9756–9767. ISSN: 02706474. DOI: 10.1523/jneurosci.19-22-09756.1999.

[28]   Benjamin E. Deverman et al. "Cre-dependent selection yields AAV variants for widespread gene transfer to the adult brain". In: *Nature Biotechnology* 34.2 (2016), pp. 204–209. ISSN: 15461696. DOI: 10.1038/nbt.3440.

[29] Roland Diggelmann et al. "Automatic spike sorting for high-density microelectrode arrays". In: *Journal of Neurophysiology* 120.6 (2018), pp. 3155–3171. ISSN: 15221598. DOI: `10.1152/jn.00803.2017`.

[30] Antonia Drinnenberg et al. "How Diverse Retinal Functions Arise from Feedback at the First Visual Synapse". In: *Neuron* 99.1 (2018), 117–134.e11. ISSN: 10974199. DOI: `10.1016/j.neuron.2018.06.001`.

[31] Felice A. Dunn, Martin J. Lankheet, and Fred Rieke. "Light adaptation in cone vision involves switching between receptor and post-receptor sites". In: *Nature* 449.7162 (2007), pp. 603–606. ISSN: 14764687. DOI: `10.1038/nature06150`.

[32] D. Endeman and M. Kamermans. "Cones perform a non-linear transformation on natural stimuli". In: *The Journal of Physiology* 588.3 (2010), pp. 435–446. ISSN: 00223751. DOI: `10.1113/jphysiol.2009.179036`.

[33] Michele Fiscella et al. "Recording from defined populations of retinal ganglion cells using a high-density CMOS-integrated microelectrode array with real-time switchable electrode selection". In: *Journal of Neuroscience Methods* 211.1 (2012), pp. 103–113. ISSN: 01650270. DOI: `10.1016/j.jneumeth.2012.08.017`.

[34] J. F. Fohlmeister, P. A. Coleman, and R. F. Miller. "Modeling the repetitive firing of retinal ganglion cells". In: *Brain Research* 510.2 (1990), pp. 343–345. ISSN: 00068993. DOI: `10.1016/0006-8993(90)91388-W`.

[35] J. F. Fohlmeister and R. F. Miller. "Impulse encoding mechanisms of ganglion cells in the tiger salamander retina". In: *Journal of Neurophysiology* 78.4 (1997), pp. 1935–1947. ISSN: 00223077. DOI: `10.1152/jn.1997.78.4.1935`.

[36] Felix Franke et al. "Bayes optimal template matching for spike sorting – combining fisher discriminant analysis with optimal filtering". In: *Journal of Computational Neuroscience* 38.3 (2015), pp. 439–459. ISSN: 15736873. DOI: `10.1007/s10827-015-0547-7`.

[37] Katrin Franke et al. "Inhibition decorrelates visual feature representations in the inner retina". In: *Nature* 542.7642 (2017), pp. 439–444. ISSN: 14764687. DOI: `10.1038/nature21394`.

[38] M. G. F. Fuortes and A. L. Hodgkin. "Changes in time scale and sensitivity in the ommatidia of Limulus". In: *The Journal of Physiology* 172.2 (1964), pp. 239–263. ISSN: 00223751. DOI: `10.1113/jphysiol.1964.sp007415`.

[39] Miguel A. García-Pérez and Eli Peli. "Visual contrast processing is largely unaltered during saccades". In: *Frontiers in Psychology* 2.SEP (2011). ISSN: 16641078. DOI: `10.3389/fpsyg.2011.00247`.

[40] A. Gelencsér et al. "Biomimetic model of the outer plexiform layer by incorporating memristive devices". In: *Physical Review E - Statistical, Nonlinear, and Soft Matter Physics* 85.4 (2012). ISSN: 15393755. DOI: `10.1103/PhysRevE.85.041918`.

[41] Tim Gollisch and Markus Meister. "Eye Smarter than Scientists Believed: Neural Computations in Circuits of the Retina". In: *Neuron* 65.2 (2010), pp. 150–164. ISSN: 08966273. DOI: `10.1016/j.neuron.2009.12.009`. URL: `http://dx.doi.org/10.1016/j.neuron.2009.12.009`.

[42] James C.R. Grove et al. "Novel hybrid action of GABA mediates inhibitory feedback in the mammalian retina". In: *PLoS Biology* 17.4 (2019), pp. 1–30. ISSN: 15457885. DOI: `10.1371/journal.pbio.3000200`.

[43] Tianruo Guo et al. "Modeling normal and rebound excitation in mammalian retinal ganglion cells". In: *Proceedings of the Annual International Conference of the IEEE Engineering in Medicine and Biology Society, EMBS*. 2012, pp. 5506–5509. ISBN: 9781424441198. DOI: `10.1109/EMBC.2012.6347241`.

[44] Tianruo Guo et al. "Understanding the Retina : A Review of Computational Models of the Retina from the Single Cell to the Network Level". In: December 2017 (2014). DOI: `10.1615/CritRevBiomedEng.2014011732`.

[45] R. D. Hamer et al. "Toward a unified model of vertebrate rod phototransduction". In: *Visual Neuroscience* 22.4 (2005), pp. 417–436. ISSN: 09525238. DOI: `10.1017/S0952523805224045`.

[46] Hans van Hateren. "A cellular and molecular model of response kinetics and adaptation in primate cones and horizontal cells". In: *Journal of Vision* 5.4 (2005), pp. 331–347. ISSN: 15347362. DOI: `10.1167/5.4.5`.

[47] J. H. van Hateren and H. P. Snippe. "Simulating human cones from mid-mesopic up to high-photopic luminances". In: *Journal of Vision* 7.4 (2007), pp. 1–11. ISSN: 15347362. DOI: `10.1167/7.4.1`.

[48] Moritz Helmstaedter et al. "Connectomic reconstruction of the inner plexiform layer in the mouse retina". In: *Nature* 500.7461 (2013), pp. 168–174. ISSN: 14764687. DOI: `10.1038/nature12346`.

[49] Arlene A. Hirano, Steven Barnes, and Nicholas C. Brecha. *Retina: Information processing: Horizontal cells*. November 2015. Elsevier, 2016, pp. 363–371. ISBN: 9780128093245. DOI: `10.1016/B978-0-12-809324-5.01402-4`. URL: `http://dx.doi.org/10.1016/B978-0-12-809324-5.01402-4`.

[50] S Hochstein and R M Shapley. "Linear and nonlinear spatial subunits in Y cat retinal ganglion cells." In: *The Journal of Physiology* 262.2 (1976), pp. 265–284. ISSN: 00223751. DOI: `10.1113/jphysiol.1976.sp011595`.

[51] Jen Chun Hsiang and Daniel Kerschensteiner. "Parallel Processing of Negative Feedback: E Unum Pluribus". In: *Neuron* 99.1 (2018), pp. 5–7. ISSN: 10974199. DOI: `10.1016/j.neuron.2018.06.041`.

[52] Saad Idrees et al. "Perceptual saccadic suppression starts in the retina". In: *Nature Communications* 11.1 (2020), pp. 1–19. ISSN: 20411723. DOI: `10.1038/s41467-020-15890-w`.

[53] Saad Idrees et al. "Retinal mechanisms of saccadic suppression and their role in processing sequential stimuli". In: *bioRxiv* (2020), pp. 1–72. DOI: `10.1101/2020.08.21.261198`.

[54] Skyler L. Jackman et al. "A Positive Feedback Synapse from Retinal Horizontal Cells to Cone Photoreceptors". In: *PLoS Biology* 9.5 (2011). Ed. by Fred Rieke, e1001057. ISSN: 1545-7885. DOI: `10.1371/journal.pbio.1001057`.

[55] Ulrike Janssen-Bienhold et al. "Molecular diversity of gap junctions between horizontal cells". In: *Progress in Brain Research* 131 (2001), pp. 93–107. ISSN: 00796123. DOI: `10.1016/s0079-6123(01)31010-5`.

[56] Jonathan Jouty et al. "Non-parametric physiological classification of retinal ganglion cells in the mouse retina". In: *Frontiers in Cellular Neuroscience* 12.December (2018). ISSN: 16625102. DOI: `10.3389/fncel.2018.00481`.

[57] Tatiana Kameneva, Hamish Meffin, and Anthony N. Burkitt. "Modelling intrinsic electrophysiological properties of on and off retinal ganglion cells". In: *Journal of Computational Neuroscience* 31.3 (2011), pp. 547–561. ISSN: 09295313. DOI: 10.1007/s10827-011-0322-3.

[58] Y. Kamiyama, T. Ogura, and S. Usui. "Ionic current model of the vertebrate rod photoreceptor". In: *Vision Research* 36.24 (1996), pp. 4059–4068. ISSN: 00426989. DOI: 10.1016/S0042-6989(96)00178-2.

[59] T. M. Kandel, E. R, Schwartz, J.H, & Jessel. "Principles of Neural Science,Fifth Edition". In: (2013).

[60] V. J. Kefalov. "Phototransduction: Phototransduction in cones". In: *Encyclopedia of the Eye* December 2010 (2010), pp. 389–396. DOI: 10.1016/B978-0-12-374203-2.00189-5.

[61] Robin Kemmler et al. "Differential regulation of cone calcium signals by different horizontal cell feedback mechanisms in the mouse retina". In: *Journal of Neuroscience* 34.35 (2014), pp. 11826–11843. ISSN: 15292401. DOI: 10.1523/JNEUROSCI.0272-14.2014.

[62] Young Joon Kim et al. "Nonlinear decoding of natural images from large-scale primate retinal ganglion recordings Author summary Overview". In: (2020), pp. 1–24.

[63] Alexandra Kling et al. "Functional Organization of Midget and Parasol Ganglion Cells in the Human Retina". In: *bioRxiv* 019005 (2020), p. 2020.08.07.240762.

[64] Dmitri E. Kourennyi et al. "Reciprocal modulation of calcium dynamics at rod and cone photoreceptor synapses by nitric oxide". In: *Journal of Neurophysiology* 92.1 (2004), pp. 477–483. ISSN: 00223077. DOI: 10.1152/jn.00606.2003.

[65] Richard H. Kramer and Christopher M. Davenport. "Lateral Inhibition in the Vertebrate Retina: The Case of the Missing Neurotransmitter". In: *PLoS Biology* 13.12 (2015), pp. 1–8. ISSN: 15457885. DOI: 10.1371/journal.pbio.1002322.

[66] S. W. Kuffler. "Discharge patterns and functional organization of mammalian retina". In: *Journal of neurophysiology* 16.1 (1953), pp. 37–68. ISSN: 00223077. DOI: 10.1152/jn.1953.16.1.37.

[67] Juncal L Peichl, Gonzälez-soriano. "Morphological types of horizontal cell in rodent retinae: A comparison of rat, mouse, gerbil, and guinea pig". In: *Visual Neuroscience* 11.3 (1994), pp. 501–517. ISSN: 14698714. DOI: 10.1017/S095252380000242X.

[68] Belle Liu et al. "pre-print-Predictive encoding of motion begins in the primate retina". In: (2020).

[69] Tatiana Malevich, Antimo Buonocore, and Ziad M. Hafed. "Rapid stimulus-driven modulation of slow ocular position drifts". In: *eLife* 9 (2020), pp. 1–21. ISSN: 2050084X. DOI: 10.7554/ELIFE.57595.

[70] Robert E. Marc and W. L.S. Liu. "Fundamental GABAergic amacrine cell circuitries in the retina: Nested feedback, concatenated inhibition, and axosomatic synapses". In: *Journal of Comparative Neurology* 425.4 (2000), pp. 560–582. ISSN: 00219967. DOI: 10.1002/1096-9861(20001002)425:4<560::AID-CNE7>3.0.CO;2-D.

[71] Pablo Martínez-Cañada et al. "A Computational Framework for Realistic Retina Modeling". In: *International Journal of Neural Systems* 26.7 (2016), pp. 1–18. ISSN: 01290657. DOI: 10.1142/S0129065716500301.

[72] R. H. Masland. "Neuronal diversity in the retina". In: *Current Opinion in Neurobiology* 11.4 (2001), pp. 431–436. ISSN: 09594388. DOI: 10.1016/S0959-4388(00)00230-0.

[73] Richard H. Masland. "The Neuronal Organization of the Retina". In: *Neuron* 76.2 (2012), pp. 266–280. ISSN: 08966273. DOI: 10.1016/j.neuron.2012.10.002.

[74] Masland RH. "The fundamental plan of the retina". In: *Nature Neuroscience* 4.9 (2001), pp. 877–886.

[75] Lane T. McIntosh et al. "Deep learning models of the retinal response to natural scenes". In: *Advances in Neural Information Processing Systems* Nips (2016), pp. 1369–1377. ISSN: 10495258. arXiv: 1702.01825.

[76] Markus Meister and Michael J Berry Ii. "The Neural Code of the Retina Review". In: *Nature* 22 (1999), pp. 435–450.

[77] Thomas A. Münch et al. "Approach sensitivity in the retina processed by a multi-functional neural circuit". In: *Nature Neuroscience* 12.10 (2009), pp. 1308–1316. ISSN: 10976256. DOI: 10.1038/nn.2389. URL: https://www.nature.com/articles/nn.2389.

[78] Bence P. Ölveczky, Stephen A. Baccus, and Markus Meister. "Segregation of object and background motion in the retina". In: *Nature* 423.6938 (2003), pp. 401–408. ISSN: 00280836. DOI: 10.1038/nature01652.

[79] S.L. Polyak. "The Retina. The Anatomy and the Histology of the Retina in Man, Ape and Monkey, including the Consideration of Visual Functions, the History of Physiological Optics, and the Histological Laboratory Technique". In: *The Journal of Nervous and Mental Disease* 96.1 (1942), pp. 114–115. ISSN: 0022-3018. DOI: 10.1097/00005053-194207000-00055.

[80] Rodrigo Publio, Rodrigo F. Oliveira, and Antonio C. Roque. "A realistic model of rod photoreceptor for use in a retina network model". In: *Neurocomputing* 69.10-12 (2006), pp. 1020–1024. ISSN: 09252312. DOI: 10.1016/j.neucom.2005.12.037.

[81] John Ross, David Burr, and Concetta Morrone. "Suppression of the magnocellular pathway during saccades". In: *Behavioural Brain Research* 80.1-2 (1996), pp. 1–8. ISSN: 01664328. DOI: 10.1016/0166-4328(96)00012-5.

[82] Joshua R. Sanes and Richard H. Masland. "The Types of Retinal Ganglion Cells: Current Status and Implications for Neuronal Classification". In: *Annual Review of Neuroscience* 38 (2015), pp. 221–246. ISSN: 15454126. DOI: 10.1146/annurev-neuro-071714-034120. URL: www.annualreviews.org.

[83] Cornelius Schröder et al. "System Identification with Biophysical Constraints: A Circuit Model of the Inner Retina". In: *bioRxiv* (2020), p. 2020.06.16.154203.

[84] Richard Schweitzer and Martin Rolfs. "Intra-saccadic motion streaks as cues to linking object locations across saccades". In: *Journal of Vision* 20.4 (2020), pp. 1–24. ISSN: 15347362. DOI: 10.1167/jov.20.4.17.

[85] Setiyawan. *Ophtalmologic Prosthesis*. Vol. 53. 9. 2013, pp. 1689–1699. ISBN: 9788578110796. arXiv: arXiv:1011.1669v3.

[86] Nishal P. Shah et al. "Inference of nonlinear receptive field subunits with spike-triggered clustering". In: *eLife* 9 (2020), pp. 1–31. ISSN: 2050084X. DOI: 10.7554/eLife.45743.

[87] T. Shirahata. "The effect of variations in sodium conductances on pacemaking in a dopaminergic retinal neuron model". In: *Acta Biologica Hungarica* 62.2 (2011), pp. 211–214. ISSN: 02365383. DOI: 10.1556/ABiol.62.2011.2.11.

[88] Takaaki Shirahata. "Simulation of rabbit A-type retinal horizontal cell that generates repetitive action potentials". In: *Neuroscience Letters* 439.1 (2008), pp. 116–118. ISSN: 03043940. DOI: 10.1016/j.neulet.2008.04.087.

[89] S.I. Fried; T.A. Muench; F.S. Werblin. *The Circuitry Underlying Directional Excitation and Inhibition to DS cells | IOVS | ARVO Journals*. 2004. (Visited on 02/24/2021).

[90] Sandra Siegert et al. "Transcriptional code and disease map for adult retinal cell types". In: *Nature Publishing Group* 15.3 (2012). ISSN: 1097-6256. DOI: 10.1038/nn.3032.

[91] Michael A. Steffen et al. "Spontaneous activity of dopaminergic retinal neurons". In: *Biophysical Journal* 85.4 (2003), pp. 2158–2169. ISSN: 00063495. DOI: 10.1016/S0006-3495(03)74642-6.

[92] Wenzhi Sun et al. "ON direction-selective ganglion cells in the mouse retina". In: *The Journal of Physiology* 576.1 (2006), pp. 197–202. ISSN: 00223751. DOI: 10.1113/jphysiol.2006.115857.

[93] Klaudia P. Szatko et al. "Neural circuits in the mouse retina support color vision in the upper visual field". In: *Nature Communications* 11.1 (2020). ISSN: 20411723. DOI: 10.1038/s41467-020-17113-8.

[94] Tamas Szikra et al. "Rods in daylight act as relay cells for cone-driven horizontal cell-mediated surround inhibition". In: *Nature Neuroscience* 17.12 (2014), pp. 1728–1735. ISSN: 15461726. DOI: 10.1038/nn.3852.

[95] Hidenori Tanaka et al. "From deep learning to mechanistic understanding in neuroscience: The structure of retinal prediction". In: *arXiv* NeurIPS (2019), pp. 1–11. arXiv: 1912.06207.

[96] A. Thiele et al. "Neural mechanisms of saccadic suppression". In: *Science* 295.5564 (2002), pp. 2460–2462. ISSN: 00368075. DOI: 10.1126/science.1068788.

[97] Wallace B. Thoreson, Norbert Babai, and Theodore M. Bartoletti. "Feedback from horizontal cells to rod photoreceptors in vertebrate retina". In: *Journal of Neuroscience* 28.22 (2008), pp. 5691–5695. ISSN: 02706474. DOI: 10.1523/JNEUROSCI.0403-08.2008.

[98] Wallace B. Thoreson and Stuart C. Mangel. "Lateral interactions in the outer retina". In: *Progress in Retinal and Eye Research* 31.5 (2012), pp. 407–441. ISSN: 13509462. DOI: 10.1016/j.preteyeres.2012.04.003.

[99] J. B. Troy and T. Shou. *The receptive fields of cat retinal ganglion cells in physiological and pathological states: Where we are after half a century of research*. 2002. DOI: 10.1016/S1350-9462(02)00002-2.

[100] Maxwell H. Turner, Gregory W. Schwartz, and Fred Rieke. "Receptive field center-surround interactions mediate context-dependent spatial contrast encoding in the retina". In: *eLife* 7 (2018), pp. 1–25. ISSN: 2050084X. DOI: 10.7554/eLife.38841.

[101] S. Usui et al. "Ionic current model of bipolar cells in the lower vertebrate retina". In: *Vision Research* 36.24 (1996), pp. 4069–4076. ISSN: 00426989. DOI: 10.1016/S0042-6989(96)00179-4.

[102] Shiro Usui et al. "Reconstruction of retinal horizontal cell responses by the ionic current model". In: *Vision Research* 36.12 (1996), pp. 1711–1719. ISSN: 00426989. DOI: 10.1016/0042-6989(96)00267-2.

[103] Rozan Vroman et al. "Extracellular ATP Hydrolysis Inhibits Synaptic Transmission by Increasing pH Buffering in the Synaptic Cleft". In: *PLoS Biology* 12.5 (2014). Ed. by Fred Rieke, e1001864. ISSN: 1545-7885. DOI: 10.1371/journal.pbio.1001864.

[104] Heinz Wässle. "Parallel processing in the mammalian retina". In: *Nature Reviews Neuroscience* 5.10 (2004), pp. 747–757. ISSN: 1471003X. DOI: 10.1038/nrn1497.

[105]　Shijun Weng, Wenzhi Sun, and Shigang He. "Identification of ON-OFF direction-selective ganglion cells in the mouse retina". In: *The Journal of Physiology* 562.3 (2005), pp. 915–923. ISSN: 00223751. DOI: 10.1113/jphysiol.2004.076695.

[106]　Adrien Wohrer. "The vertebrate retina : a functional review To cite this version : HAL Id : inria-00280693". In: (2008).

[107]　Adrien Wohrer and Pierre Kornprobst. "Virtual Retina: A biological retina model and simulator, with contrast gain control". In: *Journal of Computational Neuroscience* 26.2 (2009), pp. 219–249. ISSN: 09295313. DOI: 10.1007/s10827-008-0108-4.

[108]　Robert H Wurtz. "Vision Research". In: 48 (2008), pp. 2070–2089. DOI: 10.1016/j.visres.2008.03.021.

[109]　Robert H. Wurtz, Wilsaan M. Joiner, and Rebecca A. Berman. *Neuronal mechanisms for visual stability: Progress and problems*. 2011. DOI: 10.1098/rstb.2010.0186.

[110]　Wenjun Yan et al. "Mouse Retinal Cell Atlas: Molecular Identification of over Sixty Amacrine Cell Types". In: *Journal of Neuroscience* 40.27 (2020), pp. 5177–5195. ISSN: 15292401. DOI: 10.1523/JNEUROSCI.0471-20.2020.

[111]　Takeshi Yoshimatsu et al. "Optimal rotation of colour space by zebrafish cones in vivo". In: *F1000Research* 8 (2019), pp. 1–26.